DTU Physics
Department of Physics

Master Thesis

Theory of thermoviscous acoustofluidics in microsystems

Jonas Tobias Karlsen
s072824

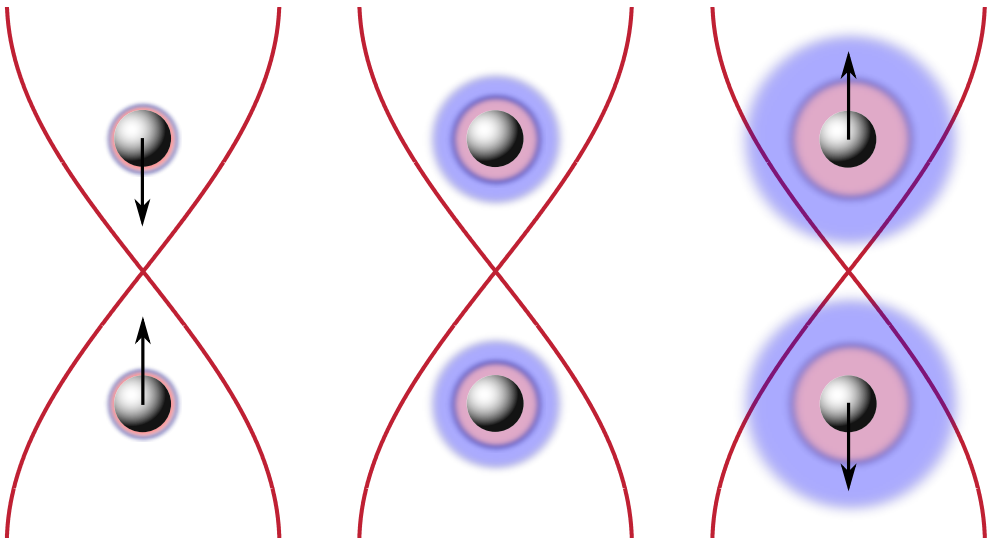

Supervisor: Professor Henrik Bruus

Department of Physics
Technical University of Denmark

14 March 2014

Frontpage illustration

The frontpage illustration shows two particles in an acoustical standing wave field experiencing a force due to scattering of the acoustic waves. As the thermal and viscous boundary layer thicknesses become comparable to the particle radius the thermoviscous corrections to the radiation force become significant and the direction of the force changes.

Abstract

Recent advances and interest in ultrasound manipulation of particles at the microscale calls for an increased theoretical understanding of acoustofluidics including the thermoviscous effects of viscosity and heat-conduction, which lead to viscous and thermal boundary layers at interfaces between materials with different thermoacoustic properties.

In this thesis we study acoustofluidics at the microscale under the unifying theme of *thermoviscous effects*. We present a mathematical theory of thermoviscous acoustofluidics describing acoustic wave propagation in a viscous, heat-conducting, Newtonian fluid. The acoustic wave propagation is described in terms of a longitudinal propagating compressional mode, a highly damped longitudinal thermal mode, and a highly damped transverse shear mode. The theory is applied to obtain a resonant field solution to the driven parallel-plate system correct to first order in $k_0\delta_\mathrm{s}$, where $k_0 = 2\pi/\lambda$ is the wavenumber and δ_s is the viscous boundary layer thickness. The theory represents an improvement over the commonly employed Prandtl-Schlichting boundary layer theory approach that is zeroth order in $k_0\delta_\mathrm{s}$. As a consequence, we are able to explain features of numerical solutions not previously accounted for. The complete description of the fields moreover allows for calculation of several quantities related to microchannel acoustofluidics such as the quality-factor of the resonance, which explains experimentally measured values around 500 as a consequence of viscous and thermal dissipation in the boundary layers near the walls.

The thermoviscous theory of acoustics is applied to the problem of scattering of sound from particles much smaller than the acoustic wavelength, and we present analytical results for the radiation force on a particle in an acoustical field, with no restrictions on the length scales of the viscous and thermal boundary layer thicknesses δ_s and δ_t relative to the particle radius a, i.e., in the limit of $\delta_\mathrm{s} \sim \delta_\mathrm{t} \sim a \ll \lambda$. This is the limit relevant to scattering of ultrasound waves from micrometer-sized particles. For the case of a typical vegetable oil droplet in water we find corrections to the acoustic radiation force of more than 100% due to thermal effects. With much ongoing experimental research in acoustofluidics aiming at focusing submicrometer-sized particles such as bacteria and vira, the corrections are interesting not only theoretically, but also from an engineering perspective.

Resumé

Nylige fremskridt og interessen for anvendelse af ultralyd til manipulering af partikler på mikroskala kræver en øget teoretisk forståelse af akustofluidik, herunder af termoviskøse effekter fra viskositet og varmeledning, hvilket fører til viskøse og termiske randlag på grænsen mellem materialer med forskellige termoakustiske egenskaber.

I denne afhandling studerer vi akustofluidik på mikroskala under temaet *termoviskøse effekter*. Vi præsenterer en matematisk teori for termoviskøs akustofluidik som beskriver akustisk bølgeudbredelse i en viskøs, varmeledende, Newtonsk væske. Den akustiske bølgeudbredelse vil blive beskrevet med en longitudinal propagerende kompressions bølge, en kraftigt dæmpet longitudinal termisk bølge, og en kraftigt dæmpet transvers bølge. Teorien vil blive anvendt til at løse for det resonante akustiske felt i det drevne parallelplade system, og vi finder en løsning korrekt til første orden i $k_0\delta_\mathrm{s}$, hvor $k_0 = 2\pi/\lambda$ er bølgetallet og δ_s er tykkelsen af det viskøse randlag. Teorien forbedrer således eksisterende løsninger, som almindeligvis er baseret på Prandtl-Schlichting grænselagsteori, der er nulte orden i $k_0\delta_\mathrm{s}$. Med den forbedrede teori er vi i stand til at forklare visse karakteristika observeret i numeriske løsninger, som ikke tidligere har været beskrevet analytisk. Den komplette beskrivelse af de akustiske felter giver ligeledes en kvantitativ forståelse af mange aspekter vedrørende akustofluidik i mikrokanaler, såsom kvalitetsfaktoren for resonansen, for hvilken vi kan forklare eksperimentelt målte værdier omkring 500, som en konsekvens af dissipation i de viskøse og termiske randlag nær væggene.

Den termoviskøse teori for akustofluidik bliver desuden anvendt til at beskrive spredning af lydbølger fra partikler, der er meget mindre end den akustiske bølgelængde, og vi præsenterer analytiske resultater for strålingskraften på en partikel i et akustisk felt uden begrænsninger på længdeskalaerne for de viskøse og termiske randlag δ_s og δ_t i forhold til partiklens radius a, det vil sige i grænsen $\delta_\mathrm{s} \sim \delta_\mathrm{t} \sim a \ll \lambda$. Dette er grænsen relevant for spredning af ultralydsbølger fra partikler af mikrometer størrelse. Betragtes en vegetabilsk oliedråbe i vand fører teorien til korrektioner af strålingskraften på mere end 100% som følge af termiske effekter. Da eksperimentel forskning i akustofluidik sigter mod at fokusere partikler under mikrometer størrelse, såsom bakterier og vira, er korrektionerne ikke kun af teoretisk interesse, men har også betydning i en ingeniørmæssig sammenhæng.

Preface

This thesis is submitted in partial fulfillment of the requirements for obtaining the degree of Master of Science in Physics and Nanotechnology at the Technical University of Denmark (DTU). The work was carried out at the Department of Physics in the Theoretical Microfluidics group (TMF) headed by Professor Henrik Bruus. The duration of this thesis work was 6 months from 16 September 2013 to 14 March 2014 corresponding to 35 ECTS points.

First and foremost, I would like to thank my supervisor Henrik Bruus for sharing his insight into physics and his great enthusiasm for the subject. It has been truly inspiring to be part of the TMF and I would like to thank the whole group for providing a pleasant and productive working environment. I have enjoyed not only the educational and inspiring discussions on physics, but also the social activities of the group ranging from board games and beer to high-roping and a moose safari in Sweden. Thanks go to PhD students Christoffer Nielsen and Peter Muller, and to my fellow MSc student and office-buddy Mikkel Ley. It has been a pleasure working beside all of you. Finally, I would like to use the opportunity to thank my parents, not for teaching me physics, but for providing me with motivation and confidence to explore the world on my own.

During the project I stayed for two weeks in Paris visiting the Laboratoire Matière et Systèmes Complexes (MSC) at Université Paris Diderot. I would like to thank both Henrik Bruus for encouraging me to come, and the MSC for hosting me there.

Jonas Tobias Karlsen
Department of Physics
Technical University of Denmark
14 March 2014

Contents

List of Figures

List of Tables

List of symbols

Symbol	Description	Unit
ρ	Mass density	kg m^{-3}
p	Pressure	Pa
T	Temperature	K
s	Entropy per mass unit	J K^{-1} kg^{-1}
ε	Internal energy per mass unit	J kg^{-1}
g	Gibbs free energy per mass unit	J kg^{-1}
$\boldsymbol{v}$	Velocity vector	m s^{-1}
$\boldsymbol{\sigma}$	Stress tensor	N m^{-2}
$\boldsymbol{\tau}$	Viscous stress tensor	N m^{-2}
Φ	Velocity scalar potential	m^2 s^{-1}
$\boldsymbol{\Psi}$	Velocity vector potential	m^2 s^{-1}
$\boldsymbol{\zeta} = \boldsymbol{\nabla} \times \boldsymbol{v}$	Vorticity vector	s^{-1}
$\square_0, \square_1, \square_2$	zeroth, first, and second-order of $\square$	
η	Dynamic viscosity	Pa s
η_b	Bulk viscosity	Pa s
$\nu_0 = \eta_0/\rho_0$	Momentum diffusion constant	m^2 s^{-1}
$\beta = \eta_\mathrm{b}/\eta + 1/3$	Viscosity ratio	
C_p	Specific heat capacity at constant pressure	J kg^{-1} K^{-1}
C_V	Specific heat capacity at constant volume	J kg^{-1} K^{-1}
$\gamma = C_p/C_V$	Specific heat capacity ratio	
k_th	Thermal conductivity	W m^{-1} K^{-1}
$D_\mathrm{th} = k_\mathrm{th}/\rho_0 C_p$	Thermal diffusion constant	m^2 s^{-1}
$\mathrm{Pr} = \nu_0/D_\mathrm{th}$	Prandtl number	
α_p	Thermal expansion coefficient	K^{-1}
c	Isentropic speed of sound	m s^{-1}
$\kappa_s = 1/\rho_0 c^2$	Isentropic compressibility	Pa^{-1}
$\kappa_T = \gamma \kappa_s$	Isothermal compressibility	Pa^{-1}

Continued on the next page

Symbol	Description	Unit
t	Time	s
f	Frequency	Hz
$\omega = 2\pi f$	Angular frequency	s^{-1}
λ	Wavelength	m
$\delta_\mathrm{s} = \sqrt{2\nu_0/\omega}$	Momentum diffusion length	m
$\delta_\mathrm{t} = \sqrt{2D_\mathrm{th}/\omega}$	Thermal diffusion length	m
$k_0 = \omega/c$	Undamped wavenumber	m^{-1}
k_c	Compressional mode wavenumber	m^{-1}
k_s	Shear mode wavenumber	m^{-1}
k_t	Thermal mode wavenumber	m^{-1}
$\Gamma_\mathrm{s} = (1+\beta)\nu_0\omega/c^2$	Viscous damping factor	
$\Gamma_\mathrm{t} = D_\mathrm{th}\omega/c^2$	Thermal damping factor	
v_bc	Actuation velocity amplitude	$\mathrm{m\ s}^{-1}$
h	Channel height	m
w	Channel width	m
$\lambda_0 = 2w$	Half-wave wavelength	m
$\omega_0 = 2\pi c/\lambda_0$	Half-wave angular frequency	s^{-1}
ω_res	Angular resonance frequency	s^{-1}
Q	Quality factor of resonance	
E_ac	Average acoustic energy density	$\mathrm{J\ m}^{-3}$
u_0	First-order velocity field amplitude	$\mathrm{m\ s}^{-1}$
$\varepsilon_\lambda = 2\pi\delta_\mathrm{s}/\lambda$		
$\varepsilon_h = 2\delta_\mathrm{s}/h$		
$\varepsilon_w = 2\delta_\mathrm{s}/w$		
a	Particle radius	m
f_0	Monopole scattering coefficient	
f_1	Dipole scattering coefficient	
$\square'$	Parameter $\square$ of fluid droplet	
Φ_ac	Acoustic contrast factor	
$x_\mathrm{c} = k_\mathrm{c}a$		
$x_\mathrm{s} = k_\mathrm{s}a$		
$x_\mathrm{t} = k_\mathrm{t}a$		

Continued on the next page

Symbol	Description	Unit
∂_k	Partial derivative with respect to k	$[k]^{-1}$
$\boldsymbol{\nabla}$	Gradient vector operator	m^{-1}
$\boldsymbol{\nabla}\cdot$	Divergence scalar operator	m^{-1}
$\boldsymbol{\nabla}\times$	Rotation vector operator	m^{-1}
∇^2	Laplacian scalar operator	m^{-2}
(x, y, z)	Cartesian coordinates	m
(r, θ, ϕ)	Spherical coordinates	
$\mathbf{e}_k$	Unit vector in the k-direction	
$\boldsymbol{n}$	Surface normal vector	
$\langle\square\rangle$	Time average of $\square$	
$\lvert\square\rvert$	Absolute value of $\square$	
$\square^*$	Complex conjugate of $\square$	
$\mathrm{Re}\,[\square]$	Real part of $\square$	
$\mathrm{Im}\,[\square]$	Imaginary part of $\square$	
$\mathrm{i} = \sqrt{-1}$	Imaginary unit	
e	Base of the natural logarithm, $\ln(\mathrm{e}) = 1$	
P_n	Legendre polynomial of order n	
P_n^m	Associated Legendre polynomial of order n	
$h_n^{(1)}$	Spherical Hankel function (1st) of order n	
$h_n^{(2)}$	Spherical Hankel function (2nd) of order n	
j_n	Spherical Bessel function of order n	
y_n	Spherical Neumann function of order n	

Chapter 1

Introduction

Acoustofluidics is the combined field of acoustics and microfluidics, which has received increasing interest in the last few decades due to its applications in bio-medical lab-on-a-chip devices. The journal *Lab on a Chip* recently published a tutorial series on acoustofluidics for use in cell and particle manipulation, covering both theory and experiments through 23 articles reviewing fundamentals and state-of-the-art experiments, theory, and modeling [1]. Experiments have demonstrated that acoustofluidic devices may be designed for applications relying on focusing, concentration, separation, and trapping of cells and micro-particles [2, 3]. Numerous applications of acoustofluidics include separation of lipids from blood cells [4], raw milk quality control [5], and detection of circulating tumor cells [6]. Lab-on-a-chip systems designed for medical purposes may eventually revolutionize the way medical diagnosis, testing, and drug-delivery is performed by providing faster, automated analysis, and personalized patient treatment.

1.1 Challenges in acoustofluidics theory and modeling

Fig. 1.1 adapted from Ref. [7] shows a sketch of a typical acoustofluidics system setup consisting of a liquid-filled microchannel mounted on a piezoelectric transducer. The figure highlights the most important physical phenomena that result from the time-harmonic actuation of the piezoelectric transducer. In this thesis we will use a simple model for actuation and study only the fluid domain of the system. We will focus on the boundary layers and the acoustic resonance of Fig. 1.1(b), and the wave-particle scattering of Fig. 1.1(c). The physics of these phenomena will be introduced in the respective chapters of this thesis and not in this overall introduction.

The basic idea of microchannel acoustofluidics is that sound may be used to move particles, commonly referred to as *acoustophoresis*. In order to achieve acoustic energy densities high enough to manipulate particles, a resonant field is excited by tuning to a resonance frequency such as the half-wave resonance illustrated in Fig. 1.1. Note the narrow viscous and thermal boundary layers of Fig. 1.1(b) resulting from diffusion of momentum and heat in the fluid due to the boundary conditions of the walls. These boundary layers will be a main concern in this thesis and we will find that a correct

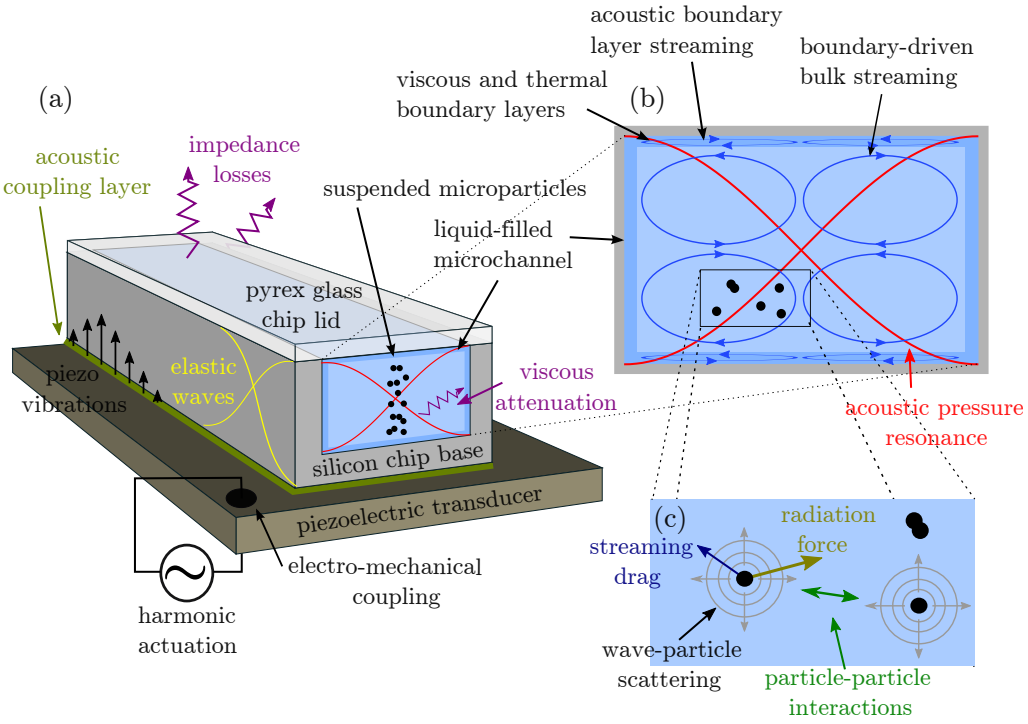

Figure 1.1: Sketch of the physics of acoustofluidics adapted from Ref. [7]. (a) Liquid-filled microchannel mounted on a piezoelectric transducer actuated harmonically at MHz frequency giving rise to a resonant acoustic standing half-wave (red) in the liquid. (b) The vertical cross-section of the channel showing the half-wave pressure resonance and the steady streaming rolls of the fluid resulting from stresses in the thermoviscous boundary layers. (c) Microparticles suspended in the channel scatter the acoustic waves, which gives rise to an acoustic radiation force on the particles.

description of the boundary layers near walls and microparticles turn out to be crucial for understanding many of the other phenomena in the sketch, such as thermoviscous attenuation, the acoustic resonance, wave-particle scattering and radiation forces, as well as the steady motion of the fluid known as acoustic streaming. These phenomena will be investigated theoretically in this thesis under the unifying theme of *thermoviscous effects* in acoustofluidics.

1.2 Motivation for studying thermal effects

Though thermoviscous theories of acoustics have been developed in the study of attenuation of sound in emulsions and suspensions [8, 9] as well as in the study of thermoacoustic engines [10, 11], the theoretical treatments of acoustofluidics in microsystems usually neglect thermal effects from the assumption that the acoustic wave propagation is isentropic [12, 13, 14, 15]. With this assumption the pressure perturbations of the acoustic wave

become proportional to the density perturbations, and one need only consider the conservation of momentum and mass expressed by the Navier-Stokes equation and the continuity equation, respectively [14].

The assumption of isentropic wave propagation corresponds to neglecting heat-conduction in the fluid. In the bulk, where the fluid may be considered almost ideal for frequencies in the MHz range [14, 15], this assumption is well justified. However, near particles and walls viscous shear stresses lead to viscous boundary layers of thickness $\delta_\mathrm{s} = \sqrt{2\nu_0/\omega}$, where $\nu_0 = \eta_0/\rho_0$ is the momentum diffusion constant, and ω is the angular frequency of the acoustic wave [15]. Likewise, the inclusion of thermal conduction leads to thermal boundary layers of thickness $\delta_\mathrm{t} = \sqrt{2D_\mathrm{th}/\omega}$, where D_th is the thermal diffusion constant. For water at room temperature and 2 MHz frequency the boundary layer thicknesses evaluate to $\delta_\mathrm{s} = 0.38$ µm and $\delta_\mathrm{t} = 0.15$ µm, respectively. The two boundary layers are thus comparable in size and we expect that thermal effects, like viscous effects [15], can lead to significant corrections to the theory of acoustofluidics, especially when considering microsystems with particle sizes similar to the boundary layer thickness.

In the field of acoustofluidics and acoustic streaming the viscous boundary layer is treated using singular Prandtl-Schlichting boundary layer theory [12, 16, 17]. This boundary layer theory approach has been employed throughout the literature in the study of acoustic streaming [18, 19, 20, 21, 22], as well as the study of thermoacoustic engines [10, 11]. However, the boundary layer theory approach is correct only to zeroth order in $k_0\delta_\mathrm{s}$, where $k_0 = 2\pi/\lambda$ is the wavenumber, and may lead to discontinuous velocity fields in the transition from the boundary layer to the bulk with the discontinuity of order $k_0\delta_\mathrm{s}$ [12, 23]. Compared to numerical simulations [24, 25] the Prandtl-Schlichting boundary layer theory is not fully satisfactory.

We find that the work on thermoviscous acoustics initiated by Epstein and Carhart in 1953 to describe attenuation of sound in emulsions and suspensions [8] provides a theoretical framework for treating thermoviscous acostofluidics in microsystems superior to the boundary layer approaches commonly employed in the isentropic limit. In this thesis we present the theory and develop it further with the aim of understanding thermoviscous effects in microsystem acoustofluidics.

1.3 Outline of this thesis

Chapter 2: Thermoviscous theory of acoustics

From the first law of thermodynamics and the conservation of mass, momentum, and energy, we derive the governing equations of thermoviscous acoustics. A perturbation series expansion is employed to derive three wave equations for the first-order fields corresponding to three modes of wave propagation in a thermoviscous fluid.

Chapter 3: Acoustic waves in 2D

We examine the theory of thermoviscous acoustics emphasizing the physical fields and derive the coupled field equations allowing for an easier comparison with isentropic the-

ories. We then set up a framework used to satisfy the boundary conditions of a hard, heat-conducting wall, and apply it to solve the driven parallel-plate system without the use of singular boundary layer theory. We investigate the solution graphically and show that the low frequency limit leads to a slowly oscillating Poiseuille flow solution.

Chapter 4: Microchannel acoustofluidics

In this chapter we investigate the driven parallel-plate solution in the limit of microchannel acoustofluidics with narrow boundary layers as compared to the channel height. We compare the analytical solution with the numerical model of Muller *et al.* [24]. Moreover, we investigate the analytical theory in relation to microchannel acoustofluidics presenting results comparable to experimental findings. Finally, we investigate higher-mode field solutions, and end with a discussion on acoustic streaming, showing that our theory is consistent with classical results.

Chapter 5: Acoustic radiation force

We review the theory of acoustic radiation forces on suspended particles and discuss thermoviscous wave-particle scattering mechanisms. Following the treatment of Epstein and Carhart [8] we solve the scattering problem of a viscous, heat-conducting spherical fluid droplet in a viscous, heat-conducting fluid medium. Having derived the scattering coefficients we investigate the time-averaged radiation force experienced by a particle in a standing wave field and show that thermoviscous theory leads to corrections of more than 100% for the case of a small oil droplet in water.

Chapter 6: Conclusion and outlook

We conclude on our findings and give suggestions for future theoretical, numerical, and experimental work.

Appendix A, B, and C

Calculations involving many algebraic details necessary for obtaining some results of the main chapters have been put in the appendices.

Chapter 2

Thermoviscous theory of acoustics

In this chapter we derive the governing equations for the first-order thermoviscous acoustic fields in a compressible, viscous, and heat-conducting Newtonian fluid. The theoretical development is inspired by the work of Bruus [13], Landau and Lifshitz [12, 26], and in particular Epstein and Carhart [8]. The main result of the chapter is the derivation of three wave equations with three distinct wavenumbers corresponding to three possible modes of wave propagation in a thermoviscous fluid, namely two longitudinal modes describing propagating compressional waves and damped thermal waves, respectively, and one transverse mode describing viscous shear waves.

2.1 Governing equations

The starting point of the theory is the first law of thermodynamics and the conservation of mass, momentum, and energy. The thermodynamics is described by the five scalar fields of temperature T, pressure p, density ρ, internal energy ε per mass unit, and entropy s per mass unit. The volume per mass unit is $1/\rho$. The first law of thermodynamics is usually given in the following form, where s and ρ are the independent variables,

$$\mathrm{d}\varepsilon = T\,\mathrm{d}s - p\,\mathrm{d}\left(\frac{1}{\rho}\right) = T\,\mathrm{d}s + \frac{p}{\rho^2}\,\mathrm{d}\rho, \tag{2.1}$$

For acoustic wave propagation it is often convenient to use T and p as independent thermodynamic variables. A standard Legendre transformation of the internal energy ε per unit mass to the Gibbs free energy g per unit mass, $g = \varepsilon - Ts + p\,\frac{1}{\rho}$, gives the first law with T and p as independent variables

$$\mathrm{d}g = -s\,\mathrm{d}T + \frac{1}{\rho}\,\mathrm{d}p. \tag{2.2}$$

Besides the first law of thermodynamics, the governing equations of thermoviscous acoustics requires the introduction of the velocity field $\boldsymbol{v}$ of the fluid as well as its stress tensor $\boldsymbol{\sigma}$, which in terms of the pressure p, velocity $\boldsymbol{v}$, dynamic shear viscosity η, and viscosity

ratio $\beta = \eta_\mathrm{b}/\eta + 1/3$, where η_b is the bulk viscosity, is given as

$$\boldsymbol{\sigma} = -p\,\mathbf{I} + \boldsymbol{\tau}, \tag{2.3a}$$

$$\boldsymbol{\tau} = \eta\left[\boldsymbol{\nabla}\boldsymbol{v} + (\boldsymbol{\nabla}\boldsymbol{v})^{\mathrm{T}}\right] + (\beta - 1)\eta\,(\boldsymbol{\nabla}\cdot\boldsymbol{v})\;\mathbf{I}. \tag{2.3b}$$

Here $\mathbf{I}$ is the unit tensor and the superscript "T" indicates tensor transposition. The tensor $\boldsymbol{\tau}$ is the viscous part of the stress tensor assuming a Newtonian fluid [13].

Mass conservation implies that the rate of change $\partial_t\rho$ of the density in a test volume with surface normal vector $\boldsymbol{n}$ is given by the influx (direction $-\boldsymbol{n}$) of the mass current density $\rho\boldsymbol{v}$. In differential form by Gauss's theorem it is

$$\partial_t\rho = \boldsymbol{\nabla}\cdot\big[-\rho\boldsymbol{v}\big]. \tag{2.4a}$$

Similarly, momentum conservation implies that the rate of change $\partial_t(\rho\boldsymbol{v})$ of the momentum density in the same test volume, is given by the stress forces $\boldsymbol{\sigma}$ acting on the surface (with normal $\boldsymbol{n}$), and the influx (direction $-\boldsymbol{n}$) of the momentum current density $\rho\boldsymbol{v}\boldsymbol{v}$. In differential form, neglecting body forces $\boldsymbol{f}$, this becomes

$$\partial_t(\rho\boldsymbol{v}) = \boldsymbol{\nabla}\cdot\big[\boldsymbol{\tau} - p\,\mathbf{I} - \rho\boldsymbol{v}\boldsymbol{v}\big]. \tag{2.4b}$$

Finally, energy conservation implies that the rate of change $\partial_t\big(\rho\varepsilon + \frac{1}{2}\rho v^2\big)$ of the energy density (internal plus kinetic), is given by the power of the stress forces $\boldsymbol{v}\cdot\boldsymbol{\sigma}$ on the surface (direction $\boldsymbol{n}$), and the influx (direction $-\boldsymbol{n}$) of heat conduction power $-k_\mathrm{th}\boldsymbol{\nabla}T$ as well as energy current density $(\rho\varepsilon + \frac{1}{2}\rho v^2)\boldsymbol{v}$. In differential form, neglecting heat sources q in the volume, this becomes

$$\partial_t\big(\rho\varepsilon + \tfrac{1}{2}\rho v^2\big) = \boldsymbol{\nabla}\cdot\big[\boldsymbol{v}\cdot\boldsymbol{\tau} + k_\mathrm{th}\boldsymbol{\nabla}T - p\,\boldsymbol{v} - \rho(\varepsilon + \tfrac{1}{2}v^2)\boldsymbol{v}\big], \tag{2.4c}$$

where we have introduced the thermal conductivity k_th.

2.2 First-order equations

Before the presence of any acoustic wave the zeroth-order state of the fluid is considered quiescent, homogeneous, and isotropic. Applying standard perturbation theory we write all fields on the form $f = f_0 + f_1$ with the exception of the velocity, for which $\boldsymbol{v} = \boldsymbol{v}_1$ since $\boldsymbol{v}_0 = \mathbf{0}$. Consequently, all terms involving only zeroth-order terms drop out of the governing differential equations, while the first-order mass, momentum, and energy equations obtained directly from Eq. (2.4) are

$$\partial_t\rho_1 = -\rho_0\boldsymbol{\nabla}\cdot\boldsymbol{v}_1, \tag{2.5a}$$

$$\rho_0\partial_t\boldsymbol{v}_1 = \boldsymbol{\nabla}\cdot\big[\boldsymbol{\tau}_1 - p_1\mathbf{I}\big], \tag{2.5b}$$

$$\rho_0\partial_t\varepsilon_1 + \varepsilon_0\partial_t\rho_1 = k_\mathrm{th}\nabla^2 T_1 - p_0\boldsymbol{\nabla}\cdot\boldsymbol{v}_1 - \varepsilon_0\rho_0\boldsymbol{\nabla}\cdot\boldsymbol{v}_1. \tag{2.5c}$$

In the energy equation, Eq. (2.5c), the two terms containing ε_0 cancel out due to the continuity equation, Eq. (2.5a), and the term $\rho_0 \partial_t \varepsilon_1$ is rewritten using the first law of thermodynamics, Eq. (2.1), which gives

$$\rho_0 T_0 \partial_t s_1 + \frac{p_0}{\rho_0} \, \partial_t \rho_1 = k_{\text{th}} \nabla^2 T_1 - p_0 \boldsymbol{\nabla} \cdot \boldsymbol{v}_1. \tag{2.6}$$

The two terms containing p_0 cancel out due to the continuity equation, Eq. (2.5a). Making use of the explicit expression for the first-order viscous stress tensor obtained from Eq. (2.3a) the resulting first-order mass, momentum, and energy equations are written on the form

$$\partial_t \rho_1 = -\rho_0 \boldsymbol{\nabla} \cdot \boldsymbol{v}_1, \tag{2.7a}$$

$$\rho_0 \partial_t \boldsymbol{v}_1 = -\boldsymbol{\nabla} p_1 + \eta_0 \nabla^2 \boldsymbol{v}_1 + \beta \eta_0 \boldsymbol{\nabla} \left(\boldsymbol{\nabla} \cdot \boldsymbol{v}_1 \right), \tag{2.7b}$$

$$\rho_0 T_0 \partial_t s_1 = k_{\text{th}} \nabla^2 T_1, \tag{2.7c}$$

Using these three first-order equations together with the thermodynamic equations of state $\rho = \rho(p, T)$ and $s = s(p, T)$, we will proceed to express everything in terms of acoustic velocity potentials. With this goal in mind we rewrite the momentum equation Eq. (2.7b) using the identity

$$\nabla^2 \boldsymbol{A} \equiv \boldsymbol{\nabla}(\boldsymbol{\nabla} \cdot \boldsymbol{A}) - \boldsymbol{\nabla} \times \boldsymbol{\nabla} \times \boldsymbol{A}, \tag{2.8}$$

and moreover differentiate once with respect to time, the resulting equation being,

$$\rho_0 \partial_t^2 \boldsymbol{v}_1 = -\partial_t \boldsymbol{\nabla} p_1 + (1 + \beta) \eta_0 \partial_t \boldsymbol{\nabla} (\boldsymbol{\nabla} \cdot \boldsymbol{v}_1) - \eta_0 \partial_t \boldsymbol{\nabla} \times \boldsymbol{\nabla} \times \boldsymbol{v}_1. \tag{2.9}$$

Let us now consider the thermodynamic equations of state $\rho(p, T)$ and $s(p, T)$. We are working within the local equilibrium hypothesis assuming applicability of classical irreversible thermodynamics. Small changes in the state functions due to pressure or temperature variation must happen according to the differentials

$$\mathrm{d}\rho = \left(\frac{\partial \rho}{\partial p} \right)_T \mathrm{d}p + \left(\frac{\partial \rho}{\partial T} \right)_p \mathrm{d}T, \tag{2.10a}$$

$$\mathrm{d}s = \left(\frac{\partial s}{\partial p} \right)_T \mathrm{d}p + \left(\frac{\partial s}{\partial T} \right)_p \mathrm{d}T, \tag{2.10b}$$

which may be linearized so that the partial derivatives of ρ and s refer to the unperturbed state of the fluid. The linearized partial derivatives are consequently described by defining the isothermal compressibility κ_T, the isobaric thermal expansion coefficient α_p, and the specific heat capacity at constant pressure C_p,

$$\kappa_T = \frac{1}{\rho} \left(\frac{\partial \rho}{\partial p} \right)_T, \tag{2.11a}$$

$$\alpha_p = -\frac{1}{\rho} \left(\frac{\partial \rho}{\partial T} \right)_p, \tag{2.11b}$$

$$C_p = T \left(\frac{\partial s}{\partial T} \right)_p. \tag{2.11c}$$

Moreover, $(\partial s/\partial p)_T$ may be expressed in terms of the isobaric thermal expansion coefficient by using Eq. (2.2) to derive the following Maxwell relation,

$$\left(\frac{\partial s}{\partial p}\right)_T = -\frac{\partial^2 g}{\partial p \partial T} = -\left(\frac{\partial(\frac{1}{\rho})}{\partial T}\right)_p = -\frac{1}{\rho}\,\alpha_p. \tag{2.12}$$

Then the linearized thermodynamic variation of Eq. (2.10) may be written as

$$\rho_1 = \rho_0\,\kappa_T\,p_1 - \rho_0\,\alpha_p\,T_1, \tag{2.13a}$$

$$s_1 = \frac{C_p}{T_0}\,T_1 - \frac{\alpha_p}{\rho_0}\,p_1. \tag{2.13b}$$

We further introduce the isentropic compressibility κ_s and the specific heat capacity at constant volume C_V,

$$\kappa_s = \frac{1}{\rho}\left(\frac{\partial \rho}{\partial p}\right)_s, \tag{2.14a}$$

$$C_V = T\left(\frac{\partial s}{\partial T}\right)_V. \tag{2.14b}$$

Then the following two identities, proven in Appendix A, hold true

$$\kappa_T = \gamma\kappa_s, \tag{2.15a}$$

$$\gamma = \frac{C_p}{C_V} = 1 + \frac{\alpha_p^2 T_0}{\rho_0 C_p \kappa_s}. \tag{2.15b}$$

To bring these parameters into the context of acoustics let us further define the isentropic speed of sound c. It is given from the isentropic compressibility as

$$c^2 = \left(\frac{\partial p}{\partial \rho}\right)_s = \frac{1}{\kappa_s \rho_0}, \tag{2.16}$$

and consequently $\kappa_s = 1/\rho_0 c^2$. The process of compression by acoustic wave propagation in a fluid is nearly adiabatic at frequencies in the MHz range with waves traveling at the isentropic speed of sound, which will be evident when deriving the wave equation.

Utilizing the thermodynamic identities of Eq. (2.13) with the above results and making use of the first-order continuity equation Eq. (2.7a) to eliminate the first-order density field ρ_1, one may derive the following expressions

$$\partial_t \boldsymbol{\nabla} p_1 = \frac{\rho_0 c^2}{\gamma}\left[\alpha_p \partial_t \boldsymbol{\nabla} T_1 - \boldsymbol{\nabla}(\boldsymbol{\nabla}\cdot\boldsymbol{v}_1)\right], \tag{2.17a}$$

$$\partial_t s_1 = \frac{C_p}{\gamma T_0}\partial_t T_1 - \frac{\alpha_p c^2}{\gamma}\boldsymbol{\nabla}\cdot\boldsymbol{v}_1, \tag{2.17b}$$

Substituting these expressions into the time-differentiated first-order momentum equation Eq. (2.9) and the first-order heat equation Eq. (2.7c) one finds

$$\partial_t^2 \boldsymbol{v}_1 - \frac{c^2}{\gamma}\boldsymbol{\nabla}(\boldsymbol{\nabla}\cdot\boldsymbol{v}_1) - (1+\beta)\nu_0\partial_t\boldsymbol{\nabla}(\boldsymbol{\nabla}\cdot\boldsymbol{v}_1) + \nu_0\partial_t\boldsymbol{\nabla}\times\boldsymbol{\nabla}\times\boldsymbol{v}_1 = -\frac{\alpha_p c^2}{\gamma}\partial_t\boldsymbol{\nabla}T_1, \quad (2.18a)$$

$$\gamma D_{\mathrm{th}}\nabla^2 T_1 - \partial_t T_1 = \frac{\gamma-1}{\alpha_p}\boldsymbol{\nabla}\cdot\boldsymbol{v}_1, \quad (2.18b)$$

Here we have introduced the momentum diffusion constant $\nu_0 = \eta_0/\rho_0$ also known as the kinematic viscosity, and the thermal diffusion constant $D_{\mathrm{th}} = k_{\mathrm{th}}/\rho_0 C_p$.

In the following development and throughout this thesis we will assume periodic time-harmonic actuation inherited by all first-order acoustic fields. Consequently we will work with the first-order fields in frequency domain. Using complex notation we write for any first-order field $A_1(\boldsymbol{r},t)$,

$$A_1(\boldsymbol{r},t) = A_1(\boldsymbol{r})\mathrm{e}^{-\mathrm{i}\omega t}, \quad (2.19)$$

which allows the substitution $\partial_t \rightarrow (-\mathrm{i}\omega)$ and thus a simple transition from time to frequency domain. The real physical fields are obtained as the real part of the complex fields.

Assuming time-harmonic fields Eq. (2.18) becomes

$$\omega^2\boldsymbol{v}_1 + \frac{c^2}{\gamma}\left(1-\mathrm{i}\gamma\Gamma_{\mathrm{s}}\right)\boldsymbol{\nabla}(\boldsymbol{\nabla}\cdot\boldsymbol{v}_1) + \mathrm{i}\omega\nu_0\boldsymbol{\nabla}\times\boldsymbol{\nabla}\times\boldsymbol{v}_1 = -\frac{\mathrm{i}\omega c^2\alpha_p}{\gamma}\boldsymbol{\nabla}T_1, \quad (2.20a)$$

$$\gamma D_{\mathrm{th}}\nabla^2 T_1 + \mathrm{i}\omega T_1 = \frac{\gamma-1}{\alpha_p}\boldsymbol{\nabla}\cdot\boldsymbol{v}_1. \quad (2.20b)$$

Here we have introduced the dimensionless bulk damping factor Γ_{s} accounting for viscous dissipation. Let us for future convenience also introduce the thermal damping factor Γ_{t} accounting for dissipation due to heat conduction. These two factors are given as

$$\Gamma_{\mathrm{s}} = \frac{(1+\beta)\nu_0\omega}{c^2}, \text{ and } \Gamma_{\mathrm{t}} = \frac{D_{\mathrm{th}}\omega}{c^2}. \quad (2.21)$$

To simplify the interpretation of the wave propagation we will now introduce the velocity potentials and set up the wave theory using these.

2.3 Velocity potentials

Any vector field may be decomposed into a sum of a longitudinal component described by the gradient of a scalar potential Φ and a transverse component described as the rotation of a vector potential $\boldsymbol{\Psi}$. Such a decomposition is known as a Helmholtz decomposition. We write

$$\boldsymbol{v}_1 = -\boldsymbol{\nabla}\Phi + \boldsymbol{\nabla}\times\boldsymbol{\Psi}, \text{ with } \boldsymbol{\nabla}\cdot\boldsymbol{\Psi} = 0. \quad (2.22)$$

Eq. (2.20b) then becomes

$$\gamma D_{\mathrm{th}} \nabla^2 T_1 + \mathrm{i}\omega T_1 + \frac{\gamma - 1}{\alpha_p} \nabla^2 \Phi = 0, \tag{2.23}$$

which shows that the temperature T_1 is a function only of the scalar potential Φ. Inserting the Helmholtz decomposition in Eq. (2.20a) leads to the following equation

$$\boldsymbol{\nabla} \left[\omega^2 \Phi + \frac{c^2}{\gamma} \left(1 - \mathrm{i}\gamma\Gamma_{\mathrm{s}}\right) \nabla^2 \Phi - \frac{\mathrm{i}\omega c^2 \alpha_p}{\gamma} T_1 \right] = \boldsymbol{\nabla} \times \left[\omega^2 \boldsymbol{\Psi} - \mathrm{i}\omega\nu_0 \nabla^2 \boldsymbol{\Psi} \right], \tag{2.24}$$

where we have used that $\boldsymbol{\nabla} \cdot \boldsymbol{\Psi} = 0$. In general both sides must vanish separately, and we will search for solutions of this kind. This leads to an equation for the vector potential $\boldsymbol{\Psi}$,

$$\nabla^2 \boldsymbol{\Psi} + k_{\mathrm{s}}^2 \boldsymbol{\Psi} = \mathbf{0}, \text{ with } k_{\mathrm{s}}^2 = \mathrm{i}\frac{\omega}{\nu_0}, \tag{2.25}$$

and an equation for the temperature field T_1 expressed in terms of the scalar potential Φ

$$T_1 = -\frac{\mathrm{i}\omega\gamma}{\alpha_p c^2} \Phi - \frac{\mathrm{i}}{\alpha_p \omega} (1 - \mathrm{i}\gamma\Gamma_{\mathrm{s}}) \nabla^2 \Phi. \tag{2.26}$$

Substituting this expression for T_1 into Eq. (2.23) we eliminate the temperature field and obtain an equation for the scalar potential Φ,

$$\nabla^2 \nabla^2 \Phi + \mathrm{i} \frac{1 - \mathrm{i}\Gamma_{\mathrm{s}} - \mathrm{i}\gamma\Gamma_{\mathrm{t}}}{(1 - \mathrm{i}\gamma\Gamma_{\mathrm{s}})\Gamma_{\mathrm{t}}} \left(\frac{\omega}{c}\right)^2 \nabla^2 \Phi + \mathrm{i} \frac{1}{(1 - \mathrm{i}\gamma\Gamma_{\mathrm{s}})\Gamma_{\mathrm{t}}} \left(\frac{\omega}{c}\right)^4 \Phi = 0. \tag{2.27}$$

The standard way to solve this bi-harmonic equation is to factorize it using that the equation

$$\nabla^2 \nabla^2 \Phi + (k_{\mathrm{c}}^2 + k_{\mathrm{t}}^2) \nabla^2 \Phi + k_{\mathrm{c}}^2 k_{\mathrm{t}}^2 \Phi = 0, \tag{2.28}$$

is equivalent to

$$(\nabla^2 + k_{\mathrm{c}}^2)(\nabla^2 + k_{\mathrm{t}}^2) \Phi = 0, \tag{2.29}$$

and then solve the two resulting harmonic equations. The wavenumbers k_{c} and k_{t} are thus obtained from solving a quadratic equation. Introducing the wavenumber of the undamped system $k_0 = \omega/c$ the result is

$$k_{\mathrm{c}}^2 = 2k_0^2 \left[A + B\right]^{-1}, \tag{2.30a}$$

$$k_{\mathrm{t}}^2 = 2k_0^2 \left[A - B\right]^{-1}, \tag{2.30b}$$

with

$$A = 1 - \mathrm{i}(\Gamma_{\mathrm{s}} + \gamma\Gamma_{\mathrm{t}}), \tag{2.30c}$$

$$B = \left[1 - 2\mathrm{i}\Gamma_{\mathrm{s}} - 2\mathrm{i}(\gamma - 2)\Gamma_{\mathrm{t}} - \left(\Gamma_{\mathrm{s}} - \gamma\Gamma_{\mathrm{t}}\right)^2\right]^{1/2}. \tag{2.30d}$$

The scalar potential Φ describes longitudinal waves. In the next section we investigate the derived wave equations. We find that k_c is the wavenumber of a compressional propagating mode, while k_t is the wavenumber of a highly damped thermal wave corresponding to thermal diffusion. A transverse wave is described by the shear wavenumber k_s of the vector potential $\boldsymbol{\Psi}$ and like the thermal wave it is heavily damped and corresponds to diffusion of momentum through viscous shear stress.

2.4 Wave equations and modes

The general solution of Eq. (2.29) is given by

$$\Phi = \phi_\mathrm{c} + \phi_\mathrm{t}, \tag{2.31}$$

where the potential ϕ_c describes a compressional propagating mode, while ϕ_t describes a thermal mode. The full first-order problem may consequently be written as the two scalar wave equations for the scalar potentials ϕ_c and ϕ_t, together with the vector wave equation for the vector potential $\boldsymbol{\Psi}$,

$$\nabla^2\phi_\mathrm{c} + k_\mathrm{c}^2\phi_\mathrm{c} = 0, \tag{2.32a}$$

$$\nabla^2\phi_\mathrm{t} + k_\mathrm{t}^2\phi_\mathrm{t} = 0, \tag{2.32b}$$

$$\nabla^2\boldsymbol{\Psi} + k_\mathrm{s}^2\boldsymbol{\Psi} = \mathbf{0}. \tag{2.32c}$$

The above three equations describe the longitudinal propagational mode, the longitudinal thermal mode, and the transverse shear mode, with the respective wavenumbers k_c, k_t, and k_s given in Eq. (2.30) and Eq. (2.25).

For frequencies in the MHz range $\Gamma_\mathrm{s} \sim \Gamma_\mathrm{t} \sim 10^{-6} \ll 1$ allowing an expansion of the expressions for k_c and k_t in Eq. (2.30). To first order in Γ_s and Γ_t one finds

$$k_\mathrm{c} \simeq \frac{\omega}{c}\left[1 + \frac{\mathrm{i}}{2}\left[\Gamma_\mathrm{s} + (\gamma-1)\Gamma_\mathrm{t}\right]\right], \tag{2.33a}$$

$$k_\mathrm{t} \simeq \frac{(1+\mathrm{i})}{\delta_\mathrm{t}}\left[1 + \frac{\mathrm{i}}{2}(\gamma-1)(\Gamma_\mathrm{s} - \Gamma_\mathrm{t})\right], \tag{2.33b}$$

$$k_\mathrm{s} = \frac{(1+\mathrm{i})}{\delta_\mathrm{s}}, \tag{2.33c}$$

where we have introduced the thermal diffusion length δ_t, as well as the momentum diffusion length δ_s. Heat and momentum diffuses from boundaries, such that δ_t and δ_s are measures for the characteristic thermal and viscous boundary layer thicknesses, respectively. They are defined as

$$\delta_\mathrm{s} = \sqrt{\frac{2\nu_0}{\omega}}, \text{ and } \delta_\mathrm{t} = \sqrt{\frac{2D_\mathrm{th}}{\omega}}. \tag{2.34a}$$

For water at 2 MHz, $\delta_\mathrm{s} \simeq 0.4$ µm and $\delta_\mathrm{t} \simeq 0.2$ µm. Consequently the length scales of the thermal and viscous boundary layer thicknesses are the same order of magnitude and

in the MHz range much smaller than the acoustic wavelength, which for water at room temperature and 2 MHz frequency is $\lambda \simeq 760$ μm.

With these numbers in mind we see that the compressional wavenumber k_c does indeed describe a propagating wave with real part of the wavenumber equal to $k_0 = \omega/c$. The imaginary part of k_c is much smaller than the real part, thus introducing a slight damping which becomes important only at very large distances compared to the wavelength.

Clearly this is not the case for the thermal and the shear modes where the real and the imaginary parts of the wavenumbers are almost equal. These waves are damped over the small distances of the respective diffusion lengths. Indeed, these two modes are best described as diffusive, responsible for heat and momentum diffusion from boundaries, but negligible outside the thin boundary layers.

We note that the small dimensionless damping factors Γ_s and Γ_t are related to the diffusion lengths δ_s and δ_t through the wavenumber. From Eq. (2.21) we obtain

$$\Gamma_\mathrm{s} = \frac{(1+\beta)}{2} k_0^2 \delta_\mathrm{s}^2, \text{ and } \Gamma_\mathrm{t} = \frac{1}{2} k_0^2 \delta_\mathrm{t}^2. \tag{2.35}$$

This is important because $k_0\delta_\mathrm{s}$ and $k_0\delta_\mathrm{t}$ are small parameters of the system, typically the same order of magnitude. For water at MHz frequencies one finds $k_0\delta_\mathrm{s} \sim 10^{-3}$. For most applications of the theory we will go only to first order in $k_0\delta_\mathrm{s}$ and $k_0\delta_\mathrm{t}$, and the above shows that Γ_s and Γ_t are of order $(k_0\delta_\mathrm{s})^2$ and $(k_0\delta_\mathrm{t})^2$, respectively. Considering the relative magnitude of the wavenumbers we note that

$$\Gamma_\mathrm{t} \sim (k_0\delta_\mathrm{t})^2 \sim (k_\mathrm{c}/k_\mathrm{t})^2 \ll 1, \tag{2.36a}$$

$$\Gamma_\mathrm{s} \sim (k_0\delta_\mathrm{s})^2 \sim (k_\mathrm{c}/k_\mathrm{s})^2 \ll 1, \tag{2.36b}$$

which will be used in the next section.

2.5 Acoustic fields from potentials

Having expressed the acoustic field theory in terms of velocity potentials we will need to find expressions for the acoustic fields in terms of the potentials, for example in order to impose certain boundary conditions on the fields.

In this section we will express the acoustic fields of velocity $\boldsymbol{v}_1$, pressure p_1, and temperature T_1 in terms of the potentials ϕ_c, ϕ_t, and $\boldsymbol{\Psi}$. We find that $\boldsymbol{\Psi}$ does not couple to neither pressure nor temperature. This is to be expected because both pressure and temperature are longitudinal wave phenomena while $\boldsymbol{\Psi}$ describes transverse waves. With hindsight, the acoustic fields are written as

$$p_1 = q_\mathrm{c}\phi_\mathrm{c} + q_\mathrm{t}\phi_\mathrm{t}, \tag{2.37a}$$

$$T_1 = b_\mathrm{c}\phi_\mathrm{c} + b_\mathrm{t}\phi_\mathrm{t}, \tag{2.37b}$$

$$\boldsymbol{v}_1 = -\boldsymbol{\nabla}(\phi_\mathrm{c} + \phi_\mathrm{t}) + \boldsymbol{\nabla} \times \boldsymbol{\Psi}. \tag{2.37c}$$

The constants q_c, q_t, b_c, and b_t will be determined in this section, and the velocity field follows trivially from the Helmholtz decomposition in Eq. (2.22). In the calculation of the constants q_c, q_t, b_c, and b_t we will neglect terms of order Γ_s and Γ_t relative to 1.

Consider first the pressure. To determine p_1 in terms of the potentials we insert the Helmholtz decomposition Eq. (2.22) into the first-order momentum equation Eq. (2.7b). One obtains

$$\boldsymbol{\nabla} p_1 = -\mathrm{i}\omega\rho_0 \boldsymbol{\nabla}\Phi - (1+\beta)\eta_0 \boldsymbol{\nabla}(\nabla^2\Phi) + \boldsymbol{\nabla} \times \left[\eta_0 \nabla^2 \boldsymbol{\Psi} - \mathrm{i}\omega\rho_0 \boldsymbol{\Psi}\right]. \tag{2.38}$$

The bracket is zero from the vector wave equation Eq. (2.25). We may then cancel the gradient to obtain the following expression for p_1

$$p_1 = -\mathrm{i}\omega\rho_0\Phi - (1+\beta)\eta_0\nabla^2\Phi. \tag{2.39}$$

Using the wave equations of Eq. (2.32) together with the wavenumbers in Eq. (2.33), and neglecting terms of order Γ_s and Γ_t relative to 1 we find the constants q_c and q_t

$$q_\mathrm{c} = -\mathrm{i}\omega\rho_0, \tag{2.40a}$$

$$q_\mathrm{t} = -\mathrm{i}\omega\rho_0 \left(1 - (1+\beta)\frac{\nu_0}{D_\mathrm{th}}\right). \tag{2.40b}$$

Consider now the temperature field. T_1 was given in terms of Φ in Eq. (2.26). Using this equation with the wave equations Eq. (2.32) and the wavenumbers Eq. (2.33) and neglecting Γ_s and Γ_t relative to 1, which from Eq. (2.36) also implies neglecting $(k_\mathrm{c}/k_\mathrm{t})^2 \ll 1$, we find the constants b_c and b_t

$$b_\mathrm{c} = -\frac{\mathrm{i}\omega(\gamma-1)}{\alpha_p c^2}, \tag{2.41a}$$

$$b_\mathrm{t} = -\frac{1}{\alpha_p D_\mathrm{th}}. \tag{2.41b}$$

This concludes the section. We now have expressions for the velocity field $\boldsymbol{v}_1$, the pressure field p_1, and the temperature field T_1 in terms of the velocity potentials ϕ_c, ϕ_t, and $\boldsymbol{\Psi}$, and we have found that the vector potential $\boldsymbol{\Psi}$ only couples to the velocity field describing transverse diffusive shear waves.

2.6 Parameter values and microsystems of interest

We end this chapter on the general thermoviscous theory of acoustics with a few remarks connecting the equations to the physical systems that will be considered in this thesis, which are microsystems relevant to lab-on-a-chip acoustophoresis applications. In order to achieve acoustic energy densities high enough to manipulate particles, a resonant cavity is most commonly used and the actuation is achieved with a piezo-electric crystal usually operating at MHz frequency [27, 28]. For most bio-medical lab-on-a-chip applications the fluid medium is water, for which the speed of sound at 25° C is 1497 m/s, as given in Table 2.1. At an actuation frequency of $f = 2$ MHz the fundamental resonance at one half wavelength is thus achieved for a cavity of length $\lambda/2 = c/2f = 374\,\mu\mathrm{m}$. For such a system

Table 2.1: Thermodynamic properties of water (wa) at 25° C [29], glycerol (gl) at 20° C [30], and air at 300 K [29], all taken at a pressure of 1 bar. The Prandtl number gives the ratio of momentum diffusion to thermal diffusion, $\mathrm{Pr} = \nu_0/D_{\mathrm{th}}$.

Parameter	Symbol	Value (wa)	Value (air)	Value (gl)	Unit
Density	ρ_0	997.1	1.161	1261	kg m^{-3}
Speed of sound	c	1497	347.4	1923	m s^{-1}
Viscosity	η_0	0.8900	0.1854	1410	mPa s
Viscosity ratio [31]	β	3.0	-	-	1
Specific heat capacity	C_p	4181	1007	2380	J kg^{-1} K^{-1}
Heat capacity ratio	γ	1.011	1.402	1.172	1
Thermal conductivity	k_{th}	0.607	2.64×10^{-2}	0.285	W m^{-1} K^{-1}
Thermal diffusivity	D_{th}	1.46×10^{-7}	2.26×10^{-5}	9.50×10^{-8}	m^2 s^{-1}
Thermal expansion coeff.	α_p	2.57×10^{-4}	3.35×10^{-3}	6.15×10^{-4}	K^{-1}
Compressibility	κ_s	4.48×10^{-10}	7.14×10^{-6}	2.14×10^{-10}	Pa^{-1}
Prandtl number	Pr	6.1	0.71	1.2×10^{4}	1

the viscous and thermal boundary layer thicknesses are 0.377 μm and 0.152 μm, respectively, as given in Table 2.2, and thus much smaller than the system size. Consequently, a small parameter of the system is $k_0\delta_{\mathrm{s}}$ or $k_0\delta_{\mathrm{t}}$, with $k_0 = \omega/c$. For the system under consideration $k_0\delta_{\mathrm{s}} = 3.17 \times 10^{-3}$ given in Table 2.2. Note that $\Gamma_{\mathrm{s}} \sim (k_0\delta_{\mathrm{s}})^2 \sim 10^{-5} \ll 1$, which means that the viscous bulk damping is negligible in such a microchannel system.

We will find in Chapter 4 that all significant dissipation takes place in the narrow boundary layers where large gradients in velocity and temperature lead to dissipation of energy. The stresses in these narrow boundary layers moreover lead to the time-averaged second-order phenomenon of acoustic streaming. In general an accurate description of the boundary layers is needed in order to correctly describe the physics of acoustofluidics. With the mode-theory developed in this chapter we see that the highly damped thermal and shear modes will describe the boundary layers, and thus singular boundary layer theory, which is zeroth order in $k_0\delta_{\mathrm{s}}$, may be avoided. At high frequencies $k_0\delta_{\mathrm{s}}$ may become significant in water and even more in air or a highly viscous fluid such as glycerol. The thermodynamic parameters of these three fluids are given in Table 2.1 and Table 2.2 lists the boundary layer thicknesses and the value of $k_0\delta_{\mathrm{s}}$ for a selection of frequencies.

Another application of the theory for which a correct description of the boundary layers becomes important is the scattering of sound from particles leading to a time-averaged radiation force on particles in acoustic wave fields. When the boundary layer thicknesses become comparable to the particle size, which is true for lab-on-a-chip applications with micrometer-sized particles at MHz-frequency (Table 2.2), thermoviscous corrections to the radiation force may be significant as shown for the viscous boundary layer in Ref. [15]. In Chapter 5 we investigate the radiation force problem using the full potential theory of thermoviscous acoustics and find large corrections to the classical theories that are valid only in the large particle limit.

Table 2.2: Viscous and thermal boundary layer thicknesses and dimensionless parameter $k_0\delta_s$ with $k_0 = \omega/c$ for a selection of frequencies in water (wa) at 25° C, glycerol (gl) at 20° C, and air at 300 K, as calculated from the parameter values of Table 2.1.

Parameter	Frequency	Value (wa)	Value (air)	Value (gl)	Unit
δ_s	2 kHz	11.9	50.4	422	µm
	2 MHz	0.377	1.59	13.3	µm
	20 MHz	0.119	0.504	4.22	µm
δ_t	2 kHz	4.82	59.9	3.89	µm
	2 MHz	0.152	1.90	0.123	µm
	20 MHz	0.0482	0.599	0.0389	µm
$k_0\delta_s$	2 kHz	1.00×10^{-4}	1.82×10^{-3}	2.76×10^{-3}	1
	2 MHz	3.17×10^{-3}	5.77×10^{-2}	8.72×10^{-2}	1
	20 MHz	1.00×10^{-2}	0.182	0.276	1

Chapter 3

Acoustic waves in 2D

The formulation of thermoviscous acoustics presented in Chapter 2 provides a rigorous analysis of acoustic wave phenomena represented as a superposition of modes. We have discussed how the compressional mode is the only propagating wave, while the thermal and shear modes are heavily damped corresponding to diffusion of heat and momentum from boundaries. From this discussion it is evident that these two damped modes are important to satisfy given boundary conditions on the temperature field T_1 and the velocity field $\boldsymbol{v}_1$, such as those of a hard, heat-conducting wall. The thermal mode is responsible for the thermal boundary layer, while the shear mode is responsible for the viscous boundary layer.

This formulation of acoustic wave phenomena as a superposition of modes provides a framework for studying the acoustic fields in the driven parallel-plate system superior to the singular boundary layer theory known as Prandtl-Schlichting boundary layer theory [12, 16, 17]. This boundary layer theory approach has been employed throughout the literature in the study of acoustic streaming in the parallel-plate geometry starting with the seminal work of Lord Rayleigh [18], and followed by later studies most notably by Nyborg [19], Hamilton *et al.* [20, 21], and Rednikov and Sadhal [22]. In the study of thermoacoustic engines the driven parallel-plate system is highly relevant and once again boundary layer theories are applied in the major works of the field [10, 11, 21].

Boundary layer theory is founded on the constraint that $\delta_\mathrm{s} \ll \lambda$ which is used to neglect pressure gradients perpendicular to the wall, i.e., the first-order pressure is assumed to vary only parallel to the channel walls. Such a treatment is correct only to zeroth order in $k_0\delta_\mathrm{s}$, where $k_0 = 2\pi/\lambda$ is the wavenumber, and may lead to discontinuous velocity fields in the transition from the boundary layer to the bulk with the discontinuity of order $k_0\delta_\mathrm{s}$ [12, 23].

In this chapter we will provide a solution to the driven parallel-plate system correct to first order in $k_0\delta_\mathrm{s}$ following an approach that does not involve singular boundary layer theory, but instead utilizes the description of thermoviscous acoustics as a superposition of modes. The work was motivated by the numerical model of Muller *et al.* including thermal effects [24] as well as the ambition of resolving the problem of discontinuous field solutions in the classical isentropic theory. We note that the solution presented in this

chapter not only incorporates thermal effects, it also represents an improvement over the classical isentropic theory by going to first order in $k_0\delta_\mathrm{s}$ instead of zeroth order. We have chosen to take the theory to first order in $k_0\delta_\mathrm{s}$ because it provides closed form solutions for wavenumbers and fields, but the formalism developed may be applied to completely lift the requirement that $k_0\delta_\mathrm{s} \ll 1$.

The chapter is structured as follows. After presenting the coupled field equations and investigating solution modes we consider the acoustic fields near a planar wall and set up a formalism that facilitate a solution satisfying the boundary conditions of hard, heat-conducting walls. This formalism is then applied to solve for the acoustic fields in the driven parallel-plate system, leading to a dispersion equation relating horizontal and vertical wavenumbers k_y and k_z. We will give approximate expressions for the wavenumbers in a few important cases and then study the generic field solution on a non-dimensional form showing that the solution correctly describes not only acoustic fields but also the low frequency shear flow limit where boundary layers become comparable to the channel height.

3.1 Field equations and modes

The velocity potential formulation has been a rigorous and instructive way of deriving the wave equations and wavenumbers associated with the different modes and the formulation provides a strong framework for solving difficult problems in various coordinate systems, as will be demonstrated when calculating the acoustic radiation force on a small particle in Chapter 5. In this chapter on standing wave phenomena we will work with the pressure field p_1, the temperature field T_1, and the velocity field $\boldsymbol{v}_1$ instead of the potentials ϕ_c, ϕ_t, and $\boldsymbol{\Psi}$. We will describe the dynamics with coupled wave and diffusion equations for the pressure field p_1 and the temperature field T_1 following an approach by Morse and Ingard [32]. With this approach we will obtain the compressional, thermal, and shear modes in a way different from the velocity potential approach, which leads to an increased intuitive understanding of the physical wave phenomena, a better understanding of the connection to the isentropic theory, and in any case an easier solution technique for the problem of standing waves in two dimensions. We emphasize that the identification of modes and the superposition of these is the key to solving thermoviscous acoustics problems.

3.1.1 Coupled field equations

We repeat here the first-order momentum, continuity, and heat equation written in time-domain on the form

$$\rho_0\partial_t\boldsymbol{v}_1 = -\boldsymbol{\nabla}p_1 - \eta_0\boldsymbol{\nabla}\times\boldsymbol{\nabla}\times\boldsymbol{v}_1 + (1+\beta)\eta_0\boldsymbol{\nabla}\left(\boldsymbol{\nabla}\cdot\boldsymbol{v}_1\right), \tag{3.1a}$$

$$\partial_t\rho_1 = -\rho_0\boldsymbol{\nabla}\cdot\boldsymbol{v}_1, \tag{3.1b}$$

$$\rho_0 T_0\partial_t s_1 = k_\mathrm{th}\nabla^2 T_1. \tag{3.1c}$$

Let us moreover write the thermodynamic identities of Eq. (2.13) on the form

$$\rho_1 = \frac{\gamma}{c^2}\left[p_1 - \frac{\alpha_p}{\gamma\kappa_s}T_1\right], \tag{3.2a}$$

$$s_1 = \frac{C_p}{T_0}\left[T_1 - \frac{(\gamma-1)\kappa_s}{\alpha_p}p_1\right]. \tag{3.2b}$$

At this point, instead of introducing the longitudinal and transverse velocity potentials Φ and $\boldsymbol{\Psi}$ we make the decomposition by writing the velocity field as the sum of a rotationless longitudinal component $\boldsymbol{v}_l$ and a divergenceless transverse (shear) component $\boldsymbol{v}_\mathrm{s}$. Consequently, we write

$$\boldsymbol{v}_1 = \boldsymbol{v}_l + \boldsymbol{v}_\mathrm{s}, \quad \text{with} \quad \boldsymbol{\nabla}\times\boldsymbol{v}_l = \boldsymbol{0}, \quad \text{and} \quad \boldsymbol{\nabla}\cdot\boldsymbol{v}_\mathrm{s} = 0. \tag{3.3}$$

Looking for general solutions for which the gradient $\boldsymbol{\nabla}p_1$ cannot be described as a rotation, the first-order momentum equation Eq. (3.1b) separates into two equations, one for the longitudinal field and one for the transverse field,

$$\rho_0\partial_t\boldsymbol{v}_l = -\boldsymbol{\nabla}p_1 + (1+\beta)\,\eta_0\boldsymbol{\nabla}\left(\boldsymbol{\nabla}\cdot\boldsymbol{v}_l\right), \tag{3.4a}$$

$$\rho_0\partial_t\boldsymbol{v}_\mathrm{s} = -\eta_0\boldsymbol{\nabla}\times\boldsymbol{\nabla}\times\boldsymbol{v}_\mathrm{s}. \tag{3.4b}$$

Evidently the solution to the equation for the transverse velocity field $\boldsymbol{v}_\mathrm{s}$ describes the shear mode, while the equation for the longitudinal velocity field is coupled to the heat equation through the pressure and describes both the compressional and the thermal mode.

To derive the wave equation for the pressure p_1 we take the time-derivative of the continuity equation Eq. (3.1b) and substitute into it the divergence of the momentum equation for $\boldsymbol{v}_l$ Eq. (3.4a) which gives

$$\nabla^2 p_1 = \left[\partial_t^2 - \frac{(1+\beta)\eta_0}{\rho_0}\partial_t\nabla^2\right]\rho_1. \tag{3.5}$$

Substituting the identity for ρ_1 in Eq. (3.2a) we obtain the wave-equation for the pressure p_1,

$$\nabla^2 p_1 = \frac{\gamma}{c^2}\left[\partial_t^2 - \frac{(1+\beta)\eta_0}{\rho_0}\partial_t\nabla^2\right]\left(p_1 - \frac{\alpha_p}{\gamma\kappa_s}T_1\right). \tag{3.6}$$

To derive the diffusion equation for the temperature T_1 we take the heat equation Eq. (3.1c) and substitute the expression for s_1 given in Eq. (3.2b). The resulting equation is written on the form

$$D_\mathrm{th}\nabla^2 T_1 = \partial_t\left[T_1 - \frac{(\gamma-1)\kappa_s}{\alpha_p}p_1\right], \tag{3.7}$$

Finally we derive the equation for the longitudinal velocity $\boldsymbol{v}_l$ determined from the pressure p_1 and the temperature T_1. Substitute the divergence of $\boldsymbol{v}_l$ in the momentum equation

for $\boldsymbol{v}_l$, Eq. (3.4a), with the expression from the continuity equation Eq. (3.1b). Then use the thermodynamic identity Eq. (3.2a) to replace ρ_1. The final result is the equation

$$\rho_0 \partial_t \boldsymbol{v}_l = -\boldsymbol{\nabla} \left[p_1 + \frac{(1+\beta)\eta_0\gamma}{\rho_0 c^2} \partial_t \left(p_1 - \frac{\alpha_p}{\gamma\kappa_s} T_1 \right) \right]. \tag{3.8}$$

We have now established the field equations needed to solve the problem of wave propagation in a thermoviscous fluid. Before investigating possible solutions of these coupled field equations we will consider the two cases where the equations decouple, namely the isentropic limit and the isothermal limit.

Isentropic limit

The isentropic limit is obtained for the case of no heat conduction letting $k_{\text{th}}, D_{\text{th}} \to 0$. Having $D_{\text{th}} \to 0$ the right-hand side of Eq. (3.7) must also vanish indicating that

$$T_1 = \frac{(\gamma-1)\kappa_s}{\alpha_p} p_1 \quad \text{(isentropic theory)}, \tag{3.9}$$

and this identity reduces the wave equation Eq. (3.6) to

$$\partial_t^2 p_1 = c^2 \left[1 + \frac{(1+\beta)\eta_0}{\rho_0 c^2} \partial_t \right] \nabla^2 p_1 \quad \text{(isentropic theory)}. \tag{3.10}$$

This is the result of the isentropic analysis presented in Ref. [14]. In the isentropic analysis the temperature field is not accounted for as the thermodynamic equation of state follows from a general Taylor expansion of $p = p(\rho, s)$ with the entropy s kept constant giving $p_1 = c^2 \rho_1$ with $c^2 = (\partial p/\partial \rho)_s$ [14]. Isentropic pressure wave propagation is nevertheless accompanied by a temperature wave-field proportional to the pressure field as given in Eq. (3.9). This result was obtained by letting $k_{\text{th}}, D_{\text{th}} \to 0$ in the general theory, but note that it follows directly from the thermodynamic identity of Eq. (3.2b) by setting $s_1 = 0$, thus confirming the correspondence between zero heat conduction and isentropic wave propagation.

Isothermal limit

If instead we go to the other limit of infinite heat conductivity letting $k_{\text{th}}, D_{\text{th}} \to \infty$ then $T_1 = 0$ by definition, and we get the isothermal theory where the wave-equation Eq. (3.6) reduces to

$$\partial_t^2 p_1 = \frac{c^2}{\gamma} \left[1 + \frac{(1+\beta)\eta_0\gamma}{\rho_0 c^2} \partial_t \right] \nabla^2 p_1 \quad \text{(isothermal theory)}, \tag{3.11}$$

thus describing waves propagating with the isothermal wave speed $c/\sqrt{\gamma} = \sqrt{1/(\rho_0 \kappa_T)}$ as a result of isothermal compression.

The general thermoviscous case

Let us now investigate the regime between the isentropic limit and the isothermal limit where the pressure p_1 and the temperature T_1 are coupled. The equations are summarized in Eq. (3.12) and we see from these that pressure waves tend to propagate while heat diffuses. Consequently there are two modes of solution depending on which process is dominant. The first corresponds to nearly isentropic wave propagation. This is the compressional mode. For the second mode p_1 is small compared to $[\alpha_p/(\gamma\kappa_s)]T_1$ such that the equations describe the process of heat diffusion, and it may thus be identified as the thermal mode.

Let us summarize the coupled field equations relevant to the investigation of these two modes. In time-domain the equations are

$$\nabla^2 p_1 = \frac{\gamma}{c^2}\left[\partial_t^2 - \frac{(1+\beta)\eta_0}{\rho_0}\partial_t\nabla^2\right]\left(p_1 - \frac{\alpha_p}{\gamma\kappa_s}T_1\right). \tag{3.12a}$$

$$D_{\mathrm{th}}\nabla^2 T_1 = \partial_t\left[T_1 - \frac{(\gamma-1)\kappa_s}{\alpha_p}p_1\right], \tag{3.12b}$$

$$\rho_0\partial_t\boldsymbol{v}_l = -\boldsymbol{\nabla}\left[p_1 + \frac{(1+\beta)\eta_0\gamma}{\rho_0 c^2}\partial_t\left(p_1 - \frac{\alpha_p}{\gamma\kappa_s}T_1\right)\right]. \tag{3.12c}$$

Having established the governing equations in time-domain we will now switch to frequency domain and investigate how the equations decouple when describing the individual modes.

As customary we assume time-harmonic first-order fields according to Eq. (2.19). The modes and wavenumbers were derived, characterized, and explained quite generally using velocity potentials in Chapter 2. Here we will derive the wavenumbers in a simple but less rigorous way obtaining the same results. We will give explicit expressions for the pressure, temperature, and velocity fields resulting from each mode, which will prove valuable for the development of standing wave solutions. Proceeding, we consider harmonic first-order fields at a given frequency ω corresponding to the complex wavenumber k, which allows the substitutions

$$\nabla^2 \to (-k^2), \quad \text{and} \quad \partial_t \to (-\mathrm{i}\omega), \tag{3.13}$$

We will use this to decouple the equations in Eq. (3.12) thus describing the two modes of longitudinal wave propagation, namely the compressional and the thermal mode.

3.1.2 Compressional propagating mode

The compressional propagating mode travels at the isentropic speed of sound c with wavenumber k_{c} almost equal to ω/c. For this mode the wave-character of Eq. (3.12a) is the dominant one. Inserting $k_{\mathrm{c}}^2 \simeq (\omega/c)^2$ in Eq. (3.12b) gives T_{c} in terms of p_{c}. One finds

$$T_{\mathrm{c}} \simeq \frac{(\gamma-1)\kappa_s}{\alpha_p}\left(1 - \mathrm{i}\Gamma_{\mathrm{t}}\right)p_{\mathrm{c}}. \tag{3.14}$$

Inserting this expression for T_c into Eq. (3.12a) gives a correction to k_c^2 which we take to first order in Γ_s and Γ_t. Moreover, we insert T_c into Eq. (3.12c) to find $\boldsymbol{v}_\mathrm{c}$ in terms of the gradient of pressure. In the end the compressional mode is defined from the equations

$$\nabla^2 p_\mathrm{c} = -k_\mathrm{c}^2 p_\mathrm{c}, \quad k_\mathrm{c}^2 = \left(\frac{\omega}{c}\right)^2 \left[1 + \mathrm{i}\Gamma_\mathrm{s} + \mathrm{i}(\gamma-1)\Gamma_\mathrm{t}\right], \tag{3.15a}$$

$$T_\mathrm{c} = \frac{(\gamma-1)\kappa_s}{\alpha_p}\left(1 - \mathrm{i}\Gamma_\mathrm{t}\right) p_\mathrm{c}, \tag{3.15b}$$

$$\boldsymbol{v}_\mathrm{c} = \frac{1}{\mathrm{i}\omega\rho_0}\left(1 - \mathrm{i}\Gamma_\mathrm{s}\right) \boldsymbol{\nabla} p_\mathrm{c}. \tag{3.15c}$$

The wavenumber obtained this way is consistent with the potential theory wavenumber given in Eq. (2.33a). The fields of the compressional mode may likewise be obtained directly from the potential theory by considering only the components due to this mode setting $p_\mathrm{c} = q_\mathrm{c}\phi_\mathrm{c}$, $T_\mathrm{c} = b_\mathrm{c}\phi_\mathrm{c}$, and $\boldsymbol{v}_\mathrm{c} = -\boldsymbol{\nabla}\phi_\mathrm{c}$.

3.1.3 Thermal mode

For the thermal mode the diffusive character of Eq. (3.12b) is the dominant one and as a first approximation we neglect the pressure term in Eq. (3.12b), which gives the wavenumber

$$k_\mathrm{t}^2 \simeq \frac{\mathrm{i}\omega}{D_\mathrm{th}} = \frac{2\mathrm{i}}{\delta_\mathrm{t}^2}. \tag{3.16}$$

Eq. (3.12a) then gives an expression for p_t in terms of T_t, which when inserted in Eq. (3.12b) gives a correction to the wavenumber k_t^2. Inserting the expression for p_t into Eq. (3.12c) one obtains $\boldsymbol{v}_\mathrm{t}$ in terms of the gradient of temperature. Going to first order in Γ_s and Γ_t one finds that the thermal mode is defined from the following equations

$$\nabla^2 T_\mathrm{t} = -k_\mathrm{t}^2 T_\mathrm{t}, \quad k_\mathrm{t}^2 = \frac{2\mathrm{i}}{\delta_\mathrm{t}^2}\left[1 + \mathrm{i}(\gamma-1)(\Gamma_\mathrm{s} - \Gamma_\mathrm{t})\right], \tag{3.17a}$$

$$p_\mathrm{t} = \mathrm{i}\left(\Gamma_\mathrm{t} - \Gamma_\mathrm{s}\right)\frac{\alpha_p}{\kappa_s} T_\mathrm{t}, \tag{3.17b}$$

$$\boldsymbol{v}_\mathrm{t} = \frac{\alpha_p \Gamma_\mathrm{t}}{\omega\rho_0\kappa_s}\boldsymbol{\nabla} T_\mathrm{t}, \tag{3.17c}$$

consistent with the potential theory of Chapter 2 considering the fields due to the thermal mode only, setting $T_\mathrm{t} = b_\mathrm{t}\phi_\mathrm{t}$, $p_\mathrm{t} = q_\mathrm{t}\phi_\mathrm{t}$, and $\boldsymbol{v}_\mathrm{t} = -\boldsymbol{\nabla}\phi_\mathrm{t}$.

3.1.4 Shear mode

The shear mode describes the transverse velocity component $\boldsymbol{v}_\mathrm{s}$ satisfying Eq. (3.4b). The mode is defined from Eq. (3.4b) which in frequency-domain is written as

$$\nabla^2 \boldsymbol{v}_\mathrm{s} = -\,k_\mathrm{s}^2 \boldsymbol{v}_\mathrm{s}, \quad k_\mathrm{s}^2 = \frac{2\mathrm{i}}{\delta_\mathrm{s}^2}, \quad \text{with} \quad \boldsymbol{\nabla}\cdot\boldsymbol{v}_\mathrm{s} = 0. \tag{3.18}$$

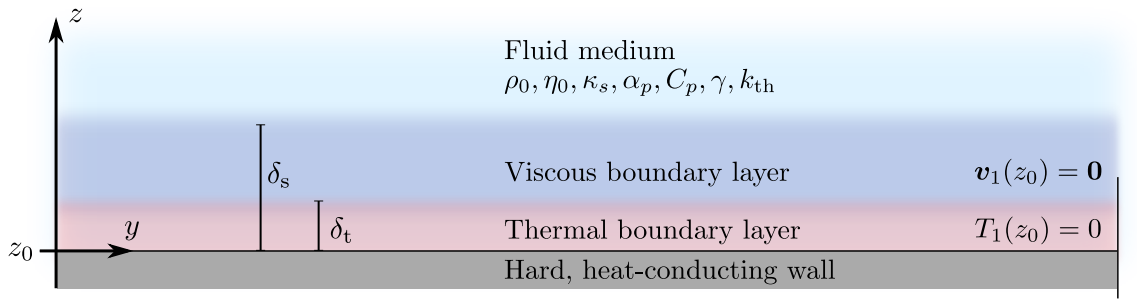

Figure 3.1: Section 3.2 considers the acoustic fields near a hard, heat-conducting planar wall. The boundary conditions of such a wall with a high heat conductivity compared to the fluid medium is the no-slip velocity condition $\boldsymbol{v}_1(z_0) = \mathbf{0}$ and constant temperature T_0 such that $T_1(z_0) = 0$ giving rise to viscous and thermal boundary layers of thickness δ_{s} and δ_{t}, respectively.

We have already discussed the nature of this overdamped transverse mode describing diffusion of momentum from boundaries on the characteristic length scale of the viscous boundary layer thickness δ_{s}. Only the shear mode has a transverse velocity component and it does not couple to pressure and temperature.

3.2 Acoustic fields near a planar wall

The formalism developed in the previous section concerning different solution modes is due to Morse and Ingard [32], who used the theory to obtain effective boundary conditions for the acoustic fields in the presence of a single planar wall. We will follow a similar approach but keep things more general in order to ensure applicability to the parallel-plate system.

We consider now a 2D system in the yz-plane with a wall in the xy-plane at $z = z_0$. We will assume that the wall is rigid and that it conducts heat much faster than the fluid and consequently we will enforce the following boundary conditions

$$T_1 = 0 \quad \text{for} \quad z = z_0, \tag{3.19a}$$

$$\boldsymbol{v}_1 = \mathbf{0} \quad \text{for} \quad z = z_0. \tag{3.19b}$$

As is evident from our previous discussion the compressional mode is the mode responsible for wave propagation in the bulk. The shear mode and the thermal mode are diffusive and will be important only near the boundary where they will be used to cancel the temperature and velocity components arising from the compressional mode such that the boundary conditions are satisfied. This gives rise to the growth of a thermal and a viscous boundary layer as illustrated in Fig. 3.1.

From this point on we will neglect $\Gamma_{\mathrm{s}} \sim (k_0\delta_{\mathrm{s}})^2$ and $\Gamma_{\mathrm{t}} \sim (k_0\delta_{\mathrm{t}})^2$ relative to 1 in accordance with our ambition of providing solutions correct to first order in $k_0\delta_{\mathrm{s}}$ and $k_0\delta_{\mathrm{t}}$.

Compressional mode

We use separation of variables to solve the equations for the compressional mode given in Eq. (3.15). Consequently, neglecting Γ_s and Γ_t relative to 1, we write

$$p_\mathrm{c} = Y(y)Z_\mathrm{c}(z), \quad k_\mathrm{c}^2 = \left(\frac{\omega}{c}\right)^2 \left[1 + \mathrm{i}\Gamma_\mathrm{s} + \mathrm{i}(\gamma-1)\Gamma_\mathrm{t}\right], \tag{3.20a}$$

$$\frac{\mathrm{d}^2 Y}{\mathrm{d}y^2} = -k_y^2 Y(y), \quad \frac{\mathrm{d}^2 Z_\mathrm{c}}{\mathrm{d}z^2} = -k_z^2 Z_\mathrm{c}(z), \quad k_\mathrm{c}^2 = k_y^2 + k_z^2, \tag{3.20b}$$

$$T_\mathrm{c}(y,z) = \frac{(\gamma-1)\kappa_s}{\alpha_p} Y(y)Z_\mathrm{c}(z), \tag{3.20c}$$

$$v_{\mathrm{c}y}(y,z) = \frac{1}{\mathrm{i}\omega\rho_0}\frac{\mathrm{d}Y}{\mathrm{d}y} Z_\mathrm{c}(z), \tag{3.20d}$$

$$v_{\mathrm{c}z}(y,z) = \frac{1}{\mathrm{i}\omega\rho_0} Y(y)\frac{\mathrm{d}Z_\mathrm{c}}{\mathrm{d}z}. \tag{3.20e}$$

Though negligible we have kept the damping factors Γ_s and Γ_t in the wavenumber k_c due to their physical significance that should not be forgotten. The compressional propagating mode will in general have a finite temperature and velocity at the wall. To satisfy the boundary conditions we first fix the temperature by adding a thermal mode.

Thermal mode

The temperature at the boundary at $z = z_0$ due to the compressional mode is $T_\mathrm{c}(y, z_0)$ and it must be exactly canceled by the thermal mode in order to fulfill the boundary condition that $T_1(y, z_0) = 0$. Consequently we write the temperature of the thermal mode on the form

$$T_\mathrm{t}(y,z) = -\frac{(\gamma-1)\kappa_s}{\alpha_p} Z_\mathrm{c}(z_0)Y(y)F_\mathrm{t}(z), \tag{3.21}$$

where $F_\mathrm{t}(z)$ must be determined subject to the boundary condition that

$$F_\mathrm{t}(z_0) = 1. \tag{3.22}$$

Inserting the above ansatz for $T_\mathrm{t}(y, z)$ into the equations for the thermal mode in Eq. (3.17) yields

$$\frac{\mathrm{d}^2 F_\mathrm{t}}{\mathrm{d}z^2} = \left(k_y^2 - \frac{2\mathrm{i}}{\delta_\mathrm{t}^2}\right) F_\mathrm{t}(z), \quad F_\mathrm{t}(z_0) = 1, \tag{3.23a}$$

$$T_\mathrm{t}(y,z) = -\frac{(\gamma-1)\kappa_s}{\alpha_p} Z_\mathrm{c}(z_0)Y(y)F_\mathrm{t}(z), \tag{3.23b}$$

$$p_\mathrm{t}(y,z) = -\mathrm{i}\,(\gamma-1)\,(\Gamma_\mathrm{t} - \Gamma_\mathrm{s})\, Z_\mathrm{c}(z_0)Y(y)F_\mathrm{t}(z), \tag{3.23c}$$

$$v_{\mathrm{t}y}(y,z) = -\,(\gamma-1)\,\frac{\Gamma_\mathrm{t}}{\omega\rho_0} Z_\mathrm{c}(z_0)\frac{\mathrm{d}Y}{\mathrm{d}y} F_\mathrm{t}(z), \tag{3.23d}$$

$$v_{\mathrm{t}z}(y,z) = -\,(\gamma-1)\,\frac{\Gamma_\mathrm{t}}{\omega\rho_0} Z_\mathrm{c}(z_0)Y(y)\frac{\mathrm{d}F_\mathrm{t}}{\mathrm{d}z}. \tag{3.23e}$$

The sum of the compressional mode and the thermal mode then fixes the temperature at the boundary in $z = z_0$, namely it assures that $T_1(y, z_0) = 0$. There is still a component of velocity at the boundary, however, which must be fixed by adding a shear mode that does not couple to the temperature.

We note that p_t and $v_{\mathrm{t}y}$ are suppressed by a factor of Γ_s or Γ_t relative to p_c and v_{cy}, respectively, and may be neglected to first order of approximation. Consequently, we may neglect the contributions from the thermal mode to the pressure and to the y-component of velocity. However, we cannot neglect the z-component of velocity due to the thermal mode because the gradient $\mathrm{d}F_\mathrm{t}/\mathrm{d}z$ is large and partly cancels the prefactor Γ_t.

Shear mode

We want to use the shear mode to cancel the y-component of velocity due to the compressional mode v_{cy} in order to fulfill the no-slip boundary condition at the wall to first order in $k_0\delta_\mathrm{s}$ and $k_0\delta_\mathrm{t}$, which means that we must require $v_{\mathrm{s}y}(y, z_0) = -v_{cy}(y, z_0)$. Consequently we write $v_{\mathrm{s}y}$ on the form

$$v_{\mathrm{s}y}(y, z) = -\frac{1}{\mathrm{i}\omega\rho_0} Z_\mathrm{c}(z_0) \frac{\mathrm{d}Y}{\mathrm{d}y} F_\mathrm{s}(z), \tag{3.24}$$

where $F_\mathrm{s}(z)$ is to be determined subject to the boundary condition

$$F_\mathrm{s}(z_0) = 1. \tag{3.25}$$

Moreover we must ensure that $\boldsymbol{v}_\mathrm{s}$ is divergence-less, which gives an expression for $v_{\mathrm{s}z}$,

$$\begin{aligned} \boldsymbol{\nabla}\cdot\boldsymbol{v}_\mathrm{s} = 0 \quad &\Rightarrow \\ v_{\mathrm{s}z}(y, z) = -\frac{k_y^2}{\mathrm{i}\omega\rho_0} Z_\mathrm{c}(z_0) Y(y) &\int F_\mathrm{s}(z)\mathrm{d}z. \end{aligned} \tag{3.26}$$

To find an equation for $F_\mathrm{s}(z)$ we insert into the equation for the shear mode Eq. (3.18). Both vector-components of the equation give the same equation for $F_\mathrm{s}(z)$ as it should. We give the resulting equation below together with the components of velocity that the shear mode adds

$$\frac{\mathrm{d}^2 F_\mathrm{s}}{\mathrm{d}z^2} = \left(k_y^2 - \frac{2\mathrm{i}}{\delta_\mathrm{s}^2}\right) F_\mathrm{s}(z), \quad F_\mathrm{s}(z_0) = 1, \tag{3.27a}$$

$$v_{\mathrm{s}y}(y, z) = -\frac{1}{\mathrm{i}\omega\rho_0} Z_\mathrm{c}(z_0) \frac{\mathrm{d}Y}{\mathrm{d}y} F_\mathrm{s}(z), \tag{3.27b}$$

$$v_{\mathrm{s}z}(y, z) = -\frac{k_y^2}{\mathrm{i}\omega\rho_0} Z_\mathrm{c}(z_0) Y(y) \int F_\mathrm{s}(z)\mathrm{d}z. \tag{3.27c}$$

Adding the compressional, thermal, and shear modes then fixes the boundary conditions on the temperature field and on the y-component of velocity to first order in $k_0\delta_\mathrm{s}$ and $k_0\delta_\mathrm{t}$. We still need to fix the z-component of velocity at the boundary, which will lead to a dispersion equation for the relation between wavenumbers k_y and k_z.

Resulting first-order fields

To get the total first-order fields we use a superposition of modes adding the compressional, thermal, and shear mode solutions. The total fields are then written as

$$p_1(y,z) = p_\mathrm{c}(y,z) + p_\mathrm{t}(y,z), \tag{3.28a}$$
$$T_1(y,z) = T_\mathrm{c}(y,z) + T_\mathrm{t}(y,z), \tag{3.28b}$$
$$v_{1y}(y,z) = v_{\mathrm{c}y}(y,z) + v_{\mathrm{s}y}(y,z) + v_{\mathrm{t}y}(y,z), \tag{3.28c}$$
$$v_{1z}(y,z) = v_{\mathrm{c}z}(y,z) + v_{\mathrm{s}z}(y,z) + v_{\mathrm{t}z}(y,z). \tag{3.28d}$$

Neglecting terms of order $\Gamma_\mathrm{s} \sim (k_0\delta_\mathrm{s})^2$ and $\Gamma_\mathrm{t} \sim (k_0\delta_\mathrm{t})^2$ relative to 1, the pressure p_t and the y-component of velocity $v_{\mathrm{t}y}$ that are due to the thermal wave become negligible. Adding it up we thus find

$$p_1(y,z) = Y(y)Z_\mathrm{c}(z), \tag{3.29a}$$
$$T_1(y,z) = \frac{(\gamma-1)\kappa_s}{\alpha_p} Y(y)\left[Z_\mathrm{c}(z) - Z_\mathrm{c}(z_0)F_\mathrm{t}(z)\right], \tag{3.29b}$$
$$v_{1y}(y,z) = \frac{1}{\mathrm{i}\omega\rho_0}\frac{\mathrm{d}Y}{\mathrm{d}y}\left[Z_\mathrm{c}(z) - Z_\mathrm{c}(z_0)F_\mathrm{s}(z)\right], \tag{3.29c}$$
$$v_{1z}(y,z) = \frac{1}{\mathrm{i}\omega\rho_0} Y(y)\left[\frac{\mathrm{d}Z_\mathrm{c}}{\mathrm{d}z} - k_y^2 Z_\mathrm{c}(z_0)\int F_\mathrm{s}(z)\mathrm{d}z - \mathrm{i}\,(\gamma-1)\,\Gamma_\mathrm{t} Z_\mathrm{c}(z_0)\frac{\mathrm{d}F_\mathrm{t}}{\mathrm{d}z}\right]. \tag{3.29d}$$

In order to have the z-component of velocity v_{1z} vanish at the boundary in $z = z_0$ we see that we must fulfill the following boundary condition on $Z_\mathrm{c}(z)$

$$\frac{\mathrm{d}Z_\mathrm{c}}{\mathrm{d}z} = Z_\mathrm{c}(z_0)\left[k_y^2\int F_\mathrm{s}(z)\mathrm{d}z + \mathrm{i}\,(\gamma-1)\,\Gamma_\mathrm{t}\frac{\mathrm{d}F_\mathrm{t}}{\mathrm{d}z}\right] \quad \text{for} \quad z = z_0. \tag{3.30}$$

We have now solved the problem formally with the expressions for the fields given in Eq. (3.29). The functions $Y(y)$, $Z_\mathrm{c}(z)$, $F_\mathrm{t}(z)$, and $F_\mathrm{s}(z)$ must satisfy their respective equations. We give these equations below for clarity, neglecting $(k_y\delta_\mathrm{s})^2$ and $(k_y\delta_\mathrm{t})^2$ relative to 1 in the equations for $F_\mathrm{s}(z)$ and $F_\mathrm{t}(z)$, noting that $k_y \sim k_0$ describing the horizontal wavenumber.

The equations are

$$\frac{\mathrm{d}^2Y}{\mathrm{d}y^2} = -k_y^2 Y(y), \quad k_\mathrm{c}^2 = k_y^2 + k_z^2, \quad k_\mathrm{c}^2 = \left(\frac{\omega}{c}\right)^2\left[1 + \mathrm{i}\Gamma_\mathrm{s} + \mathrm{i}(\gamma-1)\Gamma_\mathrm{t}\right], \tag{3.31a}$$
$$\frac{\mathrm{d}^2Z_\mathrm{c}}{\mathrm{d}z^2} = -k_z^2 Z_\mathrm{c}(z), \quad \frac{\mathrm{d}Z_\mathrm{c}}{\mathrm{d}z} = Z_\mathrm{c}(z_0)\left[k_y^2\int F_\mathrm{s}(z)\mathrm{d}z + \mathrm{i}\,(\gamma-1)\,\Gamma_\mathrm{t}\frac{\mathrm{d}F_\mathrm{t}}{\mathrm{d}z}\right] \text{ for } z = z_0, \tag{3.31b}$$
$$\frac{\mathrm{d}^2F_\mathrm{t}}{\mathrm{d}z^2} = -\frac{2\mathrm{i}}{\delta_\mathrm{t}^2}F_\mathrm{t}(z), \quad F_\mathrm{t}(z_0) = 1, \tag{3.31c}$$
$$\frac{\mathrm{d}^2F_\mathrm{s}}{\mathrm{d}z^2} = -\frac{2\mathrm{i}}{\delta_\mathrm{s}^2}F_\mathrm{s}(z), \quad F_\mathrm{s}(z_0) = 1. \tag{3.31d}$$

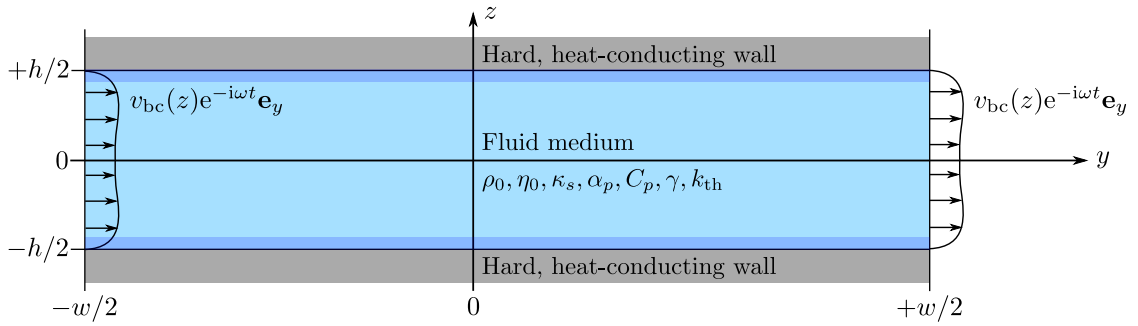

Figure 3.2: The parallel-plate system studied in Section 3.3. We consider a viscous, heat-conducting fluid medium in the yz-plane between two parallel plates in $z = \pm h/2$. Time-harmonic actuation is modeled with an actuation profile $v_{\mathrm{bc}}(z)$ at the open domain boundaries in $y = \pm w/2$ as discussed in the text.

Additional boundary conditions may be required depending on the system of interest.

The solution of these equations proceed as follows. One first solve the equations for $F_{\mathrm{t}}(z)$ and $F_{\mathrm{s}}(z)$ with the given boundary conditions as well as the equation for $Y(y)$. One may then evaluate the boundary condition on $Z_{\mathrm{c}}(z)$ and solve this equation, after which all fields are written down according to Eq. (3.29).

3.3 The parallel-plate system

We consider the system illustrated in Fig. 3.2, namely a symmetric parallel-plate system with the fluid domain of interest in the yz-plane, walls at $z = \pm h/2$, and open domain ends at $y = \pm w/2$, while the channel is considered infinitely long and hence translation invariant along the x-direction. The system is driven with a small velocity amplitude $v_{\mathrm{bc}}(z)$ at the open domain ends in $y = \pm w/2$. This is a model for the complicated actuation achieved using a piezo-transducer. The same model for actuation was used in the numerical work of Ref. [24] where the actuation velocity $v_{\mathrm{bc}}(z)$ was assumed to have a constant profile along the z-direction. A constant actuation profile may lead to problems in the corners when deriving an analytical solution, and consequently we will allow some variation in the z-direction. In relation to the experimental system, the important thing is that the frequency of actuation may be tuned to achieve resonance conditions, which happens approximately when a standing half-wave spans the width.

Having once decided to model actuation through a small velocity amplitude $v_{\mathrm{bc}}(z)$ at the domain ends in $y = \pm w/2$, it turns out that relaxing all requirements regarding this actuation profile gives solutions with physically meaningful actuation profiles. We may write down our velocity boundary condition as

$$\boldsymbol{v}_1 \cdot \mathbf{e}_y = v_{\mathrm{bc}}(z)\mathrm{e}^{-\mathrm{i}\omega t}, \quad \text{for } y = \pm w/2, \tag{3.32}$$

where we have included the time-dependence for clarity, though in the first-order fields this time-dependence is made implicit. We have not constrained the z-component of velocity

at the boundaries. The actuation in the y-component of velocity is chosen to be even, and the z-dependence is not given. We will let the z-dependence be determined from the solution itself, and consequently we write the boundary condition into the y-dependent part of v_{1y},

$$\left.\frac{\mathrm{d}Y}{\mathrm{d}y}\right|_{y=\pm w/2} = \mathrm{i}\omega\rho_0 v_{\mathrm{bc}}, \tag{3.33}$$

where we have now made the time-dependence implicit and here v_{bc} is a constant that does not depend on z. We will find that this method of relaxing the boundary conditions results in proper physical solutions.

The general solution to Eq. (3.31a) is

$$Y(y) = A\cos\left(k_y y\right) + B\sin\left(k_y y\right). \tag{3.34}$$

Here A and B are constants to be determined from the boundary conditions. Imposing the boundary conditions stated in Eq. (3.33) we get

$$\left.\frac{\mathrm{d}Y}{\mathrm{d}y}\right|_{y=\pm w/2} = \mp A k_y \sin\left(\frac{k_y w}{2}\right) + B k_y \cos\left(\frac{k_y w}{2}\right) = \mathrm{i}\omega\rho_0 v_{\mathrm{bc}}. \tag{3.35}$$

Consequently we set

$$A = 0, \quad B = \mathrm{i}\omega\rho_0 \frac{v_{\mathrm{bc}}}{k_y}\frac{1}{\cos\left(k_y w/2\right)}. \tag{3.36}$$

We have rejected solutions for which $A \neq 0$ because these solutions require that $k_y w/2 = n\pi$, where $n \in \mathbb{Z}$. However, this can only be satisfied if $\mathrm{Im}[k_y] = 0$, and with this constraint we cannot solve the equation for $Z_{\mathrm{c}}(z)$, which will be shown later. Consequently we must have $A = 0$. Then the solution is

$$Y(y) = \mathrm{i}\omega\rho_0 \frac{v_{\mathrm{bc}}}{k_y}\frac{\sin\left(k_y y\right)}{\cos\left(k_y w/2\right)}. \tag{3.37}$$

Next we find the functions $F_{\mathrm{t}}(z)$ and $F_{\mathrm{s}}(z)$. They both satisfy the same type of equation, namely Eq. (3.31c) and Eq. (3.31d). For the parallel-plate system we must require the three functions $Z_{\mathrm{c}}(z)$, $F_{\mathrm{t}}(z)$, and $F_{\mathrm{s}}(z)$ to have the same symmetry. Otherwise we cannot fulfill the no-slip condition at both boundaries. The velocity component v_{1y} moreover has the same symmetry as these three functions. All this is seen from Eq. (3.29). Considering the even symmetry that is observed numerically [24], the boundary conditions are

$$F_{\mathrm{t}}(\pm h/2) = 1, \quad F_{\mathrm{s}}(\pm h/2) = 1. \tag{3.38}$$

The solution to Eq. (3.31c) and Eq. (3.31d) with these boundary conditions is

$$F_{\mathrm{t}}(z) = \frac{\cosh\left[(1-\mathrm{i})z/\delta_{\mathrm{t}}\right]}{\cosh\left[(1-\mathrm{i})h/2\delta_{\mathrm{t}}\right]}, \quad F_{\mathrm{s}}(z) = \frac{\cosh\left[(1-\mathrm{i})z/\delta_{\mathrm{s}}\right]}{\cosh\left[(1-\mathrm{i})h/2\delta_{\mathrm{s}}\right]}. \tag{3.39a}$$

Here we have used that $\sqrt{-2\mathrm{i}} = (1-\mathrm{i})$. Having solved these equations we can move on to evaluating the boundary condition on $Z_\mathrm{c}(z)$, Eq. (3.30). Plugging into this equation and utilizing the identity for Γ_t in Eq. (2.21) gives

$$\left.\frac{\mathrm{d}Z_\mathrm{c}}{\mathrm{d}z}\right|_{z=\pm h/2} = Z_\mathrm{c}(\pm h/2)\frac{(1+\mathrm{i})}{2}\left[k_y^2\delta_\mathrm{s}\tanh\left((1-\mathrm{i})\frac{h}{2\delta_\mathrm{s}}\right)\right.$$
$$\left.+(\gamma-1)\left(\frac{\omega}{c}\right)^2\delta_\mathrm{t}\tanh\left((1-\mathrm{i})\frac{h}{2\delta_\mathrm{t}}\right)\right], \tag{3.40}$$

showing that $Z_\mathrm{c}(z)$ must be even as assumed. Under this condition the solution to Eq. (3.31b) for $Z_\mathrm{c}(z)$ is simply

$$Z_\mathrm{c}(z) = D\cos\left(k_z z\right), \tag{3.41}$$

where D is a free parameter for the amplitude. It may as well be incorporated into the constant v_bc and consequently we set $D = 1$ in the following.

Inserting the cosine solution for $Z_\mathrm{c}(z)$ of Eq. (3.41) into the boundary condition Eq. (3.40) we get a dispersion equation relating wavenumbers k_y and k_z. After some manipulation we write k_y^2 as a function of k_z,

$$k_y^2 = \frac{(\mathrm{i}-1)k_z}{\delta_\mathrm{s}}\frac{\tan\left[k_z h/2\right]}{\tanh\left[(1-\mathrm{i})h/2\delta_\mathrm{s}\right]} - \frac{(\gamma-1)\delta_\mathrm{t}}{\delta_\mathrm{s}}\left(\frac{\omega}{c}\right)^2\frac{\tanh\left[(1-\mathrm{i})h/2\delta_\mathrm{t}\right]}{\tanh\left[(1-\mathrm{i})h/2\delta_\mathrm{s}\right]}. \tag{3.42}$$

We have found all the functions $Y(y)$, $F_\mathrm{t}(z)$, $F_\mathrm{s}(z)$, and $Z_\mathrm{c}(z)$ as well as the dispersion equation relating the wavenumbers k_y and k_z, and consequently we have solved the problem. All that is left is to insert these functions in the equations for the fields Eq. (3.29). This proceeds straight-forwardly. The expression for the v_{1z} component of velocity is most conveniently written by making use of the dispersion equation to substitute k_y^2. The final result for the first-order fields is

$$p_1 = \mathrm{i}\omega\rho_0\frac{v_\mathrm{bc}}{k_y}\frac{\sin\left(k_y y\right)}{\cos\left(k_y w/2\right)}\cos\left(k_z z\right), \tag{3.43a}$$

$$T_1 = \mathrm{i}\omega\rho_0\frac{v_\mathrm{bc}}{k_y}\frac{(\gamma-1)\kappa_s}{\alpha_p}\frac{\sin\left(k_y y\right)}{\cos\left(k_y w/2\right)}\left[\cos\left(k_z z\right) - \cos\left(\frac{k_z h}{2}\right)\frac{\cosh\left[(1-\mathrm{i})z/\delta_\mathrm{t}\right]}{\cosh\left[(1-\mathrm{i})h/2\delta_\mathrm{t}\right]}\right], \tag{3.43b}$$

$$v_{1y} = v_\mathrm{bc}\frac{\cos\left(k_y y\right)}{\cos\left(k_y w/2\right)}\left[\cos\left(k_z z\right) - \cos\left(\frac{k_z h}{2}\right)\frac{\cosh\left[(1-\mathrm{i})z/\delta_\mathrm{s}\right]}{\cosh\left[(1-\mathrm{i})h/2\delta_\mathrm{s}\right]}\right], \tag{3.43c}$$

$$v_{1z} = -v_\mathrm{bc}\frac{k_z}{k_y}\frac{\sin\left(k_y y\right)}{\cos\left(k_y w/2\right)}\left\{\sin\left(k_z z\right) - \sin\left(\frac{k_z h}{2}\right)\frac{\sinh\left[(1-\mathrm{i})z/\delta_\mathrm{s}\right]}{\sinh\left[(1-\mathrm{i})h/2\delta_\mathrm{s}\right]}\right.$$
$$+(1+\mathrm{i})\frac{(\gamma-1)}{2}\left(\frac{\omega}{c}\right)^2\frac{\delta_\mathrm{t}}{k_z}\cos\left(\frac{k_z h}{2}\right)\left[\frac{\sinh\left[(1-\mathrm{i})z/\delta_\mathrm{t}\right]}{\cosh\left[(1-\mathrm{i})h/2\delta_\mathrm{t}\right]}\right.$$
$$\left.\left.-\tanh\left((1-\mathrm{i})\frac{h}{2\delta_\mathrm{t}}\right)\frac{\sinh\left[(1-\mathrm{i})z/\delta_\mathrm{s}\right]}{\sinh\left[(1-\mathrm{i})h/2\delta_\mathrm{s}\right]}\right]\right\}. \tag{3.43d}$$

Written on this form it is clear that the velocity boundary condition is fulfilled at the walls, namely that $\boldsymbol{v}_1(y, \pm h/2) = \mathbf{0}$.

3.3.1 Approximate wavenumbers

Consider the dispersion equation relating the complex wavenumbers k_y and k_z as given in Eq. (3.42). It describes possible solutions to the parallel-plate problem, all fulfilling the given boundary conditions. These different solutions will be referred to as modes, and will be investigated in more detail in Chapter 4 on microchannel acoustofluidics. For now we note that the fundamental mode is the primary mode responsible for the resonant field solutions, while the higher modes are damped.

We look for approximate solutions to the dispersion equation in the case where pressure variation perpendicular to the walls along the z-direction is small. This may seem limiting but note that the assumption of small pressure variation perpendicular to the walls is the fundamental assumption of Prandtl-Schlichting boundary layer theory, which neglects the perpendicular pressure variation all-together [12]. The boundary layer theory approach has been the standard of the field of acoustofluidics and is usually the starting point in the study of acoustic streaming [12, 18, 20, 21, 22]. With our solution of the first-order fields we have a way of extending such studies by including pressure variation perpendicular to walls.

The assumption of small pressure variation perpendicular to the walls is consistent with our solution when $k_z h/2 \ll 1$. We consequently expand the tangent in Eq. (3.42) to first order and the dispersion equation reduces to

$$k_y^2 = (\mathrm{i} - 1)\frac{1}{f_\mathrm{s}} k_z^2 - (\gamma - 1)\left(\frac{\omega}{c}\right)^2 \frac{f_\mathrm{t}}{f_\mathrm{s}}, \tag{3.44}$$

where we have defined

$$f_\mathrm{s} = \frac{\tanh\left[(1-\mathrm{i})h/2\delta_\mathrm{s}\right]}{h/2\delta_\mathrm{s}}, \quad \text{and} \quad f_\mathrm{t} = \frac{\tanh\left[(1-\mathrm{i})h/2\delta_\mathrm{t}\right]}{h/2\delta_\mathrm{t}}. \tag{3.45}$$

The second equation relating the wavenumbers is

$$k_\mathrm{c}^2 = k_y^2 + k_z^2, \quad k_\mathrm{c}^2 = \left(\frac{\omega}{c}\right)^2 \left[1 + \mathrm{i}\Gamma_\mathrm{s} + \mathrm{i}(\gamma - 1)\Gamma_\mathrm{t}\right]. \tag{3.46}$$

Using these two equations and going to first order in $k_0\delta_\mathrm{s}$ and $k_0\delta_\mathrm{t}$ one obtains the wavenumbers for the fundamental mode when pressure variation perpendicular to the walls is assumed to be small

$$k_y = \frac{\omega}{c}\sqrt{\frac{(1-\mathrm{i}) + (\gamma-1)f_\mathrm{t}}{(1-\mathrm{i}) - f_\mathrm{s}}}, \tag{3.47a}$$

$$k_z = -\mathrm{i}\frac{\omega}{c}\sqrt{\frac{f_\mathrm{s} + (\gamma-1)f_\mathrm{t}}{(1-\mathrm{i}) - f_\mathrm{s}}}. \tag{3.47b}$$

In the limit relevant to microchannel acoustophoresis where the boundary layer thickness is much smaller than the channel height, $\delta_\mathrm{s}/h \ll 1$ and $\delta_\mathrm{t}/h \ll 1$, the hyperbolic tangents in f_s and f_t may be set to unity and to first order the wavenumbers become

$$\begin{aligned} k_y &= \frac{\omega}{c}\left[1 + \frac{(1+\mathrm{i})}{2h}\left[\delta_\mathrm{s} + (\gamma-1)\delta_\mathrm{t}\right]\right] \\ k_z &= -\mathrm{i}\frac{\omega}{c}\sqrt{\frac{(1+\mathrm{i})}{h}\left[\delta_\mathrm{s} + (\gamma-1)\delta_\mathrm{t}\right]} \end{aligned}, \quad \text{for} \quad \frac{\delta_\mathrm{s}}{h}, \frac{\delta_\mathrm{t}}{h} \ll 1. \tag{3.48}$$

The wavenumber k_y does indeed describe a wave with wavenumber close to ω/c being damped slightly by the effect of viscosity and thermal conduction due to losses at the boundaries. The wavenumber k_z is small in comparison to k_y and indeed $k_z h/2 \ll 1$ consistent with boundary layer theory.

3.3.2 Dimensionless solution

In order to explore the structure of the solution and investigate various limits we write the solution with dimensionless parameters. Define the parameters ε_λ, ε_h, and ε_w, typically small in acoustophoresis applications,

$$\varepsilon_\lambda = k_0\delta_\mathrm{s} = \frac{\omega}{c}\delta_\mathrm{s} = 2\pi\frac{\delta_\mathrm{s}}{\lambda}, \tag{3.49a}$$

$$\varepsilon_h = \frac{\delta_\mathrm{s}}{h/2} = \frac{2\delta_\mathrm{s}}{h}, \tag{3.49b}$$

$$\varepsilon_w = \frac{\delta_\mathrm{s}}{w/2} = \frac{2\delta_\mathrm{s}}{w}. \tag{3.49c}$$

Likewise define the dimensionless parameters $\tilde{y}$ and $\tilde{z}$, as well as the dimensionless wavenumbers $\tilde{k}_y$ and $\tilde{k}_z$,

$$\tilde{y} = \frac{y}{w/2}, \quad \tilde{z} = \frac{z}{h/2}, \quad \tilde{k}_y = k_y\delta_\mathrm{s}, \quad \tilde{k}_z = k_z\delta_\mathrm{s}. \tag{3.50}$$

$$\tag{3.51}$$

Note moreover that the Prandtl number describing the ratio of momentum diffusion to thermal diffusion is given as $\mathrm{Pr} = \nu_0/D_\mathrm{th} = (\delta_\mathrm{s}/\delta_\mathrm{t})^2$, and consequently $\delta_\mathrm{t} = \delta_\mathrm{s}/\sqrt{\mathrm{Pr}}$. We will use these definitions to write the normalized fields on a general form dependent on the dimensionless parameters ε_λ, ε_h, ε_w, as well as the dimensionless fluid parameters Pr and γ. We write the normalized fields with a tilde and we have chosen the following normalization

$$p_1 = \rho_0 c^2\,\tilde{p}_1, \quad T_1 = \frac{1}{\alpha_p}\tilde{T}_1, \quad v_{1y} = c\,\tilde{v}_{1y}, \quad v_{1z} = c\,\tilde{v}_{1z}. \tag{3.52a}$$

With the chosen dimensionless parameters the absolute value of viscosity, system size, and actuation frequency drops out of the field expressions. We will discuss later how to bring back the physical significance of these parameters.

On dimensionless form with dimensionless parameters the fields become

$$\tilde{p}_1 = \mathrm{i}\frac{v_{\mathrm{bc}}}{c}\frac{\varepsilon_\lambda}{\tilde{k}_y}\frac{\sin\left(\tilde{k}_y\tilde{y}/\varepsilon_w\right)}{\cos\left(\tilde{k}_y/\varepsilon_w\right)}\cos\left(\tilde{k}_z\tilde{z}/\varepsilon_h\right), \tag{3.53a}$$

$$\tilde{T}_1 = \mathrm{i}(\gamma-1)\frac{v_{\mathrm{bc}}}{c}\frac{\varepsilon_\lambda}{\tilde{k}_y}\frac{\sin\left(\tilde{k}_y\tilde{y}/\varepsilon_w\right)}{\cos\left(\tilde{k}_y/\varepsilon_w\right)}\left[\cos\left(\frac{\tilde{k}_z\tilde{z}}{\varepsilon_h}\right)-\cos\left(\frac{\tilde{k}_z}{\varepsilon_h}\right)\frac{\cosh\left[(1-\mathrm{i})\sqrt{\mathrm{Pr}}\;\tilde{z}/\varepsilon_h\right]}{\cosh\left[(1-\mathrm{i})\sqrt{\mathrm{Pr}}/\varepsilon_h\right]}\right], \tag{3.53b}$$

$$\tilde{v}_{1y} = \frac{v_{\mathrm{bc}}}{c}\frac{\cos\left(\tilde{k}_y\tilde{y}/\varepsilon_w\right)}{\cos\left(\tilde{k}_y/\varepsilon_w\right)}\left[\cos\left(\frac{\tilde{k}_z\tilde{z}}{\varepsilon_h}\right)-\cos\left(\frac{\tilde{k}_z}{\varepsilon_h}\right)\frac{\cosh\left[(1-\mathrm{i})\tilde{z}/\varepsilon_h\right]}{\cosh\left[(1-\mathrm{i})/\varepsilon_h\right]}\right], \tag{3.53c}$$

$$\begin{aligned}\tilde{v}_{1z} = -\frac{v_{\mathrm{bc}}}{c}\frac{\tilde{k}_z}{\tilde{k}_y}\frac{\sin\left(\tilde{k}_y\tilde{y}/\varepsilon_w\right)}{\cos\left(\tilde{k}_y/\varepsilon_w\right)}\Bigg\{&\sin\left(\frac{\tilde{k}_z\tilde{z}}{\varepsilon_h}\right)-\sin\left(\frac{\tilde{k}_z}{\varepsilon_h}\right)\frac{\sinh\left[(1-\mathrm{i})\tilde{z}/\varepsilon_h\right]}{\sinh\left[(1-\mathrm{i})/\varepsilon_h\right]}\\&+(1+\mathrm{i})\frac{(\gamma-1)}{2\sqrt{\mathrm{Pr}}}\frac{\varepsilon_\lambda^2}{\tilde{k}_z}\cos\left(\frac{\tilde{k}_z}{\varepsilon_h}\right)\left[\frac{\sinh\left[(1-\mathrm{i})\sqrt{\mathrm{Pr}}\;\tilde{z}/\varepsilon_h\right]}{\cosh\left[(1-\mathrm{i})\sqrt{\mathrm{Pr}}/\varepsilon_h\right]}\right.\\&\left.-\tanh\left((1-\mathrm{i})\frac{\sqrt{\mathrm{Pr}}}{\varepsilon_h}\right)\frac{\sinh\left[(1-\mathrm{i})\tilde{z}/\varepsilon_h\right]}{\sinh\left[(1-\mathrm{i})/\varepsilon_h\right]}\right]\Bigg\}.\end{aligned} \tag{3.53d}$$

Here we have used that $\kappa_s = 1/(\rho_0 c^2)$.

In the general case where we cannot assume that pressure variation along the height of the channel is small, we have to solve the dispersion equation numerically. In terms of the dimensionless parameters the dispersion equation Eq. (3.42) and the two helping functions f_{s} and f_{t} may be written on the form

$$\tilde{k}_y^2 = (\mathrm{i}-1)\frac{\varepsilon_h}{f_{\mathrm{s}}}\tilde{k}_z\tan\left(\frac{\tilde{k}_z}{\varepsilon_h}\right)-(\gamma-1)\frac{f_{\mathrm{t}}}{f_{\mathrm{s}}}\varepsilon_\lambda^2, \tag{3.54a}$$

$$f_{\mathrm{s}} = \varepsilon_h\tanh\left[(1-\mathrm{i})/\varepsilon_h\right], \quad \text{and} \quad f_{\mathrm{t}} = \frac{\varepsilon_h}{\sqrt{\mathrm{Pr}}}\tanh\left[(1-\mathrm{i})\sqrt{\mathrm{Pr}}/\varepsilon_h\right]. \tag{3.54b}$$

The second equation relating the wavenumbers is $k_{\mathrm{c}}^2 = k_y^2 + k_z^2$, where k_{c} has a small imaginary part corresponding to bulk damping from viscous dissipation and heat conduction as we have seen. To first order the bulk damping may be neglected and in terms of the dimensionless parameters the second equation relating the wavenumbers reads

$$\tilde{k}_y^2 + \tilde{k}_z^2 = \varepsilon_\lambda^2. \tag{3.54c}$$

The two equations may be solved numerically to yield the wavenumbers $\tilde{k}_y$ and $\tilde{k}_z$ for given values of ε_λ and ε_h. In the next section we investigate the possible field solutions using

an approach which highlights the differences in the fields as we tune the dimensionless parameters.

3.3.3 Investigation of field solutions

In order to study the form of the field solutions in various limits we consider the form in Eq. (3.53) where the fields are written on dimensionless form using the dimensionless parameters ε_λ, ε_h, and ε_w. These parameters all vary with frequency. In order to keep the study generic we start out considering the form of the fields at resonance conditions as functions of ε_λ and ε_h. The following approach will be employed:

1. Choose desired fluid parameters and actuation boundary velocity: γ, Pr, and v_{bc}/c.

2. Set desired parameter value of $\varepsilon_\lambda = k_0\delta_{\mathrm{s}}$. Having gone to first order in this parameter we may try to study the range $0 < \varepsilon_\lambda \lesssim 0.15$.

3. Set desired parameter value of $\varepsilon_h = 2\delta_{\mathrm{s}}/h$. We can study all values, $\varepsilon_h > 0$.

4. Solve the dispersion equations Eq. (3.54) to get wavenumbers $\tilde{k}_y$ and $\tilde{k}_z$. In the general case this is done numerically.

5. Tune the parameter ε_w to achieve fundamental resonance conditions for the given parameter values of ε_λ and ε_h. In the general case this is done numerically by minimizing $|\cos(\tilde{k}_y/\varepsilon_w)|$.

6. Plot the fields normalized by the maximum field value. By normalizing the field solutions we may study how the shape of the solution changes as a function of parameter values.

Note that tuning ε_w to maximize the field amplitudes in step 5 corresponds to adjusting the width of the channel to achieve fundamental resonance conditions. For acoustically resonant fields the fundamental resonance is achieved for $w \simeq \lambda/2$ corresponding to $\varepsilon_w \simeq 2\varepsilon_\lambda/\pi$, however, as ε_h is increased above 1 the maximum field amplitudes are achieved for increasingly larger values of ε_w as we observe a transition from resonant acoustic fields to viscosity dominated shear flow. This will be studied in more detail in a later section.

The procedure for plotting described above is somewhat generic and allows investigation of the field solutions as functions of ε_λ and ε_h with a minimum of parameters referring to the specific fluid. Indeed, the absolute value of viscosity, system size, and actuation frequency drops out of the field expressions and by normalizing the fields we study only the form of the solutions. The only thing referring to a specific fluid is the Prandtl number, the squareroot of which gives the ratio of viscous to thermal boundary layer thicknesses, as well as the heat capacity ratio γ.

After studying the generic behavior of the fields as functions of ε_λ and ε_h with no reference to the value of viscosity, system size, and actuation frequency, we may want to find the corresponding physical system. To do so, one simply calculates the frequency

corresponding to the value of ε_λ. As $\varepsilon_\lambda = \omega\delta_s/c$ one finds

$$\omega = \frac{c^2\varepsilon_\lambda^2}{2\nu_0}, \tag{3.55}$$

and thus we have reintroduced frequency and viscosity by calculating the frequency required to fix ε_λ to its desired value. Referring to the fluid parameters of Table 2.1 and Table 2.2 we see that one may indeed find relevant physical systems for which $0 < \varepsilon_\lambda \lesssim 0.2$ without going beyond 20 MHz frequencies which is feasible in experiments.

Having once calculated the frequency we may evaluate the numerical value of δ_s for the fluid in question, and that in turn allows us to calculate the system height and width corresponding to the chosen value of ε_h and the calculated value of ε_w, respectively. Thus we reintroduce the length scales corresponding to the dimensionless parameters through the relations

$$\delta_s = \sqrt{\frac{2\nu_0}{\omega}}, \quad h = \frac{2\delta_s}{\varepsilon_h}, \quad w = \frac{2\delta_s}{\varepsilon_w}. \tag{3.56}$$

with the frequency ω calculated from ε_λ according to Eq. (3.55).

In the plotting we fix the value of Pr and γ to those of water at room temperature. Fig. 3.3 shows generic plots of the fields and how they change as ε_λ is varied, while Fig. 3.5 shows generic plots of the fields and their dependence on ε_h. When varying ε_λ in Fig. 3.3 we are studying the effect of a non-zero $\varepsilon_\lambda = k_0\delta_s$ thus going beyond boundary layer theory which neglects pressure variation perpendicular to walls. Row (a) of Fig. 3.3 shows how increasing the value of ε_λ from $\varepsilon_\lambda = 0.001$ to $\varepsilon_\lambda = 0.15$ leads to a significant pressure variation in the $\tilde{z}$-direction. For a small value of ε_λ this almost parabolic pressure variation along $\tilde{z}$ was recently observed in the numerical simulations of Muller *et al.* [24], and we will compare this model to our theory in Chapter 4.

Fig. 3.3 shows how the field solution changes when ε_λ is increased with a significant $\tilde{z}$-variation in all fields. We find that the $\tilde{z}$-variation of the fields also depend on ε_h because as ε_h is increased to 1 the boundary layers begin to overlap. In Fig. 3.4 we have plotted the quantity $1 - p_1(\tilde{z}=0)/p_1(\tilde{z}=1)$ in the $(\varepsilon_\lambda, \varepsilon_h)$-plane. Referring to the lineplot of Fig. 3.3 row (a), we see that this quantity gives a measure for the effect of a finite $k_0\delta_s$ by describing the deviation from zero pressure variation along the $\tilde{z}$-direction. Fig. 3.4 is generated in the isentropic limit assuming that thermal effects have little effect on the wavenumber, making the figure completely generic with no reference to the fluid medium because Pr and γ drop out of the equations for the wavenumbers. We may consequently identify contours corresponding to a given fluid and frequency as shown in the figure using the values for water, air, and glycerol given in Table 2.2. The figure also indicates the contours of constant channel aspect-ratio $\alpha = h/w$ for the fundamental half-wave resonance. These are found from

$$\alpha = \frac{h}{w} = \frac{\varepsilon_w}{\varepsilon_h} \quad \Rightarrow \quad \varepsilon_h = \frac{1}{\alpha}\varepsilon_w \simeq \frac{2}{\pi\alpha}\varepsilon_\lambda, \tag{3.57}$$

where we have used that the fundamental half-wave resonance is achieved for $w \simeq \lambda/2$ corresponding to $\varepsilon_w \simeq 2\varepsilon_\lambda/\pi$, which is approximately true when $\varepsilon_h < 1$. Fig. 3.4 shows

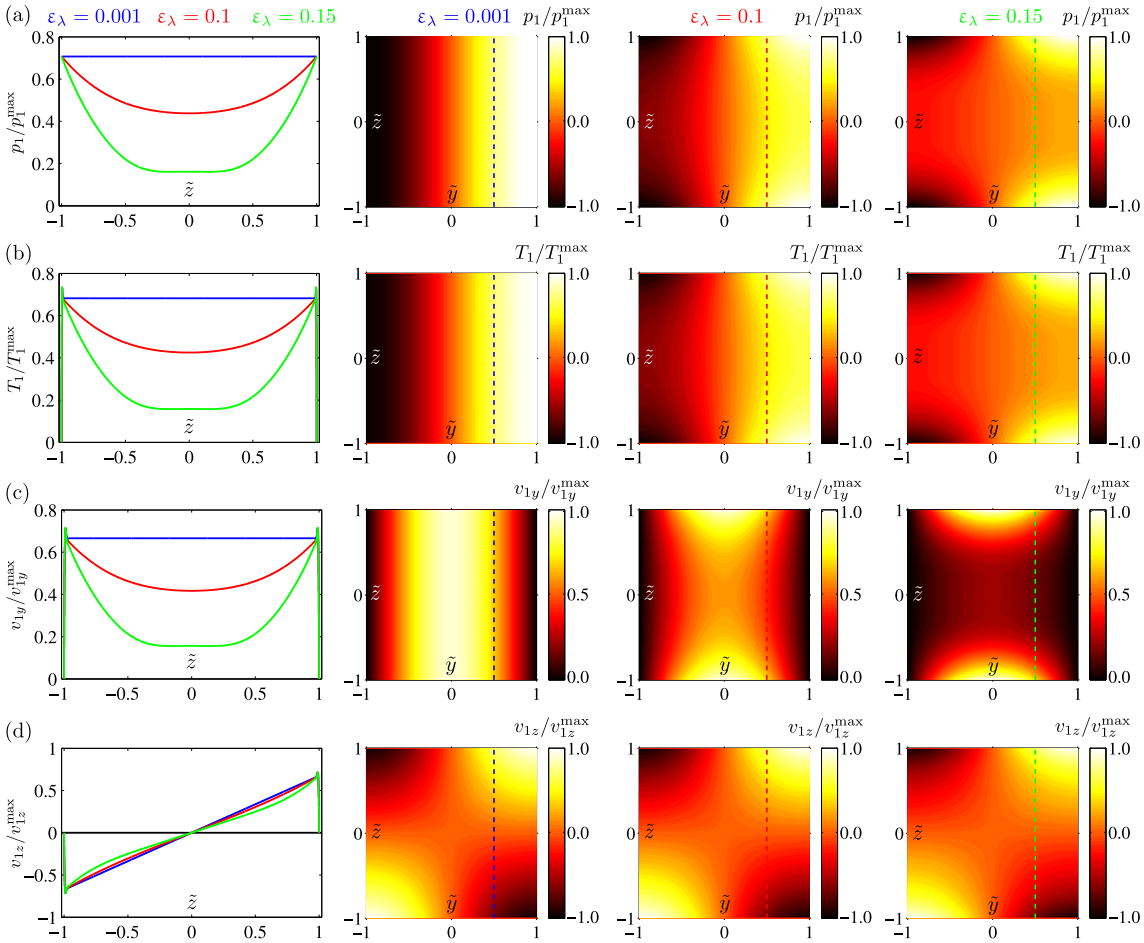

Figure 3.3: In this figure we study the effect of a finite $\varepsilon_\lambda = k_0\delta_s$ on the acoustic fields. Row (a) The pressure field p_1. Row (b) The temperature field T_1. Row (c) The velocity field component v_{1y}. Row (d) The velocity field component v_{1z}. The fields are normalized by their maximum amplitude. For each row the lineplot shows the field variation along the $\tilde{z}$-direction taken at $\tilde{y} = 0.5$ as indicated in the contour plots with a dashed line. The first column of contourplots correspond to $\varepsilon_\lambda = 0.001$ (blue), the second $\varepsilon_\lambda = 0.1$ (red), and the last $\varepsilon_\lambda = 0.15$ (green). In all plots the value of ε_h is fixed at $\varepsilon_h = 0.005$, corresponding to very narrow boundary layers as compared to the height.

that significant effects of finite $\varepsilon_\lambda = k_0\delta_s$ may be observed for real fluids at MHz frequencies. For water significant effects require frequencies beyond 20 MHz, but with fluids such as air or glycerol one may see more than 10% deviation already at 2 MHz.

It should be noted that this dependence of the first-order fields on $\tilde{z}$ may lead to focusing of acoustically hard particles in the middle of the channel cross-section, not only along the horizontal $\tilde{y}$-direction to the pressure node, but also along the vertical $\tilde{z}$-direction where the pressure may be lowered significantly at the center as seen in the lineplot of Fig. 3.3 row (a).

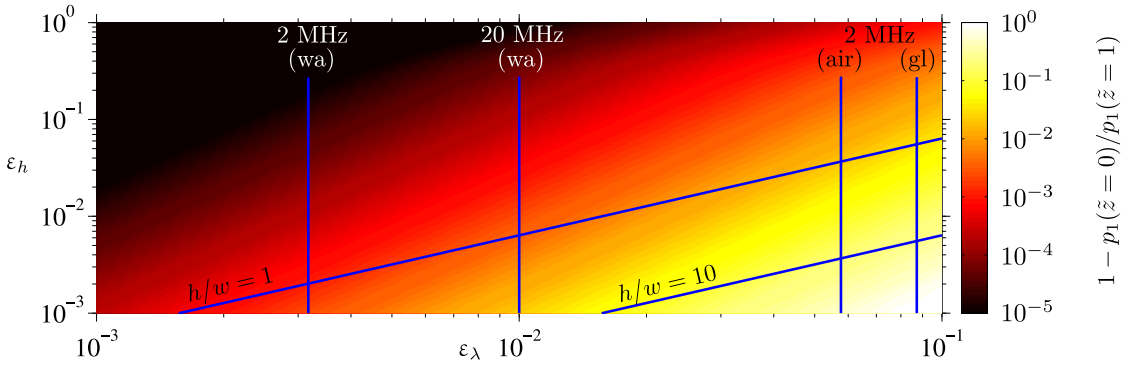

Figure 3.4: Contourplot of $1 - p_1(\tilde{z} = 0)/p_1(\tilde{z} = 1)$ taken at $\tilde{y} = 0.5$ showing the deviation from zero pressure variation along the $\tilde{z}$-direction as a result of finite $\varepsilon_\lambda = k_0\delta_s$ in the isentropic limit plotted in the $(\varepsilon_\lambda, \varepsilon_h)$-plane. Contours corresponding to water (wa) at 2 MHz and 20 MHz, and glycerol (gl) and air at 2 MHz are indicated. Contours of constant channel aspect-ratio $\alpha = h/w$ of 1 and 10 assuming half-wave resonances are indicated. The figure shows that significant effects of finite $\varepsilon_\lambda = k_0\delta_s$ may be observed for real fluids at MHz frequencies with deviations from constant bulk pressure profiles well above 10% for air and glycerol at 2 MHz.

In Fig. 3.5 we study how the field solution changes as $\varepsilon_h = 2\delta_s/h$ is increased corresponding to increasing the boundary layer thickness δ_s relative to the height of the channel h. When $\varepsilon_h = 1$ the two boundary layers thus begin to overlap. Referring to the plots of v_{1y} in row (c) of Fig. 3.5 we see that for $\varepsilon_h = 20$ the profile along $\tilde{z}$ is parabolic, while an inspection of the contourplots shows that v_{1y} is constant in the $\tilde{y}$-direction. We expect that this shear-flow dominated regime suppresses the resonance completely.

The analytical solution thus describes the transition from a resonant near-horizontal bulk field to a viscosity-dominated shear flow as the boundary layer thickness is increased corresponding to decreasing the frequency. The regime of microchannel acoustofluidics where the boundary layers are much smaller than the channel height $\delta_s \ll h$ gives rise to acoustically resonant field solutions that will be studied and compared to numerical simulations in Chapter 4. The other solution regime is the low frequency shear flow regime where the boundary layers become comparable to the height of the channel $\delta_s \sim h$. This low frequency shear flow limit will be investigated in the next section.

3.3.4 Low frequency shear flow limit

As discussed in relation to Fig. 3.5 we have found that the field solution of Eq. (3.53) describes a regime where the boundary layer overlap becomes so pronounced that the flow profile $v_{1y}(\tilde{z})$ becomes parabolic resembling a Poiseuille flow. Fig. 3.6 investigates the shear flow solution regime and the transition to shear flow solutions in more detail. In Fig. 3.6(a) we have illustrated the regime of shear flow solutions and clarified the conditions that must be fulfilled for this regime. In particular the boundary layer thickness must be comparable to the system size much smaller than the wavelength, i.e., $\varepsilon_h \sim \varepsilon_w \gg \varepsilon_\lambda$.

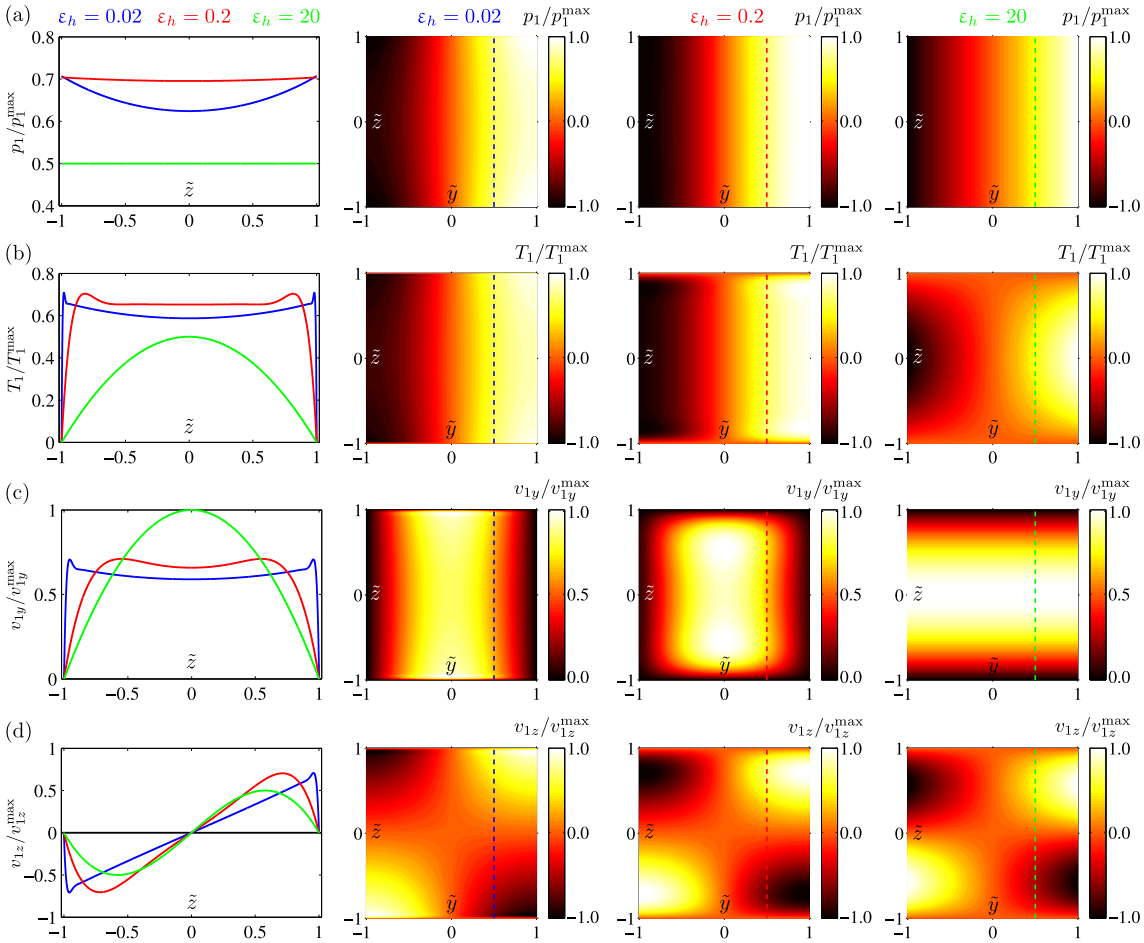

Figure 3.5: In this figure we study the effect of increasing $\varepsilon_h = 2\delta_s/h$ on the acoustic fields. Row (a) The pressure field p_1. Row (b) The temperature field T_1. Row (c) The velocity field component v_{1y}. Row (d) The velocity field component v_{1z}. The fields are normalized by their maximum amplitude. For each row the lineplot shows the field variation along the $\tilde{z}$-direction taken at $\tilde{y} = 0.5$ as indicated in the contour plots with a dashed line. The first column of contourplots correspond to $\varepsilon_h = 0.02$ (blue), the second $\varepsilon_h = 0.2$ (red), and the last $\varepsilon_h = 20$ (green). In all plots the value of ε_λ is fixed at $\varepsilon_\lambda = 0.1$. Increasing $\varepsilon_h = 2\delta_s/h$ corresponds to increasing the boundary layer thickness δ_s relative to the height of the channel h. When $\varepsilon_h > 1$ the two boundary layers thus overlap. Notice in particular the plots of v_{1y} in row (c). For $\varepsilon_h = 20$ the profile along $\tilde{z}$ becomes parabolic, while an inspection of the contourplots shows that the field becomes constant in the $\tilde{y}$-direction.

The plots of Fig. 3.6(b)-(d) were generated like those of Fig. 3.5 with the field amplitudes maximized to try to achieve resonance conditions for each value of ε_h. Considering the flow profile $v_{1y}(\tilde{z})$ we see from Fig. 3.6(b) how increasing the value of ε_h from 0.05 to 1 gives profiles from the acoustic resonant regime with narrow boundary layers to the

parabolic profile in the shear flow regime. Note that each solution is normalized by the maximum amplitude in the full channel. The shear flow profile would have much smaller amplitude than the acoustic profiles because the resonance is suppressed in the shear flow regime. This may be recognized from Fig. 3.6(d) showing a lineplot of $v_{1y}(\tilde{y})$ along the horizontal direction of the channel where the acoustic regime results in a cosine profile. The figure shows how the horizontal wave is slowly suppressed when ε_h is increased. There is still some resonant wave character in the horizontal direction for $\varepsilon_h = 1$, but for $\varepsilon_h = 4$ the velocity $v_{1y}(\tilde{y})$ becomes constant along the $\tilde{y}$-direction consistent with a Poiseuille flow solution.

A poiseuille flow solution has a linear pressure drop along the length of the channel in the horizontal $\tilde{y}$-direction. As seen in Fig. 3.6(c) the analytical solution does indeed change from a sine-wave along $\tilde{y}$ in the acoustic regime of small ε_h to the expected linear pressure variation along $\tilde{y}$ for $\varepsilon_h = 4$.

We proceed to show that our analytical solution does indeed describe a low frequency Poiseuille flow as indicated in the plots of Fig. 3.6. Considering the regime illustrated in Fig. 3.6(a) we assume that $\varepsilon_h = 2\delta_\mathrm{s}/h > 10$ such that the shear flow requirement of the boundary layer extending along the whole height of the channel is fulfilled. If one assumes that pressure variation along the height of the channel is insignificant, which is true in the shear flow limit, then the wavenumbers may be approximated analytically as given in Eq. (3.47). Written on dimensionless form the wavenumbers are

$$\tilde{k}_y = \varepsilon_\lambda \sqrt{\frac{(1-\mathrm{i}) + (\gamma-1) f_\mathrm{t}}{(1-\mathrm{i}) - f_\mathrm{s}}}, \quad \tilde{k}_z = -\mathrm{i}\varepsilon_\lambda \sqrt{\frac{f_\mathrm{s} + (\gamma-1) f_\mathrm{t}}{(1-\mathrm{i}) - f_\mathrm{s}}}, \tag{3.58}$$

with f_s and f_t given in terms of the dimensionless parameters in Eq. (3.54b). In the case under consideration we may further expand in the parameter $1/\varepsilon_h < 1$. One finds for f_s and f_t

$$f_\mathrm{s} = (1-\mathrm{i})\left[1 - \frac{1}{3}\frac{(1-\mathrm{i})^2}{\varepsilon_h^2}\right], \quad f_\mathrm{t} = (1-\mathrm{i})\left[1 - \frac{1}{3}\frac{(1-\mathrm{i})^2\,\mathrm{Pr}}{\varepsilon_h^2}\right]. \tag{3.59}$$

Going to first order in $1/\varepsilon_h$ we obtain the wavenumbers

$$\tilde{k}_y = \frac{\sqrt{3\gamma}}{2}(1+\mathrm{i})\varepsilon_h \varepsilon_\lambda, \quad \tilde{k}_z = -\mathrm{i}\tilde{k}_y. \tag{3.60}$$

Considering the pressure solution in Eq. (3.53) it becomes apparent that in order to get a pressure constant along $\tilde{z}$ and linear in $\tilde{y}$ corresponding to a Poiseuille flow, one must require that

$$\frac{\tilde{k}_y}{\varepsilon_w} \ll 1, \quad \frac{\tilde{k}_z}{\varepsilon_h} \ll 1, \tag{3.61}$$

and go to first order when expanding in these parameters. Using the wavenumbers in Eq. (3.60) we see that this is equivalent to requiring that

$$\frac{\varepsilon_\lambda \varepsilon_h}{\varepsilon_w} \ll 1, \quad \varepsilon_\lambda \ll 1. \tag{3.62}$$

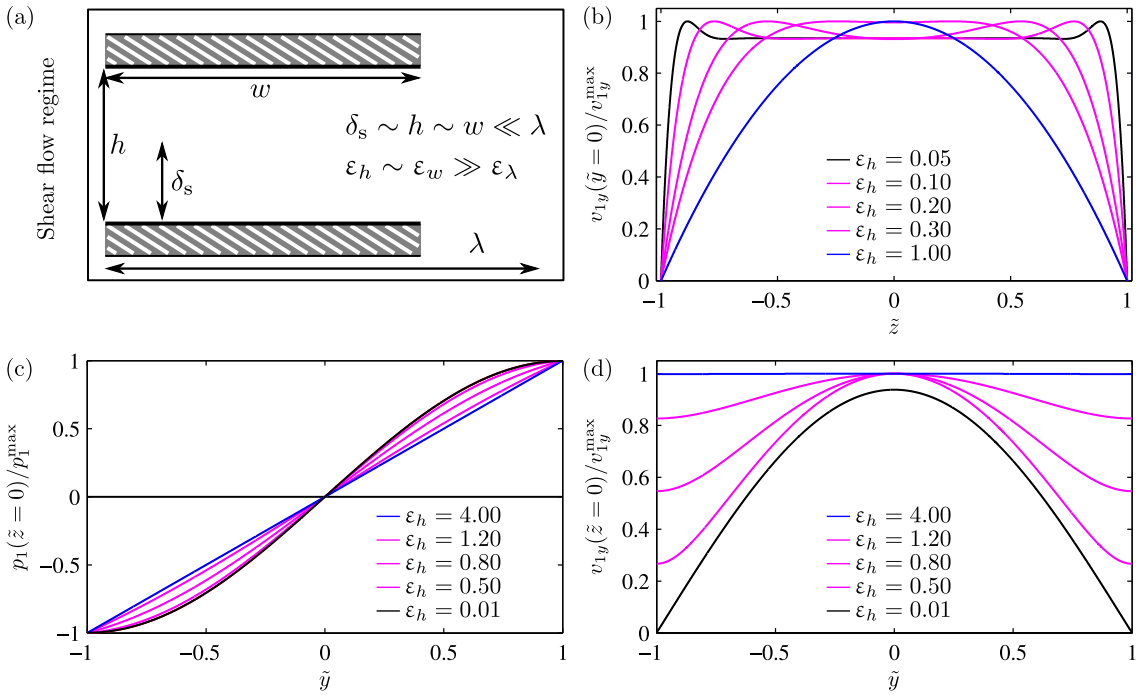

Figure 3.6: In this figure we study the transition from resonant acoustic fields to shear flow solutions when increasing ε_h corresponding to increasing boundary layer thicknesses. For $\varepsilon_h = 1$ the two boundary layers begin to overlap. In all plots the value of ε_λ is fixed at $\varepsilon_\lambda = 0.01$, and the fields are normalized by the maximum amplitude in the full channel. (a) Illustration of the shear flow solution regime and the conditions that must be met. (b) Lineplot of the normalized horizontal velocity component $v_{1y}(\tilde{z})$ along the vertical $\tilde{z}$-direction showing the growth of the viscous boundary layers and the resulting parabolic profile as ε_h is increased to 1. (c) Lineplot of the normalized pressure along the horizontal $\tilde{y}$-direction going from a sine-wave to a linear dependence of $\tilde{y}$ as ε_h is increased. (d) Lineplot of the horizontal velocity component $v_{1y}(\tilde{y})$ along the $\tilde{y}$-direction going from a cosine wave in the acoustic regime of small ε_h to a constant profile along $\tilde{y}$ in the shear flow regime as ε_h is increased. All observations of the fields in the shear flow limit are consistent with the classical Poiseuille flow solution oscillating at low frequency.

Now, ε_h and ε_w must be large in comparison to ε_λ and they are almost equal when comparing to the much smaller number ε_λ. Consequently, the first requirement above reduces to the second and we are left with the requirement that $\varepsilon_\lambda \ll 1$, which then allows an expansion to first order in the parameters $\tilde{k}_y/\varepsilon_w$ and $\tilde{k}_z/\varepsilon_h$ when expanding the fields. It is clear that $1/\varepsilon_h \gg \varepsilon_\lambda$ and expansions in $1/\varepsilon_h$ are at another level of approximation. Consequently, when going to first order in $\tilde{k}_y/\varepsilon_w$ and $\tilde{k}_z/\varepsilon_h$ (i.e., to first order in ε_λ) then the expansion in $1/\varepsilon_h$ should be at least to second order.

The pressure p_1 and the velocity components v_{1y} and v_{1z} of the shear flow limit are thus found from Eq. (3.53) going to first order in $\tilde{k}_y/\varepsilon_w$ and $\tilde{k}_z/\varepsilon_h$ (i.e., to first order in

ε_λ) and to second order in $1/\varepsilon_h$. One finds

$$\tilde{p}_1 = \mathrm{i}\frac{v_{\mathrm{bc}}}{c}\frac{\varepsilon_\lambda}{\varepsilon_w}\tilde{y}, \tag{3.63a}$$

$$\tilde{v}_{1y} = -\mathrm{i}\frac{v_{\mathrm{bc}}}{c}\frac{1}{\varepsilon_h^2}\left(1-\tilde{z}^2\right), \tag{3.63b}$$

$$\tilde{v}_{1z} = 0. \tag{3.63c}$$

Written with dimensional parameters the solution is

$$p_1 = -\frac{\Delta p}{w}y, \tag{3.64a}$$

$$\boldsymbol{v}_1 = \frac{\Delta p\, h^2}{8\eta_0 w}\left(1-\frac{4z^2}{h^2}\right)\mathbf{e}_y, \tag{3.64b}$$

where we have defined the pressure drop across the channel width, Δp, as

$$\Delta p = -\mathrm{i}\omega\rho_0 v_{\mathrm{bc}} w. \tag{3.64c}$$

Clearly, this is nothing but a slowly oscillating Poiseuille flow. In the limit of low frequencies the analytical solution of Eq. (3.43) thus results in a physically meaningful shear flow solution and a correct variation of the fields, attributable to a correct description of the boundary layers in the full domain of the channel.

Chapter 4

Microchannel acoustofluidics

The aim of this chapter is to study the field solution of the parallel-plate system found in Chapter 3 in a limit relevant to microchannel acoustofluidics. The development of an analytical solution that correctly resolves the boundary layers to first order in $k_0\delta_s$ was in part motivated by the numerical work of Muller *et al.* [24] with the numerical solution showing features of order $k_0\delta_s$ such as pressure variation perpendicular to walls, neglected in boundary layer theory approaches [12, 20, 22]. The system considered by Muller *et al.* models an experimental setup well characterized through a number of experiments published in Refs. [25, 27, 28, 33]. Fig. 4.1 is adapted from Refs. [27, 28] and shows the experimental setup. In our theoretical model we are concerned only with the vertical cross-section of the channel and assume translation invariance along the x-direction. For a start we are applying the theory of Chapter 3 assuming a parallel-plate configuration and consequently neglecting effects of the vertical sidewalls. Since the resonant component of velocity is the y-component this approximation is not as crude as it may seem. The actuation boundary condition then models vibrating walls. In Section 4.2.4 we discuss a possible way of extending the theory to include vertical sidewalls and we show that this leads to corrections of order $k_0\delta_s$ not affecting the resonant character of the fields.

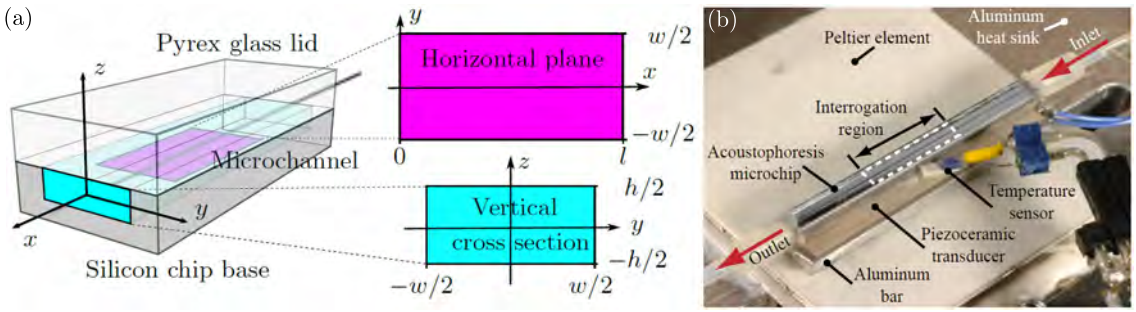

Figure 4.1: Adapted from Refs. [27, 28] showing the experimental system modeled in this chapter. (a) Schematic drawing of the long water-filled channel of width $w = 380\ \mu\text{m}$ and height $h = 160\ \mu\text{m}$. (b) Photo and description of the experimental setup by Augustsson *et al.* [27].

Referring to Fig. 4.1 we consider the model of Ref. [24] with channel width $w = 380\,\mu\text{m}$ and height $h = 160\ \mu\text{m}$ actuated at the vertical boundaries with the velocity amplitude $v_{\text{bc}} = \omega d_0$, with $d_0 = 0.1$ nm, a typical value of displacements resulting in resonant field amplitudes corresponding to experiments [24, 33]. For the fluid medium we will use the values for water at room temperature given in Table 2.1. In the numerical work of Ref. [24] the fundamental horizontal half-wave resonance was assumed to be excited at the frequency f_0 for which $w = \lambda_0/2$ giving $f_0 = c/2w = 1.97$ MHz. The boundary layer thicknesses evaluate to $\delta_{\text{s}} = 0.38\ \mu\text{m}$ and $\delta_{\text{t}} = 0.15\ \mu\text{m}$ and consequently $\delta_{\text{s}}/h \ll 1$ and $\delta_{\text{t}}/h \ll 1$. We will refer to this limit as the microchannel acoustofluidics limit. The aim of this chapter is to understand this limit using the analytical theory of Chapter 3. We will consider the resonance frequency, the acoustic energy density, the acoustic fields, the quality-factor of the resonance, characteristic timescales of the system, higher-mode solutions and inclusion of sidewalls, as well as the time-averaged second-order phenomenon of acoustic streaming.

4.1 Fundamental resonant mode

In this section we study the fundamental resonant mode obtained from the analytical theory in Chapter 3 and compare the results to those of the numerical model published in Ref. [24]. The fundamental resonant mode is obtained from the analytical field solution of Eq. (3.43) with the wavenumbers chosen for the fundamental horizontal half-wave, and the frequency tuned to resonance conditions where the field amplitudes are maximized. As will be shown in the next few sections the theory predicts a resonance frequency shifted away from the simple half-wave condition of $f_0 = c/2w$. Though the frequency shift is relatively small the acoustic energy density is twice as large at the true resonance frequency f_{res} as compared to the energy density at f_0.

4.1.1 Fundamental mode wavenumbers

In the limit of microchannel acoustophoresis where the boundary layer thicknesses are much smaller than the channel height, $\delta_{\text{s}}/h \ll 1$ and $\delta_{\text{t}}/h \ll 1$, the dispersion equation was solved analytically and the approximate wavenumbers given in Eq. (3.48). These are the fundamental mode wavenumbers, repeated here for clarity

$$\left.\begin{aligned} k_y^0 &= \frac{\omega}{c}\left[1 + \frac{(1+\text{i})}{2h}\left[\delta_{\text{s}} + (\gamma-1)\delta_{\text{t}}\right]\right] \\ k_z^0 &= -\text{i}\frac{\omega}{c}\sqrt{\frac{(1+\text{i})}{h}\left[\delta_{\text{s}} + (\gamma-1)\delta_{\text{t}}\right]} \end{aligned}\right\}, \quad \text{for} \quad \frac{\delta_{\text{s}}}{h}, \frac{\delta_{\text{t}}}{h} \ll 1, \tag{4.1}$$

where the superscript "0" indicates that $n = 0$ for the fundamental mode. The wavenumber k_y describes a wave with wavenumber close to ω/c being damped slightly by the effect of viscosity and thermal conduction from the boundaries. The wavenumber k_z is small in comparison to k_y and indeed $k_z h/2 \ll 1$ as must be the case for the fundamental mode in the limit of $\delta_{\text{s}} \ll h$.

4.1.2 Resonance condition

Consider the solution of the fields in Eq. (3.43). At resonance the field amplitudes are maximized and consequently resonance is achieved by tuning the frequency ω such that the prefactor $1/|\cos(k_y w/2)|$ becomes a maximum, i.e. $|\cos(k_y w/2)|$ should be minimized. The resonance frequency for the loss-less system is denoted ω_0 at which a standing half-wave spans the width, $w = \lambda_0/2$, giving $\omega_0 = \pi c/w$. Then the function to be minimized may be written down using the wavenumbers of Eq. (4.1) as

$$\cos\left(\frac{k_y w}{2}\right) = \cos\left(\frac{\pi}{2}\left[1 + \frac{1}{2h}\left[\delta_\mathrm{s} + (\gamma-1)\delta_\mathrm{t}\right]\right]\frac{\omega}{\omega_0} + \mathrm{i}\frac{\pi}{4h}\left[\delta_\mathrm{s} + (\gamma-1)\delta_\mathrm{t}\right]\frac{\omega}{\omega_0}\right). \tag{4.2}$$

Now, since

$$|\cos(A + \mathrm{i}\epsilon)|^2 = \cos^2 A\ \cosh^2\epsilon + \sin^2 A\ \sinh^2\epsilon, \tag{4.3}$$

the minima is found when the real part of the argument is equal to $(\pi/2 + p\pi)$, $p \in \mathbb{Z}$, such that the real part vanishes and the remaining term is suppressed by the factor $\sinh^2\epsilon \simeq \epsilon^2$, where $\epsilon \ll 1$. For the fundamental resonance with $p = 0$ we get to first order

$$\omega_\mathrm{res} = \left(1 - \frac{1}{2h}\left[\delta_\mathrm{s} + (\gamma-1)\delta_\mathrm{t}\right]\right)\omega_0. \tag{4.4}$$

The theory predicts a shift in resonance frequency not previously accounted for. As the energy lineshape function is very narrow around resonance the seemingly insignificant shift in the resonance frequency turns out to have crucial importance for obtaining the maximum energy density of the resonant field, as will be illustrated in Section 4.1.4.

4.1.3 Acoustic fields

Fig. 4.2 presents contourplots of the analytical solution for the fundamental resonant fields. Comparing to the numerical solution in Ref. [24] we find that the analytical solution correctly captures the features of the numerical solution, with the z-component of velocity an order $k_0\delta_\mathrm{s} \sim 10^{-3}$ smaller than the resonant y-component having the correct variation. The amplitudes are off in comparison to the numerical work in Ref. [24] because the shift in resonance frequency away from the simple condition of $f_0 = c/2w$ was not accounted for in Ref. [24] and consequently the amplitudes are lower. To compare the analytical theory with the numerical model without any fitting parameters, resonance conditions must be achieved in both models. With courtesy of Peter Muller [24] the numerical model was obtained and adapted to simulate the parallel-plate system at resonance frequency and we may thus compare the fields.

Fig. 4.3 presents lineplots along the height of the channel in $y = w/4$ indicated with blue dashed lines in the 2D plot of Fig. 4.2. The left column shows the variation along the full height of the channel, while the right column is a zoom of the the boundary layer region near $z = -h/2$. The figure presents a perfect agreement between the numerical model and the analytical theory. Note that there are no fitting parameters. Both models are actuated at the open boundaries with the same amplitude of velocity with the resulting resonant

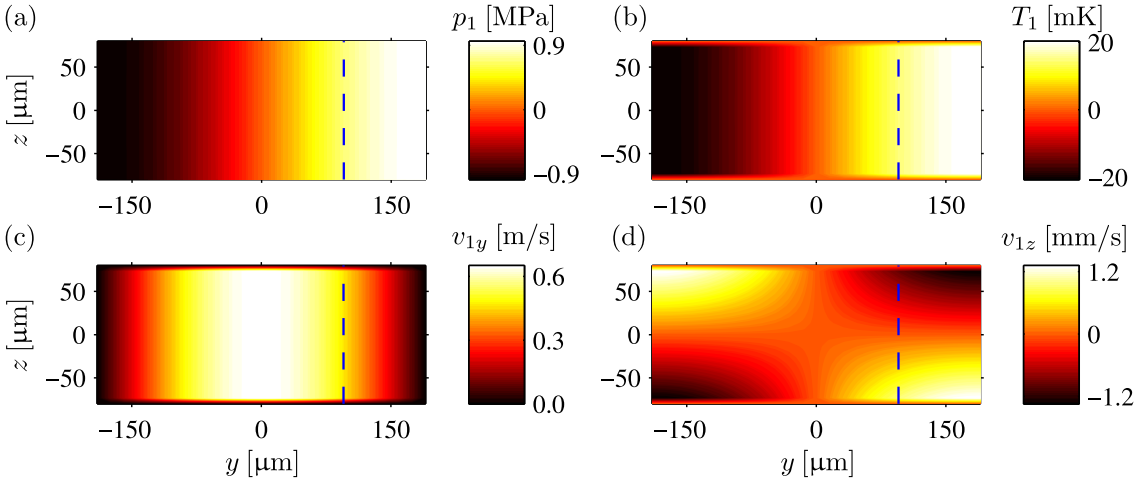

Figure 4.2: Contour plots of the analytical acoustic fields for the fundamental resonant mode in the vertical cross-section of the microchannel shown in Fig. 4.1. The dashed blue lines in $y = w/4$ indicate where the lineplots of Fig. 4.3 are taken. (a) Pressure field p_1. (b) Temperature field T_1. (c) Velocity field component v_{1y}. (d) Velocity field component v_{1z}. Note the scales on the velocity field components. The z-component of velocity is an order $k_0\delta_\mathrm{s} \sim 10^{-3}$ smaller than the resonant y-component.

field amplitude about 500 times larger. In the numerical model resonance is achieved with a frequency sweep and a fit of the acoustic energy density as a function of frequency as shown in Fig. 4.4(b), while in the analytical model resonance is achieved by maximizing the amplitudes using the field expressions of Eq. (3.43) as explained in Section 4.1.2.

4.1.4 Energy density and lineshape function

The energy density is an important quantity because it allows calculation of resonant field amplitudes, quality factors, and forces that may be observed in experiments. The acoustic energy stored in the system consists of the kinetic energy as well as the potential energy of the compressed fluid. The time-averaged acoustic energy density $\mathcal{E}_\mathrm{ac}$ is thus calculated as

$$\mathcal{E}_\mathrm{ac} = \frac{1}{2}\rho_0 \left\langle v_1^2 \right\rangle + \frac{1}{2}\kappa_s \left\langle p_1^2 \right\rangle = \frac{1}{4}\left(\rho_0 |v_1|^2 + \kappa_s |p_1|^2\right), \tag{4.5}$$

where we have used that the time-average of a product of two time-harmonic fields can be calculated as $\langle A(t)B(t)\rangle = \mathrm{Re}\left[A_0 B_0^*\right]/2$.

It is often convenient to consider the averaged acoustic energy density E_ac obtained as the average over volume of $\mathcal{E}_\mathrm{ac}$. For a harmonically oscillating system we moreover note that the potential and kinetic energies are equal. Consequently, we may evaluate the average acoustic energy density E_ac from the pressure alone, which simplifies calculations considerably.

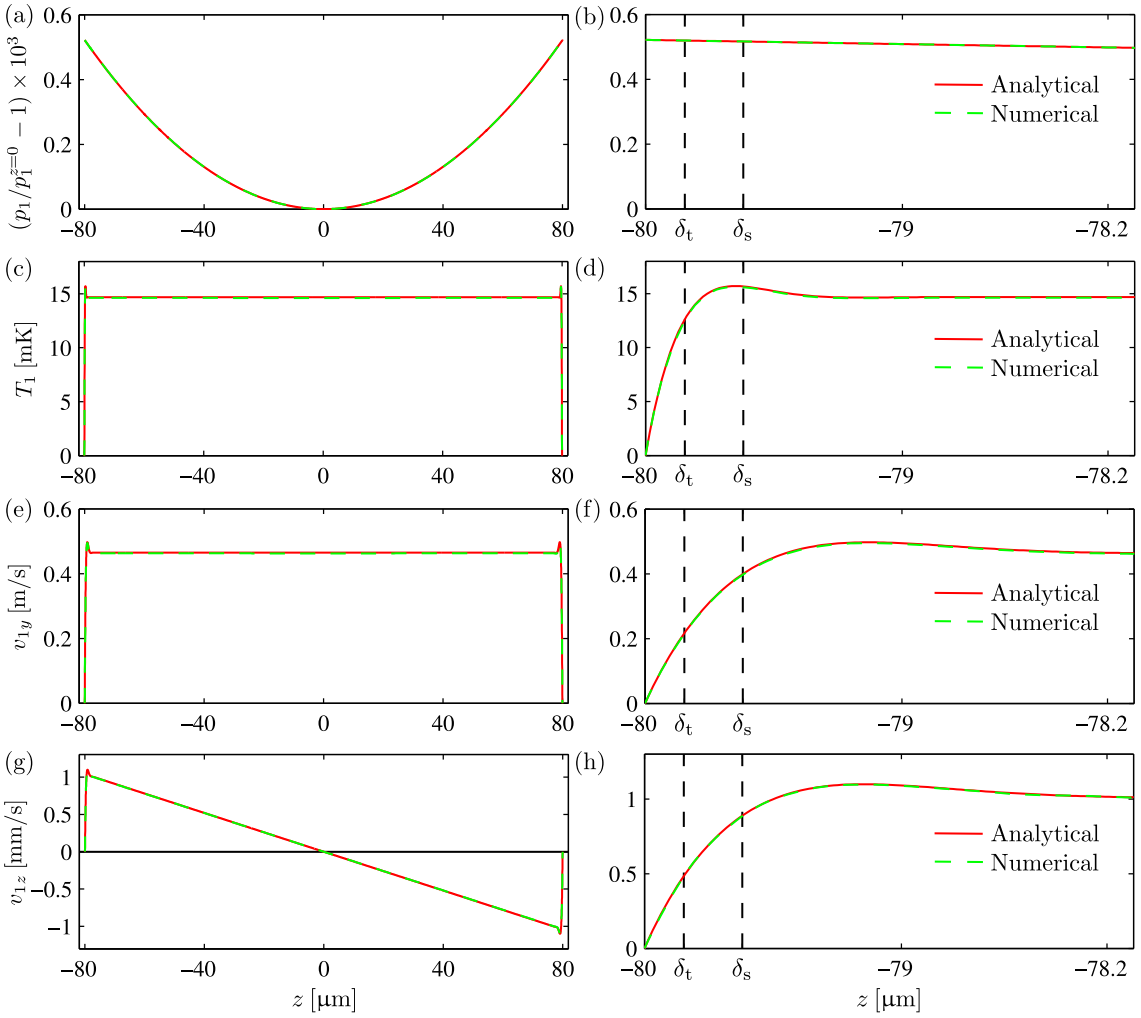

Figure 4.3: Lineplots of the analytical and numerical solution of the acoustic fields for the fundamental resonant mode taken at the cutlines in $y = w/4$ as indicated with dashed blue lines in the contourplots of Fig. 4.2. There is a perfect agreement between the analytical theory and the numerical model of Muller *et al.* [24]. This is not a fit and there are no free parameters. The left column shows the variation along the full height of the channel, while the right column is a zoom of the boundary layer region near $z = -h/2$. (a)-(b) Pressure field p_1. The plot shows $(p_1/p_1^{z=0} - 1) \times 10^3$ in order to show the pressure variation along the height of the channel which is first order in $k_0\delta_s$. (c)-(d) Temperature field T_1. (e)-(f) Velocity field component v_{1y}. (g)-(h) Velocity field component v_{1z}.

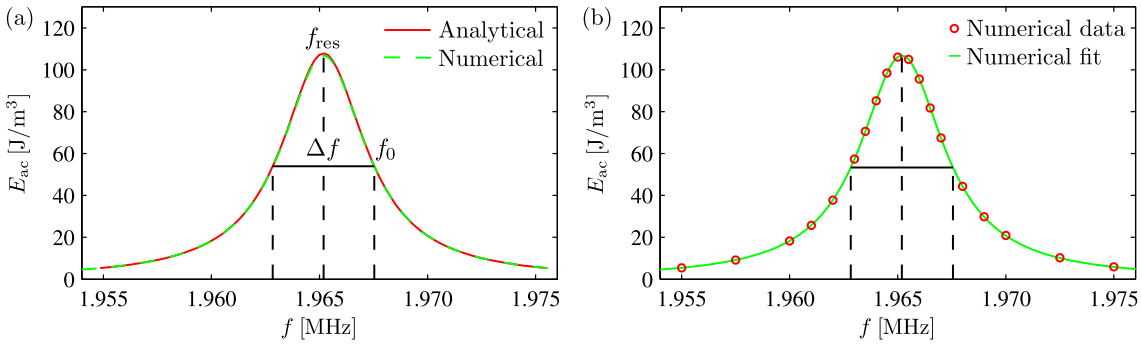

Figure 4.4: Average acoustic energy density E_{ac} plotted as a function of actuation frequency f. The resonance is sharply peaked around the resonance frequency f_{res} shifted downwards from the half-wavelength resonance frequency $f_0 = c/2w$ of the lossless system. The full-width-half-maximum Δf is indicated with a horizontal black line. (a) Analytical Lorentzian energy lineshape function of Eq. (4.8) compared to the energy lineshape function obtained from the numerical model. There is good agreement with no free parameters. (b) Data from the numerical model. The numerical energy lineshape function was obtained as the fit of the data points indicated in the figure.

For the 2D system under consideration,

$$\begin{aligned} E_{ac} &= \frac{1}{hw}\int_{-h/2}^{h/2} \mathrm{d}z \int_{-w/2}^{w/2} \mathrm{d}y \left(\frac{1}{4}\rho_0 |v_1|^2 + \frac{1}{4}\kappa_s |p_1|^2 \right), \\ &\simeq \frac{1}{hw}\int_{-h/2}^{h/2} \mathrm{d}z \int_{-w/2}^{w/2} \mathrm{d}y \left(\frac{1}{2}\kappa_s |p_1|^2 \right). \end{aligned} \tag{4.6}$$

Inserting the pressure obtained in Eq. (3.43) with variation along the z-direction neglected since $k_z h/2 \ll 1$, and moreover using that $k_y \simeq \omega/c \simeq \pi/w$ near resonance due to the smallness of δ_s/h and δ_t/h one finds

$$\begin{aligned} E_{ac} &\simeq \frac{1}{2w}\kappa_s \omega^2 \rho_0^2 \frac{v_{bc}^2}{|k_y|^2} \frac{1}{|\cos\left(k_y w/2\right)|^2} \int_{-w/2}^{w/2} \mathrm{d}y |\sin\left(k_y y\right)|^2, \\ &\simeq \frac{1}{4}\rho_0 v_{bc}^2 \frac{1}{|\cos\left(k_y w/2\right)|^2}. \end{aligned} \tag{4.7}$$

Here it was used that $\kappa_s = 1/\rho_0 c^2$. For the factor $1/|\cos(k_y w/2)|^2$ we cannot neglect the small imaginary part of the wavenumber because the energy density would then diverge at resonance conditions. Instead we expand around resonance conditions to obtain the energy lineshape function $E_{ac}(\omega)$. A few calculational details are given in Section B.1 of Appendix B. The result is the Lorentzian energy lineshape function

$$E_{ac} = \frac{\rho_0 v_{bc}^2}{\pi^2} \frac{\omega_{res}^2}{(\omega - \omega_{res})^2 + \Gamma_{sys}^2 \omega_{res}^2}, \quad \text{for} \quad \omega \simeq \omega_{res}. \tag{4.8}$$

Here we have defined the complete thermoviscous damping factor of the parallel-plate microsystem Γ_{sys} as

$$\Gamma_{\text{sys}} = \frac{1}{2h}\left[\delta_{\text{s}} + (\gamma - 1)\delta_{\text{t}}\right]. \tag{4.9}$$

The Lorentzian energy lineshape function is plotted in Fig. 4.4 with the datapoints and the fit obtained from the numerical model. Again, without any fitting parameters, we find perfect agreement between the analytical theory and the numerical model. The energy lineshape function was measured experimentally for a system similar to that of Fig. 4.1 showing the same Lorentzian form of the main resonance peak [33].

4.1.5 Quality factor of the resonance

The quality factor of the resonance known as the Q-factor is another important quantity that may be measured experimentally [33]. The Q-factor of the resonance is defined as

$$Q = 2\pi \frac{\text{Energy stored}}{\text{Energy dissipated per cycle}}, \tag{4.10}$$

and may be obtained from the energy lineshape function as

$$Q = \frac{\omega_{\text{res}}}{\Delta\omega}, \tag{4.11}$$

where $\Delta\omega$ is the full-width half-maximum of the energy lineshape function. Consequently we may evaluate the Q-factor from the expression for E_{ac} in Eq. (4.8). The result is

$$\Delta\omega = 2\Gamma_{\text{sys}}\omega_{\text{res}}, \tag{4.12a}$$

$$Q = \frac{1}{2\Gamma_{\text{sys}}} = \frac{h}{\delta_{\text{s}} + (\gamma - 1)\delta_{\text{t}}}. \tag{4.12b}$$

We note that $\omega_0 - \omega_{\text{res}} = \Gamma_{\text{sys}}\omega_0 \simeq \Gamma_{\text{sys}}\omega_{\text{res}}$, so that the frequency shift away from the simple resonance condition is approximately equal to the half-width half-maximum of the energy lineshape function.

For the system under consideration we find $Q = 418$ which is the correct order of magnitude as compared to experiments with measured values of 577 and 209 [33]. The losses are introduced by viscous shear loss in the viscous boundary layers and by heat conduction into the walls through the thermal boundary layers. Q-factors agreeing well with experiments cannot be obtained without considering these two mechanisms. For a 1D system with bulk losses only, one obtains Q-factors of order 10^{-5} [14]. With the analytical theory we have thus explained the Q-factors obtained experimentally [33], and we have identified the most important damping mechanism of the experimental system to be the dissipation in the narrow boundary layers.

From the definition of the Q-factor it follows that $Q/2\pi$ gives the number of cycles necessary to dissipate the stored energy if the actuation stops, or alternatively the number of cycles necessary to build up the resonant field once the actuation starts. Consequently,

$$\tau_{\text{res}} = \frac{Q}{2\pi}\tau_{\text{cycle}} = \frac{Q}{\omega} \simeq 34\ \mu\text{s}. \tag{4.13}$$

is the timescale on which the resonance is set up or shut down once the actuation is turned on or off.

4.2 Higher-mode wavenumbers

We are concerned with the dispersion equations relating the complex wavenumbers k_y and k_z and we will look for higher mode solutions in the limit relevant to microchannel acoustophoresis applications. For simplicity we consider the isentropic limit without heat conduction, where the dispersion equation Eq. (3.42) reduces. The equations for the wavenumbers are then

$$k_y^2 = \frac{(\mathrm{i}-1)}{\delta_\mathrm{s}} \frac{k_z}{\tanh\left[(1-\mathrm{i})h/2\delta_\mathrm{s}\right]} \tan\left(\frac{k_z h}{2}\right), \tag{4.14a}$$

$$k_\mathrm{c}^2 = k_y^2 + k_z^2, \quad k_\mathrm{c} = (\omega/c)\left[1 + \mathrm{i}\Gamma_\mathrm{s}/2\right]. \tag{4.14b}$$

4.2.1 Analytical solution of the dispersion equation

To find an analytical approximation we first note that $\tanh\left[(1-\mathrm{i})x\right] = 1$ for $x \gg 1$, and consequently in the microchannel acoustofluidics limit we may set $\tanh\left[(1-\mathrm{i})h/2\delta_\mathrm{s}\right] = 1$. Assuming that pressure variation perpendicular to the walls is small such that $k_z h/2 \ll 1$ and expanding the tangent around zero leads to the fundamental resonant mode as shown in Section 3.3.1. For higher mode solutions we cannot make this assumption.

Combining the two equations in Eq. (4.14) we obtain an equation for k_z,

$$k_\mathrm{c}^2 = k_z^2 - (1-\mathrm{i})\frac{1}{\delta_\mathrm{s}} k_z \tan\left(\frac{k_z h}{2}\right). \tag{4.15}$$

We will normalize the equation using the following normalization, different from that of Chapter 3,

$$\tilde{k}_\mathrm{c} = k_\mathrm{c} h, \quad \tilde{k}_z = k_z h, \quad \tilde{k}_y = k_y h. \tag{4.16}$$

Then

$$\tilde{k}_\mathrm{c}^2 = \tilde{k}_z^2 - (1-\mathrm{i})\frac{h}{\delta_\mathrm{s}} \tilde{k}_z \tan\left(\frac{\tilde{k}_z}{2}\right). \tag{4.17}$$

Note that $\tilde{k}_\mathrm{c} = k_\mathrm{c} h \simeq \pi h/w \sim 1$, and consequently the left hand side of Eq. (4.17) is of order unity. Introducing the small parameter $\varepsilon_h = 2\delta_\mathrm{s}/h \sim 10^{-3}$, Eq. (4.17) may be written

$$\tilde{k}_\mathrm{c}^2 = \tilde{k}_z \left[\tilde{k}_z - (1-\mathrm{i})\frac{2}{\varepsilon_h} \tan\left(\frac{\tilde{k}_z}{2}\right)\right]. \tag{4.18}$$

Since the right hand side has to be of order unity in order to match the left hand side the tangent must be of order ε_h in order to cancel the prefactor $1/\varepsilon_h$. Consequently the argument must be close to an integer times π. We write

$$\tilde{k}_z = 2\pi n + \tilde{\varepsilon}, \quad n = 1, 2, ... \tag{4.19}$$

Expanding $\tan(\tilde{k}_z/2)$ to first order in $\tilde{\varepsilon}$ around $n\pi$ yields

$$\tan\left(\frac{\tilde{k}_z}{2}\right) = \tan\left(n\pi + \frac{\tilde{\varepsilon}}{2}\right) \simeq \tan(n\pi) + [1 + \tan(n\pi)]^2 \frac{\tilde{\varepsilon}}{2} = \frac{\tilde{\varepsilon}}{2}. \tag{4.20}$$

Inserting the expansion into the normalized dispersion equation Eq. (4.17) and rearranging, we get the following quadratic equation for $\tilde{\varepsilon}$

$$\left[1 - (1 - \mathrm{i})\frac{h}{2\delta_\mathrm{s}}\right]\tilde{\varepsilon}^2 + 4\pi n\left[1 - (1 - \mathrm{i})\frac{h}{4\delta_\mathrm{s}}\right]\tilde{\varepsilon} + (2\pi n)^2 - \tilde{k}_\mathrm{c}^2 = 0. \tag{4.21}$$

In the limit of microchannel acoustofluidics terms of order h/δ_s are much larger than unity and the equation reduces to give

$$\tilde{\varepsilon}^2 + 2\pi n\tilde{\varepsilon} - \frac{\delta_\mathrm{s}}{h}(1 + \mathrm{i})\left[(2\pi n)^2 - \tilde{k}_\mathrm{c}^2\right] = 0. \tag{4.22}$$

This is a standard quadratic equation. Going to first order in δ_s/h the solution is

$$\tilde{\varepsilon}_\pm = -\pi n\left[1 \pm \left(1 + 2(1 + \mathrm{i})\frac{\delta_\mathrm{s}}{h}\left[1 - \left(\frac{\tilde{k}_\mathrm{c}}{2\pi n}\right)^2\right]\right)\right]. \tag{4.23}$$

The second root arising from the minus sign is the physical solution where $\tilde{\varepsilon}$ is indeed small. Consequently we set $\tilde{\varepsilon} = \tilde{\varepsilon}_-$ to find the approximate higher-mode wavenumbers $\tilde{k}_z = 2\pi n + \tilde{\varepsilon}$. Finally using $k_z = \tilde{k}_z/h$ the approximate solution for the higher-mode wavenumbers is

$$k_z^n = \frac{2\pi n}{h}\left[1 + (1 + \mathrm{i})\frac{\delta_\mathrm{s}}{h}\left[1 - \left(\frac{k_\mathrm{c}h}{2\pi n}\right)^2\right]\right], \quad n = 1, 2, ... \tag{4.24}$$

We expect this analytical result to be a good approximation as long as $\tilde{\varepsilon}/2 \ll 1$ such that the first-order expansion of the tangent remains a good approximation. This means the result is valid as long as n remains sufficiently small. We may find the values of n for which $\tilde{\varepsilon}/2 < 0.1$. Using the parameters of the system under consideration we find that $\tilde{\varepsilon}/2 < 0.1$ for $n < 13$.

4.2.2 Numerical solution of the dispersion equation

The dispersion equation may of course also be solved numerically. Take the normalized dispersion equation Eq. (4.17) and split the wavenumber into real and imaginary parts

$$\tilde{k}_z = \tilde{k}_z^\mathrm{r} + \mathrm{i}\tilde{k}_z^\mathrm{i}, \quad \tilde{k}_z^\mathrm{r}, \tilde{k}_z^\mathrm{i} \in \mathbb{R}. \tag{4.25}$$

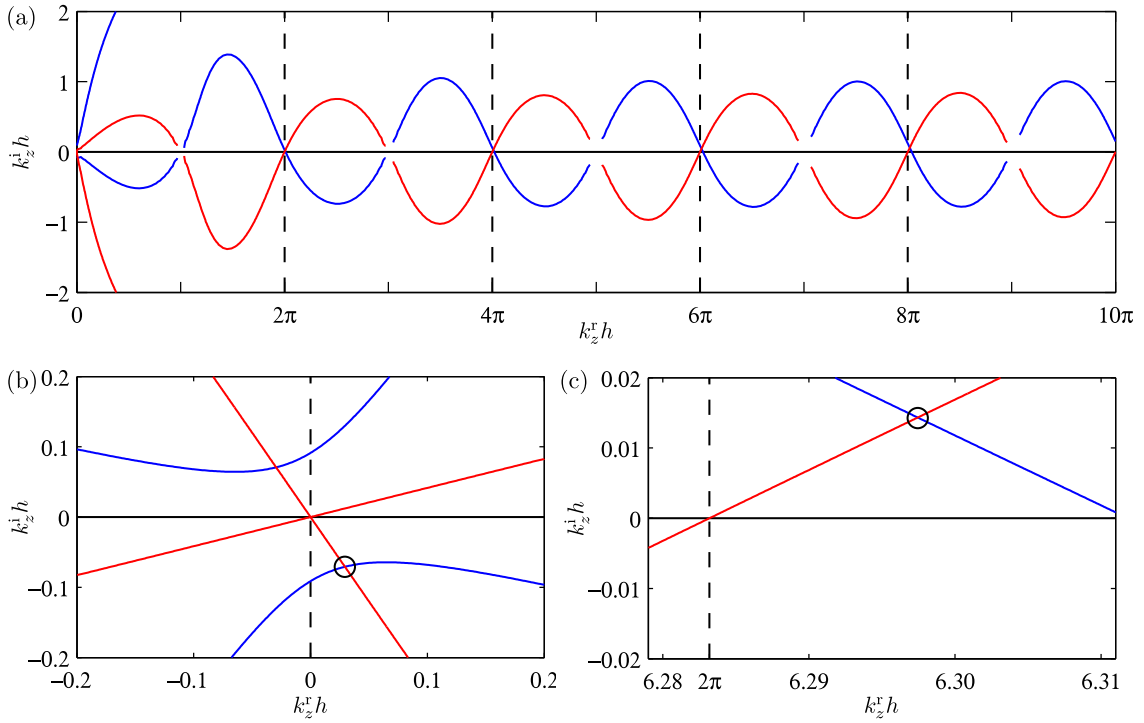

Figure 4.5: Graphical solution of the dispersion equation Eq. (4.17) for the wavenumber k_z. Red/blue graphs show contours of solutions for the real/imaginary equations in Eq. (4.26) in the $(\tilde{k}_z^{\mathrm{r}}, \tilde{k}_z^{\mathrm{i}})$-plane. Solutions of the dispersion equation are found where both equations are satisfied at intersections. (a) Solutions are close to periodic with the real part approximately equal to $\tilde{k}_z^{\mathrm{r}} \simeq n2\pi$, $n \in \mathbb{Z}$. (b) Zoom showing the fundamental mode solution for which $k_z h/2 \ll 1$ with the analytical result of Eq. (4.1) indicated with a black circle. (c) The first higher mode solution for which $n = 1$ with the black circle indicating the analytical result of Eq. (4.24).

Plugging this into Eq. (4.17) gives the following two equations from the requirement that the real and the imaginary part of the equation must be satisfied independently

$$(\tilde{k}_z^{\mathrm{r}})^2 - (\tilde{k}_z^{\mathrm{i}})^2 - h^2(\omega/c)^2\left[1 - (\Gamma_{\mathrm{s}}/2)^2\right] - \frac{h}{\delta_{\mathrm{s}}}\left[G^{\mathrm{r}}(\tilde{k}_z^{\mathrm{r}} + \tilde{k}_z^{\mathrm{i}}) - G^{\mathrm{i}}(\tilde{k}_z^{\mathrm{i}} - \tilde{k}_z^{\mathrm{r}})\right] = 0, \quad (4.26a)$$

$$2\tilde{k}_z^{\mathrm{r}}\tilde{k}_z^{\mathrm{i}} - \Gamma_{\mathrm{s}}h^2(\omega/c)^2 - \frac{h}{\delta_{\mathrm{s}}}\left[G^{\mathrm{r}}(\tilde{k}_z^{\mathrm{i}} - \tilde{k}_z^{\mathrm{r}}) + G^{\mathrm{i}}(\tilde{k}_z^{\mathrm{r}} + \tilde{k}_z^{\mathrm{i}})\right] = 0, \quad (4.26b)$$

where $G^{\mathrm{r}}, G^{\mathrm{i}} \in \mathbb{R}$ are defined from $\tan[(\tilde{k}_z^{\mathrm{r}} + \mathrm{i}\tilde{k}_z^{\mathrm{i}})/2] = G^{\mathrm{r}} + \mathrm{i}G^{\mathrm{i}}$, with explicit expressions given in Eq. (B.8).

Using Matlab we implicitly plot the zero contours of the two equations in Eq. (4.26) in the $(\tilde{k}_z^{\mathrm{r}}, \tilde{k}_z^{\mathrm{i}})$-plane using `ezplot`. The points at which the two zero contours intersect then give the solutions to the dispersion equation. One could also use a numeric method to search for solutions in given intervals. Fig. 4.5 shows the graphical solution. We find that

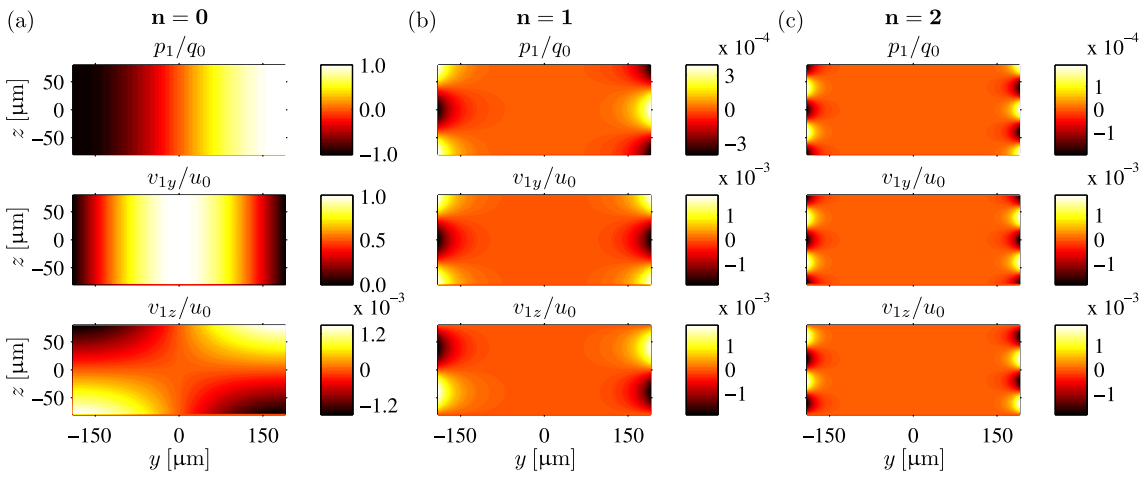

Figure 4.6: Higher mode field solutions. The pressure fields are normalized by the fundamental mode ($n = 0$) pressure amplitude q_0, while the velocity fields are normalized by the fundamental mode amplitude of v_{1y} denoted as u_0. (a) Fundamental mode, $n = 0$. (b) First higher mode, $n = 1$. (c) Second higher mode, $n = 2$. The higher-order modes are damped in the bulk and take significant values only at the domain ends in $y = \pm w/2$.

solutions are close to periodic in $\tilde{k}_z^{\mathrm{r}}$ as predicted from the analytical solution in Eq. (4.24), with solutions generally having a very small imaginary part while the real part grows between solutions with approximately 2π.

4.2.3 Higher-mode field solutions

We investigate the first few higher-mode field solutions using the analytical wavenumbers obtained from Eq. (4.24) and for the fundamental mode Eq. (3.48). Inserting the wavenumbers in the expressions for the first-order fields of Eq. (3.43) in the isentropic limit we may evaluate the pressure field p_1 and the velocity field $\boldsymbol{v}_1$ for the the higher-mode field solutions. With the parameters of Table 2.1 we obtain the following numeric values for the wavenumbers

$$\begin{aligned} k_y^0 &= \left[8.27 \times 10^3 + \mathrm{i}\, 9.81 \times 10^0\right] \ \mathrm{m}^{-1}, \quad k_z^0 = \left[1.83 \times 10^2 - \mathrm{i}\, 4.42 \times 10^2\right] \ \mathrm{m}^{-1}, \\ k_y^1 &= \left[9.12 \times 10^1 - \mathrm{i}\, 3.85 \times 10^4\right] \ \mathrm{m}^{-1}, \quad k_z^1 = \left[3.94 \times 10^4 + \mathrm{i}\, 8.91 \times 10^1\right] \ \mathrm{m}^{-1}, \\ k_y^2 &= \left[1.86 \times 10^2 - \mathrm{i}\, 7.83 \times 10^4\right] \ \mathrm{m}^{-1}, \quad k_z^2 = \left[7.87 \times 10^4 + \mathrm{i}\, 1.85 \times 10^2\right] \ \mathrm{m}^{-1}. \end{aligned} \tag{4.27a}$$

From the relative size of the real and imaginary parts of the wavenumbers it is clear that the fundamental mode has a wave-behavior in the y-direction while the higher mode solutions are damped in the y-direction and have wave-behavior along the z-direction instead.

Fig. 4.6 presents graphical results for the fundamental mode and the first two higher-mode field solutions. The phases in the figure were chosen to maximize the features of the characteristic solutions. The plot confirms that the higher the mode, the more damped it is in the y-direction such that the solution takes significant values only near the domain

ends at $y = \pm w/2$, where velocities oscillate almost as perfect sines along the z-direction as discussed in more detail in the next section. The higher modes have a lower amplitude as compared to the fundamental mode, with velocities comparable to the fundamental mode only at the domain ends in $y = \pm w/2$.

4.2.4 Inclusion of sidewalls using a superposition of modes

Fig. 4.7(a) shows the velocity component $v_{1z}(z)$ evaluated at the domain end in $y = w/2$ for the fundamental mode and the first two higher-mode solutions. As is evident from these plots combined with the expressions for the higher-mode wavenumbers and the first-order fields, the higher-mode solutions for v_{1z} constitute an approximate sine-basis along the z-direction at the domain ends in $y = \pm w/2$. The fundamental mode has a completely different character with the v_{1z} component growing exponentially in the boundary layer and falling off approximately linear along the z-direction.

The analytical solution for the first-order fields found in Chapter 3 is for the parallel-plate system with no restrictions on the v_{1z} component at the domain ends in $y = \pm w/2$. We see that a possible way to include sidewalls and fulfill the no-slip condition on the v_{1z} component at the domain ends in $y = \pm w/2$ is to use a superposition of modes. Indeed, the higher mode solutions are negligible with respect to the fundamental resonant field in the bulk, but at the domain ends they are comparable in amplitude to the fundamental mode and may thus be used to extinguish the velocity component v_{1z}.

Due to symmetry we need only consider one of the domain ends and we choose $y = w/2$. The following result for $v_{1z}^n(w/2, z)$ is obtained using the solution of Eq. (3.43) in the isentropic limit

$$v_{1z}^n(w/2, z) = A_n \left[\sin\left(k_z^n z\right) - B_n \sinh\left[(1 - \mathrm{i})z/\delta_\mathrm{s}\right]\right], \quad n = 0, 1, 2, \ldots, \tag{4.28a}$$

where

$$A_n = -v_\mathrm{bc}\frac{k_z^n}{k_y^n}\frac{\sin\left(k_y^n w/2\right)}{\cos\left(k_y^n w/2\right)}, \quad B_n = \frac{\sin\left(k_z^n h/2\right)}{\sinh\left[(1 - \mathrm{i})h/(2\delta_\mathrm{s})\right]}, \quad n = 0, 1, 2, \ldots . \tag{4.28b}$$

For the higher-order modes we will use the analytical wavenumbers of Eq. (4.24) going to zeroth order in $\delta_\mathrm{s}/h \ll 1$, which gives the wavenumbers

$$k_z^n \simeq \frac{2\pi n}{h}, \quad n = 1, 2, \ldots, \tag{4.29}$$

and thus $B_n = 0$ for $n = 1, 2, \ldots$. Then

$$v_{1z}^n(w/2, z) \simeq A_n \sin\left(2\pi n \frac{z}{h}\right), \quad n = 1, 2, \ldots, \tag{4.30}$$

and consequently $v_{1z}^n(w/2, z)$ approximately constitute a complete sine-basis in the z-direction as seen for the first two higher modes in Fig. 4.7(a).

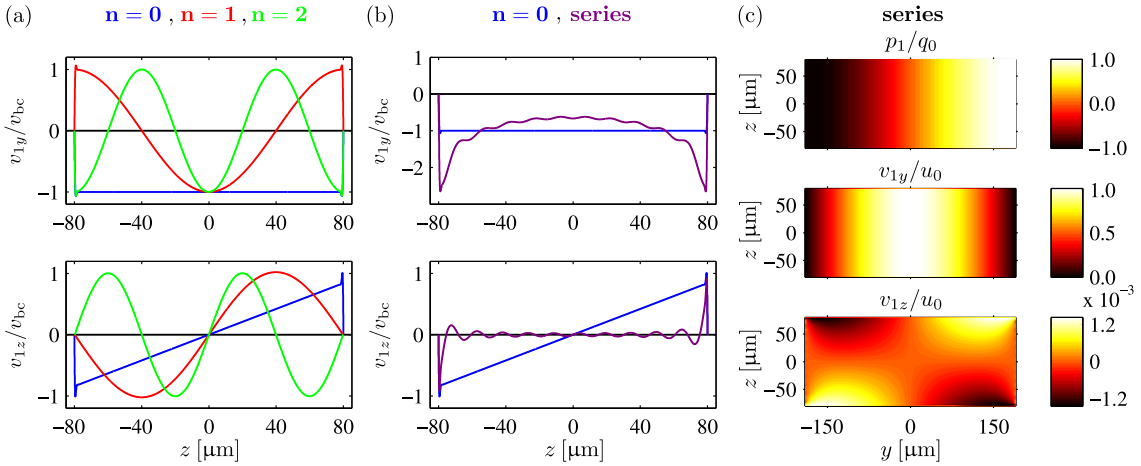

Figure 4.7: (a) Line-plots along the z-direction for the velocity fields evaluated at the domain end in $y = w/2$ for the fundamental mode (blue), the first higher-mode (red), and the second higher-mode (green). The velocities are normalized by the driving velocity v_{bc}. Phases are chosen to show the characteristics of each mode. (b) Same as in (a) showing the fundamental mode (blue) and a superposition of modes according to Eq. (4.33) which fulfills the no-slip condition of sidewalls, truncated at $N = 10$ (violet). (c) Contour plot of the field solution calculated from Eq. (4.33) as a superposition of modes with $N = 10$ to include the effects of sidewalls. The pressure is normalized by the pressure amplitude of the fundamental mode ($n = 0$) denoted q_0, and the velocities are normalized by the fundamental mode amplitude of v_{1y} denoted by u_0.

Projecting $v_{1z}^0(w/2, z)$ onto the $v_{1z}^n(w/2, z)$-basis then corresponds to making a Fourier decomposition onto a general sine-basis on $z \in [-h/2, h/2]$. We write

$$v_{1z}^0(w/2, z) = \sum_{n=1}^{\infty} C_n \sin\left(2\pi n \frac{z}{h}\right), \tag{4.31a}$$

$$C_n = \frac{2}{h} \int_{-h/2}^{h/2} v_{1z}^0(w/2, z) \sin\left(2\pi n \frac{z}{h}\right) \mathrm{d}z. \tag{4.31b}$$

Some details on the evaluation of the expansion coefficients C_n are given in Section B.2.2 of Appendix B. The result is

$$C_n = (-1)^n 8\pi n A_0 \left[\frac{\sin\left(k_z^0 h/2\right)}{(k_z^0)^2 h^2 - (2\pi n)^2} + \mathrm{i} B_0 \frac{\sin\left(k_{\mathrm{s}} h/2\right)}{k_{\mathrm{s}}^2 h^2 - (2\pi n)^2} \right], \tag{4.32}$$

with $k_{\mathrm{s}} = (1 + \mathrm{i})/\delta_{\mathrm{s}}$ the usual shear wavenumber. The absolute value of the expansion coefficients C_n falls off as $1/n$ but due to the alternating sign the series is convergent [34].

From the calculations above we see that we may fulfill the requirement that $v_{1z}(\pm w/2, z) = 0$, corresponding to the no-slip boundary condition of sidewalls, by using the following su-

perposition of modes

$$p_1 = p_1^0 - \sum_{n=1}^{N} \frac{C_n}{A_n} p_1^n, \quad \boldsymbol{v}_1 = \boldsymbol{v}_1^0 - \sum_{n=1}^{N} \frac{C_n}{A_n} \boldsymbol{v}_1^n. \tag{4.33}$$

Fig. 4.7 shows the result of such a series solution using the truncation number $N = 10$. Note that the inclusion of higher mode solutions used to extinguish the v_{1z}-component of velocity at $y = \pm w/2$ alters the actuation profile of the v_{1y}-component of velocity at $y = \pm w/2$. Clearly this does not change the resonant character of the fundamental mode which is a result in itself. It means that the exact actuation profile is not important to the resonant character of the first-order fields, and thus a full-chip model including elastic walls is not needed for studying the first-order fields. However, the actuation profile may change features of order $k_0\delta_s$ for example in the v_{1z} component of velocity, and such changes could be important to the second-order fields.

4.3 Acoustic streaming in microchannels

Motivated by the experiments of Kundt [35] the phenomenon of acoustic streaming was first investigated theoretically by Lord Rayleigh [18]. The second-order time-averaged steady motion of the fluid has later been the subject of several analytical studies most notably by Schlichting [17], Nyborg [19], Hamilton *et al.* [20, 21], and Rednikov and Sadhal [22], as well as comprehensive numerical modeling by Muller *et al.* [24, 25]. Landau and Lifshitz [12] presents the classical Rayleigh-Schlichting theory employing boundary layer theory to solve the adiabatic second-order problem for the parallel-plate system in the limit of $\delta_s \ll h \ll \lambda$. The boundary layer approach relies on the simplified boundary layer equations for the first-order fields from which the simplified second-order boundary layer equations follow [12]. The bulk streaming rolls (Rayleigh streaming) illustrated in Fig. 4.8(a) are driven by tiny streaming rolls in the narrow boundary layers (Schlichting streaming) set up from the large shear stresses in the boundary layers. The Schlichting streaming rolls cannot be seen in Fig. 4.8(a) due to the thickness of the boundary layers $\delta_s \ll h$. However, in Fig. 4.8(b) a lineplot of the second-order streaming velocity near the boundary layer region is shown for $y = w/4$, and one observes the sign-change in the streaming velocity when moving along the z-direction from inside the boundary layer to outside the boundary layer indicating the transition from the Schlichting streaming to the Rayleigh streaming. This graph is generated from a numerical simulation using the model of Muller *et al.* [24].

In the classical analytical theory the asymptotic limit of the boundary layer solution for the second-order velocity gives an effective bulk streaming boundary condition that is used to solve the bulk equation. Since the boundary layer is very narrow $\delta_s \ll h$ the boundary layer streaming field near the wall (Schlichting streaming) is neglected and the effective boundary condition is used to solve for the streaming in the bulk (Rayleigh streaming).

Following this approach Muller *et al.* presented an anaytical solution in the limit of $\delta_s \ll h \sim \lambda$ [25], while the case of $\delta_s \sim h \ll \lambda$ was considered by Hamilton *et al.* [20, 21]. These analytical studies of streaming are all based on boundary layer theory neglecting

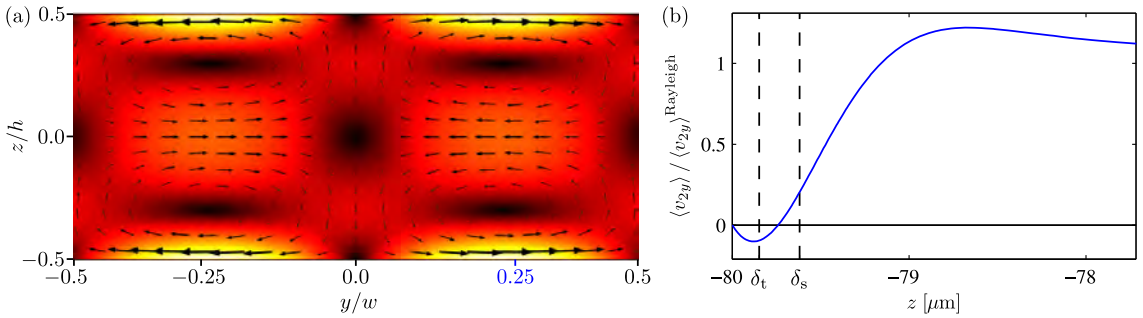

Figure 4.8: The second-order time-averaged steady motion of the fluid known as acoustic streaming as calculated from the thermoviscous numerical model of Muller *et al.* [24]. (a) Time-averaged second-order velocity field $\langle \boldsymbol{v}_2 \rangle$, with the color and the length of the arrows indicating the magnitude of the velocity. The four bulk streaming rolls known as Rayleigh streaming rolls are driven by Schlichting streaming rolls in the narrow boundary layers not visible. (b) Lineplot of the second-order time-averaged velocity field component $\langle v_{2y} \rangle$ taken along the z-direction in $y = w/4$, normalized by the adiabatic Rayleigh streaming boundary condition amplitude [18]. The plot shows only the region near the boundary layer at the bottom of the channel, showing the change in sign indicating the transition from the Schlichting boundary layer streaming to the bulk Rayleigh streaming.

pressure variation along the height of the channel, and a solution with no requirements on all length scales for which $\delta_s \sim h \sim \lambda$ has never been presented.

With the theory developed in Chapter 3 a solution in the full domain for which $\delta_s \sim h \sim \lambda$ may be within reach and we expect that a significant pressure variation along the height of the channel could change the streaming velocity field significantly. In this thesis we have not attempted to derive such a solution because streaming has not been a main concern in this work. We nevertheless wish to discuss this important aspect of microchannel acoustofluidics with a focus on the framework needed to take this step and provide a general solution.

Considering the isentropic limit we will set up a general formalism, and then consider the limit of $\delta_s \ll h$. In this limit we will make use of the first-order fields derived in Chapter 3 to obtain the effective boundary condition on the streaming velocity field obtained by Rayleigh using boundary layer theory [18]. Since streaming is not a main part of this thesis the calculation of the effective streaming boundary condition will only be outlined, with most calculations put in Section B.3 of Appendix B.

4.3.1 Second-order equations

Continuing the perturbation expansion to second order the second-order momentum equation and continuity equation are obtained from Eq. (2.4b) and Eq. (2.4a), respectively. In the isentropic limit the equation of state is obtained as a Taylor expansion of the pressure

$p(\rho, s)$ with the entropy s kept constant. One obtains

$$\rho_0 \partial_t \boldsymbol{v}_2 = -\boldsymbol{\nabla} p_2 - \rho_1 \partial_t \boldsymbol{v}_1 - \rho_0 \left(\boldsymbol{v}_1 \cdot \boldsymbol{\nabla}\right) \boldsymbol{v}_1 + \eta_0 \nabla^2 \boldsymbol{v}_2 + \beta \eta_0 \boldsymbol{\nabla} \left(\boldsymbol{\nabla} \cdot \boldsymbol{v}_2\right), \tag{4.34a}$$

$$\partial_t \rho_2 = -\rho_0 \boldsymbol{\nabla} \cdot \boldsymbol{v}_2 - \boldsymbol{\nabla} \cdot (\rho_1 \boldsymbol{v}_1), \tag{4.34b}$$

$$p_2 = c^2 \rho_2 + \frac{1}{2} \partial_\rho \left\{ c^2 \right\} \rho_1^2. \tag{4.34c}$$

Here it was used that $c^2 = (\partial p / \partial \rho)_s$ in the third equation when expanding the pressure $p(\rho, s)$. In the isentropic limit the dynamic viscosity η can only be perturbed by pressure and density changes, and here we have assumed that such perturbations are negligible. Taking the time-average and rearranging, the momentum equation and the continuity equation become

$$\nu_0 \nabla^2 \langle \boldsymbol{v}_2 \rangle + \beta \nu_0 \boldsymbol{\nabla} \left(\boldsymbol{\nabla} \cdot \langle \boldsymbol{v}_2 \rangle\right) - \frac{1}{\rho_0} \boldsymbol{\nabla} \langle p_2 \rangle = \frac{1}{\rho_0} \langle \rho_1 \partial_t \boldsymbol{v}_1 \rangle + \langle (\boldsymbol{v}_1 \cdot \boldsymbol{\nabla}) \boldsymbol{v}_1 \rangle, \tag{4.35a}$$

$$\boldsymbol{\nabla} \cdot \langle \boldsymbol{v}_2 \rangle = -\frac{1}{\rho_0} \boldsymbol{\nabla} \cdot \langle \rho_1 \boldsymbol{v}_1 \rangle, \tag{4.35b}$$

where it was used that a full time derivative averages to zero over one period, namely $\langle \partial_t \boldsymbol{v}_2 \rangle = \boldsymbol{0}$ since $\boldsymbol{v}_2$ must vary periodically around a constant mean value.

4.3.2 Vorticity equation

Taking the rotation of the momentum equation gives an equation for the rotation of the velocity field, which together with the continuity equation and the boundary conditions at boundaries $\partial\Omega$ specifies the problem

$$\nu_0 \nabla^2 \left(\boldsymbol{\nabla} \times \langle \boldsymbol{v}_2 \rangle\right) = \boldsymbol{\nabla} \times \left[\frac{1}{\rho_0} \langle \rho_1 \partial_t \boldsymbol{v}_1 \rangle + \langle \left(\boldsymbol{v}_1 \cdot \boldsymbol{\nabla}\right) \boldsymbol{v}_1 \rangle \right], \tag{4.36a}$$

$$\boldsymbol{\nabla} \cdot \langle \boldsymbol{v}_2 \rangle = -\frac{1}{\rho_0} \boldsymbol{\nabla} \cdot \langle \rho_1 \boldsymbol{v}_1 \rangle, \tag{4.36b}$$

$$\langle \boldsymbol{v}_2 \rangle = \boldsymbol{0}, \quad \text{for } \boldsymbol{r} \in \partial\Omega. \tag{4.36c}$$

Consider now Eq. (4.36a). Only the x-component is non-zero if we consider fields in the 2D yz-plane and translation-invariance along the x-direction. For simplicity we consequently introduce the scalar fields

$$\langle \zeta_2(y, z) \rangle = \left[\boldsymbol{\nabla} \times \langle \boldsymbol{v}_2 \rangle\right]_x, \tag{4.37a}$$

$$\langle S(y, z) \rangle = \left[\boldsymbol{\nabla} \times \left\{ \frac{1}{\rho_0} \langle \rho_1 \partial_t \boldsymbol{v}_1 \rangle + \langle \left(\boldsymbol{v}_1 \cdot \boldsymbol{\nabla}\right) \boldsymbol{v}_1 \rangle \right\} \right]_x. \tag{4.37b}$$

Then the scalar equation corresponding to Eq. (4.36a) in 2D becomes

$$\nu_0 \nabla^2 \langle \zeta_2 \rangle = \langle S \rangle. \tag{4.38}$$

It describes the time-averaged vorticity $\langle \zeta_2 \rangle$ generated by the source $\langle S \rangle$.

4.3.3 Streaming velocity field and potential equations

Following the approach by Muller [23] we decompose the second-order velocity field $\langle \boldsymbol{v}_2 \rangle$ into a gradient field and a rotation. For the 2D system we write

$$\langle \boldsymbol{v}_2 \rangle = \boldsymbol{\nabla} \langle \phi_2(y,z) \rangle + \boldsymbol{\nabla} \times [\langle \psi_2(y,z) \rangle \hat{\boldsymbol{x}}] \,. \tag{4.39}$$

Written out in components

$$\langle v_{2y} \rangle = \partial_y \langle \phi_2 \rangle + \partial_z \langle \psi_2 \rangle \,, \tag{4.40a}$$
$$\langle v_{2z} \rangle = \partial_z \langle \phi_2 \rangle - \partial_y \langle \psi_2 \rangle \,. \tag{4.40b}$$

The divergence and the rotation of the decomposition gives

$$\nabla^2 \langle \phi_2 \rangle = \boldsymbol{\nabla} \cdot \langle \boldsymbol{v}_2 \rangle \,, \tag{4.41a}$$
$$\nabla^2 \langle \psi_2 \rangle = - [\boldsymbol{\nabla} \times \langle \boldsymbol{v}_2 \rangle]_x \,. \tag{4.41b}$$

Using the vorticity equation Eq. (4.38) and the continuity equation Eq. (4.36b) we get the governing equations for $\langle \phi_2 \rangle$ and $\langle \psi_2 \rangle$

$$\nabla^2 \langle \phi_2 \rangle = -\frac{1}{\rho_0} \boldsymbol{\nabla} \cdot \langle \rho_1 \boldsymbol{v}_1 \rangle \,, \tag{4.42a}$$
$$\nu_0 \nabla^2 \nabla^2 \langle \psi_2 \rangle = - \langle S \rangle \,. \tag{4.42b}$$

Solving these equations with the appropriate boundary conditions on the second-order velocity field $\langle \boldsymbol{v}_2 \rangle$ gives a complete description of acoustic streaming in the full domain of the two-dimensional cross-section. We have not attempted to do so in this thesis, but one approach would be to use a Fourier series expansion for the homogeneous equations and a Green's function method for the inhomogeneous equations.

4.3.4 Approximate equations in the boundary layer region

The variation of the two potentials $\langle \phi_2 \rangle$ and $\langle \psi_2 \rangle$ are inherited from the first-order fields and consequently $\partial_y \sim k_y$ and $\partial_z \sim 1/\delta_\mathrm{s}$ in the boundary layer. As shown in Section B.3 this means that the problem may be reduced to the following set of equations valid to first order in $k_y \delta_\mathrm{s}$,

$$\nu_0 \partial_z^3 \langle v_{2y} \rangle = - \langle S \rangle \,, \tag{4.43a}$$
$$\langle S \rangle = -\frac{1}{2} \partial_z \partial_y \left\{ |v_{1y}|^2 \right\} - \frac{1}{2} \partial_z^2 \left\{ \mathrm{Re} \left[v_{1y}^* v_{1z} \right] \right\} . \tag{4.43b}$$

Moreover $\langle v_{2z} \rangle \sim k_y \delta_\mathrm{s} \langle v_{2y} \rangle$ and consequently it may be neglected to zeroth order in $k_y \delta_\mathrm{s}$.

4.3.5 Effective bulk streaming boundary condition

Considering only the $\langle v_{2y} \rangle$-component of the streaming velocity in the boundary layer we derive an effective boundary condition for the bulk streaming velocity field equivalent to that of Rayleigh obtained using singular boundary layer theory [12, 18]. The vorticity source $\langle S \rangle$ of Eq. (4.38) given in Eq. (4.37b) is negligible in the bulk in the microchannel acoustofluidics limit because the variation of the first-order fields along the height of the channel is negligible such that the bulk wave field is essentially horizontal and the rotation thus vanishes.

Consider solving Eq. (4.38) in the boundary layer, and in the bulk where $\langle S \rangle \simeq 0$ as discussed above. The equations and solutions in these two regions may be written as

In the boundary layer *In the bulk*

$$\nu_0 \nabla^2 \langle \zeta_2 \rangle = \langle S \rangle \,, \qquad \nu_0 \nabla^2 \langle \zeta_2 \rangle^{\text{bulk}} \simeq 0, \tag{4.44a}$$

$$\langle \zeta_2 \rangle = \langle \zeta_2 \rangle^{\text{hom}} + \langle \zeta_2 \rangle^{\text{part}} \,, \qquad \langle \zeta_2 \rangle^{\text{bulk}} = \langle \zeta_2 \rangle^{\text{hom}} \,, \tag{4.44b}$$

where

$$\nu_0 \nabla^2 \langle \zeta_2 \rangle^{\text{part}} = \langle S \rangle \quad \text{(Particular solution)}, \tag{4.44c}$$

$$\nu_0 \nabla^2 \langle \zeta_2 \rangle^{\text{hom}} = 0 \qquad \text{(Homogeneous solution)}. \tag{4.44d}$$

Consequently, the bulk solution is identical to the homogeneous solution obtained from solving the homogeneous equation. The boundary layer solution is the sum of the homogeneous solution and a particular solution.

The enforcement of the no-slip boundary condition at walls in $z = z_0$ requires the sum of the velocity components from the particular solution and the homogeneous solution (bulk solution) to be zero at $z = z_0$. Considering only the $\langle v_{2y} \rangle$-component of velocity we thus have

$$\langle v_{2y} \rangle^{\text{bulk}}_{z=z_0} = - \langle v_{2y} \rangle^{\text{part}}_{z=z_0} \,, \tag{4.45}$$

where $\langle v_{2y} \rangle^{\text{part}}_{z=z_0}$ is a particular solution of Eq. (4.44c) valid in the boundary layer, evaluated at $z = z_0$.

$\langle v_{2y} \rangle^{\text{bulk}}_{z=z_0}$ may thus be interpreted as an effective boundary condition on the bulk streaming velocity field. Using this boundary condition to solve the homogeneous equation valid in the bulk corresponds to putting the source terms $\langle S \rangle$ of the boundary layer into a linesource at the boundary in $z = z_0$.

In the boundary layer a particular solution may be obtained directly by combining the two equations of Eq. (4.43) and integrating three times, which formally gives

$$\langle v_{2y} \rangle^{\text{part}} = \frac{1}{2\nu_0} \left[\int \mathrm{d}z \int \mathrm{d}z \left\{ \partial_y \{ |v_{1y}|^2 \} \right\} + \int \mathrm{d}z \left\{ \text{Re} \left[v_{1y}^* v_{1z} \right] \right\} \right]. \tag{4.46}$$

As we consider a particular solution we are not concerned with the integration "constant" which may depend on y. Moreover, in the expression above any non-z-dependent terms

in $\partial_y\{|v_{1y}|^2\}$ and $\mathrm{Re}[v_{1y}^* v_{1z}]$ may be thrown away before the integration. Such terms are accounted for in the solution of the homogeneous equation and would have vanished from differentiation if calculating the explicit vorticity source density. Using the equation above we do not need to evaluate the explicit vorticity source density, but only $\partial_y\{|v_{1y}|^2\}$ and $\mathrm{Re}[v_{1y}^* v_{1z}]$.

The evaluation of $\partial_y\{|v_{1y}|^2\}$ and $\mathrm{Re}[v_{1y}^* v_{1z}]$ in the boundary layer region from the complex first-order fields and the subsequent integrations which must be carried out in order to derive the effective boundary condition on the second-order bulk streaming velocity field are tedious and not particularly instructive. We have left the calculations in Section B.3. In the limit studied by Rayleigh where $\delta_\mathrm{s} \ll h$ the result of the calculation is

$$\left\langle v_{2y} \right\rangle_{z=z_0}^{\mathrm{bulk}} = \frac{3}{8}\frac{u_0^2}{c}\sin\left(2k_y^\mathrm{r} y\right), \tag{4.47}$$

where u_0 is the amplitude of v_{1y} in the bulk standing wave, and $k_y = k_y^\mathrm{r} + \mathrm{i}k_y^\mathrm{i}$ with $k_y^\mathrm{r}, k_y^\mathrm{i} \in \mathbb{R}$. In the theory of Rayleigh the amplitude u_0 is arbitrary because the first-order velocity field in the bulk has an assumed horizontal wave form. In our theory it is given as

$$u_0^2 = \frac{2v_\mathrm{bc}^2}{\cosh\left(k_y^\mathrm{i} w\right) - 1}, \tag{4.48}$$

as calculated in Section B.3, Eq. (B.55).

The effective bulk streaming velocity boundary condition as given in Eq. (4.47) agrees with the result obtained by Rayleigh and Landau & Lifshitz using singular boundary layer theory [12, 18]. The solution of Rayleigh assumes a horizontal bulk wave with a real wavenumber k, while our solution for the first-order fields has complex wavenumbers k_y and k_z. To go from the Rayleigh result to our result one quite naturally has to let $k \to k_y^\mathrm{r}$ because our solution comes from a complete description of the first-order fields which includes damping and variation in the vertical z-direction.

If one wishes to solve for the bulk Rayleigh streaming velocity field $\langle \boldsymbol{v}_2 \rangle$ with the effective boundary condition, the easiest way to do so is to go back to Eq. (4.35). Multiplying Eq. (4.35a) by ρ_0 and realizing that the source terms on the right-hand side of the equation have zero rotation in the bulk because the variation in the z-direction is negligible they may be reformulated as gradient terms and absorbed together with $\boldsymbol{\nabla}\langle p_2 \rangle$ into an effective pressure gradient $\boldsymbol{\nabla}\chi_2$. Since the right-hand side of the continuity equation Eq. (4.35b) moreover is zero in the bulk due to the phase-difference between ρ_1 and $\boldsymbol{v}_1$ of $\pi/2$, the bulk equations reduce to the standard equations of incompressible creeping flow as discussed in Ref. [25].

4.3.6 Outlook on streaming

The main motivation for considering streaming in this thesis was to show that the classical result obtained in the isentropic limit by Rayleigh [18] is consistent with the complete description of the first-order fields given in Chapter 3. Having shown that this is true

we note that the strength of our first-order solution is that it is valid in the full domain without the use of boundary layer theory. Consequently we can go further than effective boundary conditions for the bulk field, and we may be able to solve the full second-order problem expressed by the potential equations Eq. (4.42) in the full domain.

Having considered only the isentropic limit a straight-forward extension of this work on streaming is to include thermal effects in the second-order equations. When doing so the perturbations of the viscosity η with temperature were recently shown to have a significant effect on the effective bulk streaming velocity boundary condition with corrections of $\sim 20\%$ for water at room temperature [22]. Using boundary layer theory a corrected boundary condition was derived,

$$\langle v_{2y}^{\mathrm{bnd}} \rangle^{\mathrm{thermoviscous}} = \frac{3}{8} \frac{u_0^2}{c} \sin(2ky) \left[1 + \frac{2}{3} (\gamma - 1) \frac{\sqrt{\mathrm{Pr}}}{1 + \mathrm{Pr}} \left(1 - \frac{(\partial_T \eta)_p}{\eta_0 \alpha_p} \right) \right]. \tag{4.49}$$

With our theory we should be able to verify this result and perhaps take it further by providing a solution valid in the full domain.

Preliminary studies show that the perturbations of the viscosity η with pressure are the same order of magnitude as those introduced by temperature. When considering second-order effects in thermoviscous acoustofluidics such small perturbations of the parameter values with temperature and pressure could potentially lead to significant corrections. For water one may obtain accurate descriptions of the parameter values as functions of temperature and pressure from the exhaustive fit of the state function given by the International Association for the Properties of Water and Steam [36, 37, 38]. Preliminary studies show that there is a need to investigate these effects in future work.

Chapter 5

Acoustic radiation force

The acoustic radiation force is the time-averaged force experienced by a particle in an acoustical field due to scattering of the acoustic waves from the particle. Theoretical studies of the acoustic radiation force date back to King in 1934 [39] and Yosioka and Kawasima in 1955 [40] who considered the force on an incompressible and a compressible particle, respectively, in an inviscid ideal fluid. Their work was summarized and generalized in 1962 by Gorkov [41]. We will refer to the result of Gorkov as the classical ideal theory. It is limited to inviscid ideal fluids and consequently all thermoviscous effects are neglected. Moreover, it is valid only for particles with a radius a much smaller than the acoustic wavelength λ.

Subsequent work on the acoustic radiation force where thermoviscous effects have been treated as presented by Doinikov [42, 43, 44] and by Danilov and Mironov [45], have focused on developing general theoretical schemes for calculation of acoustic radiation forces. The immediate applicability of these works suffer in great deal from the generality of the developed formalisms and as pointed out by Settnes and Bruus [15], analytical expressions are given only in the special limits of $\delta \ll a \ll \lambda$ and $a \ll \delta \ll \lambda$, where δ is the boundary layer thicknesses. For micrometer sized particles at MHz frequency relevant to lab-on-a-chip applications, however, $\delta \sim a \ll \lambda$. In 2012 Settnes and Bruus [15] consequently extended the classical theory of Gorkov to include the effect of viscosity. In this chapter we extend the radiation force theory to include the effect of both viscosity and heat conduction and we give closed form analytical expressions in the limit of $\delta_\mathrm{s} \sim \delta_\mathrm{t} \sim a \ll \lambda$ relevant to acoustophoresis applications.

Our approach to the full thermoviscous scattering problem was developed by Epstein and Carhart in 1953 [8]. The scope of their work was a theory for the absorption of sound in emulsions such as water fog in air. In 1972 Allegra and Hawley further developed the theory to include elastic solid particles suspended in a fluid in order to calculate attenuation of sound in suspensions and emulsions [9]. The seminal work of these authors have become known as ECAH theory within the field of ultrasound characterization of emulsions and suspensions, and combined with the multiple wave scattering theories of Refs. [46, 47] it has been applied to calculate homogenized complex wavenumbers of suspensions and emulsions [48, 49].

The field of ultrasound characterization driven by engineering applications and the field of acoustic radiation forces seem to have developed in parallel. Indeed the scopes of the work in the two fields are very different. In the works of Epstein and Carhart and Allegra and Hawley and in a recent comprehensive review of the field of ultrasound characterization by Challis in 2005 there is no mention of radiation forces [8, 9, 49]. However, the microscopic scattering problem of a particle suspended in a fluid remains the same, and having once solved for the amplitude of the scattered wave the radiation force on the particle may be obtained from a far-field calculation as shown by Settnes and Bruus [15].

As ECAH theory has overcome some of the problems of thermoviscous scattering currently receiving renewed interest within the field of acoustic radiation forces it was a natural step to bring the two together in this thesis. There are quite a few misprints in the seminal paper by Epstein and Carhart [8]. Some of them were corrected by Allegra and Hawley [9], but we nevertheless felt a need to go through the somewhat tedious calculations in order to bring the theory into the field of acoustic radiation forces. This is the aim of this chapter.

5.1 Physical system

We consider a viscous, heat-conducting fluid droplet immersed in a viscous, heat-conducting fluid medium perturbed by an acoustical wave field. The spherical fluid droplet is placed at the center of the coordinate system in $r = 0$ and has a radius a such that the boundary between the sphere and the fluid medium is at $r = a$. Let unprimed variables and parameters characterize the region of the fluid medium, $r \geq a$, while primed variables and parameters characterize the region of the fluid droplet, $r \leq a$. For example the parameter κ_s' is the compressibility of the fluid droplet, while κ_s is the compressibility of the fluid medium. Parameter ratios between the fluid droplet and the fluid medium are denoted with a tilde, e.g. $\tilde{\kappa}_s = \kappa_s'/\kappa_s$.

We solve the first-order scattering problem in accordance with our general scheme of approximation for which terms of order $(k_0\delta_\mathrm{s})^2, (k_0\delta_\mathrm{t})^2$ and $(k_0 a)^2$ are neglected relative to 1 from the assumption that the acoustic wavelength is much larger than the boundary layer thicknesses and the particle radius, $\delta_\mathrm{s} \sim \delta_\mathrm{t} \sim a \ll \lambda$. These assumptions are made for the surrounding fluid medium parameters and for the fluid droplet parameters, and are applicable to microparticle acoustophoresis applications because we do not put any constraints on the relative size of the boundary layer thicknesses compared to the particle size. We solve the problem using a partial wave expansion method assuming that the scattered sound wave radiated from the particle may be represented as an expansion in multipole modes. In the long-wavelength limit, also known as the Rayleigh limit, where $k_\mathrm{c} a \ll 1$ only the monopole mode and the dipole mode are important [15]. Before proceeding with the involved mathematical treatment we refer the reader to Fig. 5.1, which illustrates the physical mechanisms responsible for the radiation of sound with monopole, dipole, and multipole geometry from a particle subject to a periodic acoustical field.

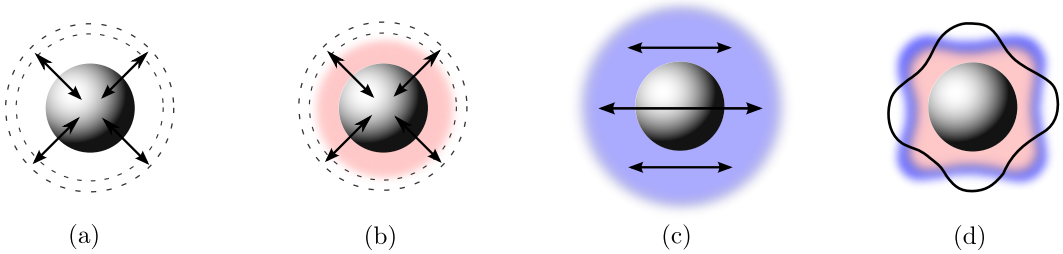

Figure 5.1: Thermoviscous acoustic wave scattering mechanisms and radiation geometries. (a) Mechanical contrast: The incident periodic pressure field compresses the particle relative to the fluid which leads to monopole radiation. (b) Thermal contrast: The incident periodic temperature field leads to thermal expansion of the particle relative to the fluid giving rise to monopole radiation, and the growth of a diffusive thermal boundary layer. (c) Density contrast: A difference in inertia between particle and fluid causes the particle in the periodic wave field to move periodically back-and-forth with respect to the fluid leading to the growth of a viscous boundary layer and emission of dipole radiation. (d) Particle resonances: For large particles or high frequencies the acoustic wavelength becomes comparable to the particle size and may excite particle resonances modeled as multipole radiation sources.

5.2 Partial wave expansion

In Chapter 2 we derived the three wave equations corresponding to the three possible modes of wave propagation in a fluid, namely the longitudinal compressional mode describing propagating waves, the longitudinal diffusive thermal mode, and the transverse diffusive shear mode. The wave equations and wavenumbers corresponding to the three modes were given in Eq. (2.32) and Eq. (2.33), respectively.

In spherical coordinates (r, θ, ϕ) the scalar wave equation separates into three ordinary differential equations describing the dependence of the radial distance r, the polar angle θ, and the azimuthal angle ϕ. In general the radial dependence is solved by spherical Bessel or Hankel functions, the θ-dependence is solved by associated Legendre polynomials, and the ϕ-dependence is solved by exponential or sine functions. More background and details can be found in any advanced book on wave phenomena, for example the electromagnetics book of Ref. [50]. Each solution is known as a partial wave and the full solution is expanded in terms of these. The partial wave expansion method is a standard approach to scattering problems in acoustics, electromagnetics, and quantum theory. All waves in distinct parts of space are expanded using the partial wave expansion and with the appropriate boundary conditions this solves the scattering problem.

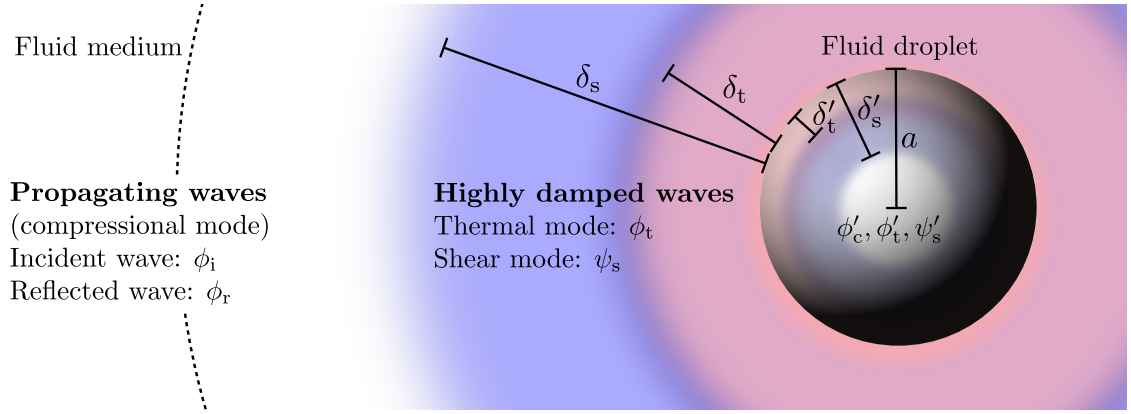

Figure 5.2: In a viscous, heat-conducting fluid medium described with parameters $\rho_0, \eta_0, \kappa_s, \alpha_p, C_p, \gamma$, and k_th, a compressional propagating incident wave ϕ_i is scattered from a viscous, heat-conducting fluid droplet described with parameters $\rho'_0, \eta'_0, \kappa'_s, \alpha'_p, C'_p, \gamma'$, and k'_th, giving rise to a compressional scattered wave and highly damped thermal and shear waves both outside in the fluid medium $(\phi_\mathrm{r}, \phi_\mathrm{t}, \psi_\mathrm{s})$ and inside in the fluid droplet $(\phi'_\mathrm{c}, \phi'_\mathrm{t}, \psi'_\mathrm{s})$. Viscous and thermal boundary layers appear as consequences of the highly damped waves both outside and inside the fluid droplet. The droplet has a radius a comparable to the boundary layer thicknesses $\delta_\mathrm{s}, \delta_\mathrm{t}, \delta'_\mathrm{s}, \delta'_\mathrm{t}$, but much smaller than the acoustic wavelength λ.

We are concerned with a problem exhibiting azimuthal symmetry, such that the fields and potentials have no ϕ-dependence. This also reduces the associated Legendre polynomials to the ordinary Legendre polynomials when solving the scalar wave equations. Avoiding singular solutions and considering the direction of wave propagation the solution to the scalar wave equations Eq. (2.32a) and Eq. (2.32b) for ϕ_c and ϕ_t may then be written down immediately.

For the vector wave equation in Eq. (2.32c) describing the vector potential $\mathbf{\Psi}$ some care must be taken. Indeed, the vector wave equation does not separate nicely in spherical coordinates as it does in cartesian coordinates. Moreover the vector potential is required to be divergenceless $\boldsymbol{\nabla}\cdot\mathbf{\Psi} = 0$. The solution to the vector wave equation is obtained from the solution of the corresponding scalar wave equation as described in Appendix C. Only one solution is divergenceless with the correct symmetry as shown in Section C.2. This solution is described with associated Legendre polynomials and only the ϕ-component of the vector potential is non-zero. To simplify notation we write $\mathbf{\Psi} = \psi_\mathrm{s}\,\mathbf{e}_\phi$.

The above considerations allow us to expand the solutions to the wave equations:

In the fluid medium, $r \geq a$:

$$\phi_\mathrm{i} = \phi_0 \sum_{n=0}^{\infty} \mathrm{i}^n (2n+1) j_n(k_\mathrm{c} r) P_n(\cos\theta), \tag{5.1a}$$

$$\phi_\mathrm{r} = \phi_0 \sum_{n=0}^{\infty} \mathrm{i}^n (2n+1) A_n h_n^{(1)}(k_\mathrm{c} r) P_n(\cos\theta), \tag{5.1b}$$

$$\phi_\mathrm{t} = \phi_0 \sum_{n=0}^{\infty} \mathrm{i}^n (2n+1) B_n h_n^{(1)}(k_\mathrm{t} r) P_n(\cos\theta), \tag{5.1c}$$

$$\psi_\mathrm{s} = \phi_0 \sum_{n=0}^{\infty} \mathrm{i}^n (2n+1) C_n h_n^{(1)}(k_\mathrm{s} r) P_n^1(\cos\theta), \tag{5.1d}$$

In the fluid droplet, $r \leq a$:

$$\phi_\mathrm{c}' = \phi_0 \sum_{n=0}^{\infty} \mathrm{i}^n (2n+1) A_n' j_n(k_\mathrm{c}' r) P_n(\cos\theta), \tag{5.1e}$$

$$\phi_\mathrm{t}' = \phi_0 \sum_{n=0}^{\infty} \mathrm{i}^n (2n+1) B_n' j_n(k_\mathrm{t}' r) P_n(\cos\theta), \tag{5.1f}$$

$$\psi_\mathrm{s}' = \phi_0 \sum_{n=0}^{\infty} \mathrm{i}^n (2n+1) C_n' j_n(k_\mathrm{s}' r) P_n^1(\cos\theta). \tag{5.1g}$$

In the above expansion ϕ_i describes the incident propagating wave, ϕ_r the scattered reflected propagating wave, ϕ_t the scattered diffusive thermal wave, and ψ_s the scattered diffusive shear wave. The primed potentials describe the compressional, thermal, and shear waves inside the fluid droplet. The setup is illustrated in Fig. 5.2. Note that P_n is the ordinary Legendre polynomial while P_n^1 is the associated Legendre polynomial. The parameter ϕ_0 is an arbitrary amplitude of the incident wave and has units of $\mathrm{m}^2\,\mathrm{s}^{-1}$. We have chosen the expansion coefficients of the incident wave to be those of a plane wave travelling in the positive z-direction,

$$\phi_i = \phi_0\, \mathrm{e}^{\mathrm{i}k_\mathrm{c} z} = \phi_0\, \mathrm{e}^{\mathrm{i}k_\mathrm{c} r\cos\theta} = \phi_0 \sum_{n=0}^{\infty} \mathrm{i}^n (2n+1) j_n(k_\mathrm{c} r) P_n(\cos\theta). \tag{5.2}$$

Indeed, this problem exhibits azimuthal symmetry. The scattering coefficients obtained from this configuration are general due to linearity of the first-order scattering problem ensuring that any azimuthal symmetric incident wave field may be expanded in terms of plane waves.

5.3 Boundary conditions

The spherical fluid droplet has a radius a and is centered at $r = 0$. Neglecting surface tension the appropriate boundary conditions at the interface in $r = a$ are those of continuous velocity, continuous normal stress, continuous temperature, and continuous heat flux.

The general stress boundary condition of continuous $\sigma_{ij}n_j$ simply states that there can be no discontinuous change in force across any infinitesimal area and may be considered a statement of Newton's third law. Of course this is only true when neglecting surface tension. With the symmetry of our problem these boundary conditions are written as

$$\begin{aligned} v_{1r} &= v'_{1r}, \quad & v_{1\theta} &= v'_{1\theta}, \quad & T_1 &= T'_1, \\ \sigma^{(1)}_{rr} &= \sigma^{(1)\prime}_{rr}, \quad & \sigma^{(1)}_{r\theta} &= \sigma^{(1)\prime}_{r\theta}, \quad & k_{\mathrm{th}}\partial_r T_1 &= k'_{\mathrm{th}}\partial_r T'_1, \end{aligned} \qquad \text{for} \quad r = a. \tag{5.3}$$

The primed variables and fields refer to the region of the fluid droplet at $r \leq a$, while the unprimed variables and fields refer to the fluid medium at $r \geq a$. In the stress boundary conditions the full stress tensor including pressure is used, and the superscript "(1)" indicates that we are considering only first-order contributions in linear scattering theory.

The boundary conditions must be written in terms of the potentials in order to use the partial wave expansion of Eq. (5.1). The pressure and temperature were found to be proportional to the two scalar potentials as given in Eq. (2.37). The velocity field is given from the Helmholtz decomposition. In spherical coordinates with azimuthal symmetry the two components of velocity are

$$v_{1r} = -\partial_r\Phi + \frac{1}{r\sin\theta}\partial_\theta\left\{\sin\theta\,\psi_{\mathrm{s}}\right\}, \tag{5.4a}$$

$$v_{1\theta} = -\frac{1}{r}\partial_\theta\Phi - \frac{1}{r}\partial_r\left\{r\,\psi_{\mathrm{s}}\right\}. \tag{5.4b}$$

The stress tensor components in spherical coordinates for an incompressible fluid are given in Landau and Lifshitz [12]. Considering a compressible fluid we add the divergence term in the diagonal according to Eq. (2.3a). Using the expression for the pressure in Eq. (2.39) and neglecting Γ_{s} and Γ_{t} relative to 1 we find

$$\sigma^{(1)}_{rr} = \mathrm{i}\omega\rho_0\left(\phi_{\mathrm{c}} + M\phi_{\mathrm{t}}\right) + 2\eta_0\left[-\partial_r^2\Phi + \frac{1}{\sin\theta}\partial_\theta\left\{\sin\theta\left(-\frac{1}{r^2}\psi_{\mathrm{s}} + \frac{1}{r}\partial_r\psi_{\mathrm{s}}\right)\right\}\right], \tag{5.5a}$$

$$\text{with} \quad M = 1 - \frac{2\nu_0}{D_{\mathrm{th}}},$$

$$\sigma^{(1)}_{r\theta} = \eta_0\left[-2\partial_\theta\left\{\frac{1}{r}\partial_r\Phi - \frac{1}{r^2}\Phi\right\} - \left(\partial_r^2\psi_{\mathrm{s}} - \frac{2}{r^2}\psi_{\mathrm{s}}\right) + \frac{1}{r^2}\partial_\theta\left\{\frac{1}{\sin\theta}\partial_\theta\left\{\sin\theta\,\psi_{\mathrm{s}}\right\}\right\}\right], \tag{5.5b}$$

Some details on the calculation of the stress tensor components are given in Section C.3 of Appendix C.

Having expressed the boundary conditions in terms of the velocity potentials, we may now proceed to insert the partial wave expansion of Eq. (5.1) into the boundary conditions for $r = a$ in Eq. (5.3). The polar dependence can be expressed in terms of ordinary Legendre polynomials by making use of the Legendre equation and the definition of the associated Legendre polynomials [51]

$$\frac{1}{\sin\theta}\frac{\mathrm{d}}{\mathrm{d}\theta}\left(\sin\theta\frac{\mathrm{d}}{\mathrm{d}\theta}P_n(\cos\theta)\right) + n(n+1)P_n(\cos\theta) = 0, \tag{5.6a}$$

$$P_n^m(x) = \left(1-x^2\right)^{m/2}\frac{\mathrm{d}^m}{\mathrm{d}x^m}P_n(x), \quad \text{for} \quad m = 0, 1, 2, \ldots\,, \tag{5.6b}$$

from which we obtain the following two identities

$$P_n^1(\cos\theta) = -\frac{\mathrm{d}}{\mathrm{d}\theta}P_n(\cos\theta), \tag{5.7a}$$

$$\frac{1}{\sin\theta}\frac{\mathrm{d}}{\mathrm{d}\theta}\left(\sin\theta\, P_n^1(\cos\theta)\right) = n(n+1)P_n(\cos\theta). \tag{5.7b}$$

The two identities of Eq. (5.7) are used to express the angular dependence in the boundary conditions in terms of the ordinary Legendre functions. Since polynomials of different order n are linearly independent we can equate the coefficients of both sides for each order n. This provides a general theoretical scheme for solving the scattering problem to desired order n, although numerically the matrix inversion may be problematic [49]. This is the method referred to within the field of ultrasound characterization of emulsions and suspensions as ECAH theory [49].

Considering here the Rayleigh limit where the wavelength is much larger than the particle radius, $k_\mathrm{c}a \ll 1$, the dominant contributions to the scattered field are due to the $n = 0$ monopole term and the $n = 1$ dipole term [15]. In the following equations we will shorten notation by introducing the normalized wavenumbers x_c, x_t, and x_s,

$$x_\mathrm{c} = k_\mathrm{c}a, \quad x_\mathrm{t} = k_\mathrm{t}a, \quad \text{and} \quad x_\mathrm{s} = k_\mathrm{s}a, \tag{5.8}$$

and likewise for primed variables. Note that the Rayleigh limit is obtained when $x_\mathrm{c} \ll 1$. In the general case that we want to consider the thermal and the viscous boundary layers are comparable to the radius of the particle, which means that x_t and x_s are neither small nor large as compared to 1.

Inserting the expansion of Eq. (5.1) into the boundary conditions in Eq. (5.3) and making use of the identities in Eq. (5.7) and the linear independence of the Legendre

polynomials we obtain the following system of coupled linear equations valid for $n \geq 1$,

$$x_{\mathrm{c}} j_n'(x_{\mathrm{c}}) + A_n x_{\mathrm{c}} h_n'(x_{\mathrm{c}}) + B_n x_{\mathrm{t}} h_n'(x_{\mathrm{t}}) - C_n n(n+1) h_n(x_{\mathrm{s}}) = A_n' x_{\mathrm{c}}' j_n'(x_{\mathrm{c}}') + B_n' x_{\mathrm{t}}' j_n'(x_{\mathrm{t}}') - C_n' n(n+1) j_n(x_{\mathrm{s}}'), \tag{5.9a}$$

$$j_n(x_{\mathrm{c}}) + A_n h_n(x_{\mathrm{c}}) + B_n h_n(x_{\mathrm{t}}) - C_n \left[x_{\mathrm{s}} h_n'(x_{\mathrm{s}}) + h_n(x_{\mathrm{s}})\right] = A_n' j_n(x_{\mathrm{c}}') + B_n' j_n(x_{\mathrm{t}}') - C_n' \left[x_{\mathrm{s}}' j_n'(x_{\mathrm{s}}') + j_n(x_{\mathrm{s}}')\right], \tag{5.9b}$$

$$b_{\mathrm{c}} j_n(x_{\mathrm{c}}) + A_n b_{\mathrm{c}} h_n(x_{\mathrm{c}}) + B_n b_{\mathrm{t}} h_n(x_{\mathrm{t}}) = A_n' b_{\mathrm{c}}' j_n(x_{\mathrm{c}}') + B_n' b_{\mathrm{t}}' j_n(x_{\mathrm{t}}'), \tag{5.9c}$$

$$k_{\mathrm{th}} b_{\mathrm{c}} x_{\mathrm{c}} j_n'(x_{\mathrm{c}}) + A_n k_{\mathrm{th}} b_{\mathrm{c}} x_{\mathrm{c}} h_n'(x_{\mathrm{c}}) + B_n k_{\mathrm{th}} b_{\mathrm{t}} x_{\mathrm{t}} h_n'(x_{\mathrm{t}}) = A_n' k_{\mathrm{th}}' b_{\mathrm{c}}' x_{\mathrm{c}}' j_n'(x_{\mathrm{c}}') + B_n' k_{\mathrm{th}}' b_{\mathrm{t}}' x_{\mathrm{t}}' j_n'(x_{\mathrm{t}}'), \tag{5.9d}$$

$$\begin{aligned}\eta_0 \Big(&\left[x_{\mathrm{c}} j_n'(x_{\mathrm{c}}) - j_n(x_{\mathrm{c}})\right] + A_n \left[x_{\mathrm{c}} h_n'(x_{\mathrm{c}}) - h_n(x_{\mathrm{c}})\right] + B_n \left[x_{\mathrm{t}} h_n'(x_{\mathrm{t}}) - h_n(x_{\mathrm{t}})\right] \\ &-(C_n/2)\left[x_{\mathrm{s}}^2 h_n''(x_{\mathrm{s}}) + (n^2+n-2) h_n(x_{\mathrm{s}})\right]\Big) \\ = \eta_0' \Big(&A_n' \left[x_{\mathrm{c}}' j_n'(x_{\mathrm{c}}') - j_n(x_{\mathrm{c}}')\right] + B_n' \left[x_{\mathrm{t}}' j_n'(x_{\mathrm{t}}') - j_n(x_{\mathrm{t}}')\right] \\ &-(C_n'/2)\left[x_{\mathrm{s}}'^2 j_n''(x_{\mathrm{s}}') + (n^2+n-2) j_n(x_{\mathrm{s}}')\right]\Big),\end{aligned} \tag{5.9e}$$

$$\begin{aligned}&\eta_0 \left[x_{\mathrm{s}}^2 j_n(x_{\mathrm{c}}) - 2x_{\mathrm{c}}^2 j_n''(x_{\mathrm{c}})\right] + A_n \eta_0 \left[x_{\mathrm{s}}^2 h_n(x_{\mathrm{c}}) - 2x_{\mathrm{c}}^2 h_n''(x_{\mathrm{c}})\right] \\ &\quad + B_n \eta_0 \left[x_{\mathrm{s}}^2 M h_n(x_{\mathrm{t}}) - 2x_{\mathrm{t}}^2 h_n''(x_{\mathrm{t}})\right] + 2n(n+1) C_n \eta_0 \left[x_{\mathrm{s}} h_n'(x_{\mathrm{s}}) - h_n(x_{\mathrm{s}})\right] \\ &= A_n' \eta_0' \left[x_{\mathrm{s}}'^2 j_n(x_{\mathrm{c}}') - 2x_{\mathrm{c}}'^2 j_n''(x_{\mathrm{c}}')\right] + B_n' \eta_0' \left[x_{\mathrm{s}}'^2 M' j_n(x_{\mathrm{t}}') - 2x_{\mathrm{t}}'^2 j_n''(x_{\mathrm{t}}')\right] \\ &\quad + 2n(n+1) C_n' \eta_0' \left[x_{\mathrm{s}}' j_n'(x_{\mathrm{s}}') - j_n(x_{\mathrm{s}}')\right].\end{aligned} \tag{5.9f}$$

In the equations above we have used the implicit notation that $h_n = h_n^{(1)}$ since the spherical Hankel functions are all of the first kind. Moreover, a prime on any spherical Bessel or Hankel function indicates differentation with respect to the argument. Epstein and Carhart were the first to write down these equations [8]. We note that in their seminal paper there is a misprint in the last term of the second equation.

5.4 Monopole scattering coefficient

We obtain the monopole scattering coefficient f_0 by solving for the expansion coefficient A_0 in the partial wave expansion for the propagating scattered wave. Describing the scattered wave with the scattering coefficients f_n instead of the expansion coefficients A_n is a matter of convention. We will use the scattering coefficients f_n over the expansion coefficients A_n as it simplifies expressions and follows the tradition of the seminal work on

acoustic radiation force by Gorkov [15, 41, 52]. The monopole scattering coefficient f_0 is then obtained from $A_0 = -(\mathrm{i}/3)x_\mathrm{c}^3 f_0$.

From the partial wave expansion Eq. (5.1) and the boundary conditions Eq. (5.3) one obtains the equations of order $n = 0$ similar to those given in Eq. (5.9) for $n \geq 1$. The boundary conditions for $v_{1\theta}$ and $\sigma_{r\theta}^{(1)}$ are trivially satisfied for the $n = 0$ equations because there is no angular dependence in the zeroth-order Legendre and associated Legendre polynomials, $P_0(x) = 1$ and $P_0^1(x) = 0$. $P_0^1(x) = 0$ leads to $\psi_\mathrm{s} = 0$ at this order and the coefficients C_0 and C_0' drop out of the equations leaving 4 equations with 4 unknowns. Physically, the absence of angular dependence in the monopole equations is a consequence of the monopole mode corresponding to radial compression and expansion.

The resulting equations of order $n = 0$ are written in Eq. (C.18) in Section C.4. The solution to this inhomogeneous system of linear equations proceeds straight-forwardly but is rather tedious and requires some work. It is presented in Section C.4 of Appendix C. The approximations made in that section are in accordance with our general scheme of approximation with terms of order $(k_0\delta_\mathrm{s})^2, (k_0\delta_\mathrm{t})^2$ and $(k_0 a)^2$ neglected relative to 1 from the assumption that the acoustic wavelength is much larger than the boundary layer thicknesses and the particle radius. This is true both for the fluid medium parameters and for the fluid droplet parameters.

The result of the calculations in Section C.4 is most conveniently written on the form

$$f_0 = 1 - \tilde{\kappa}_s + 3(\gamma - 1)\left(1 - \frac{\tilde{\alpha}_p}{\tilde{\rho}_0 \tilde{C}_p}\right)^2 H(x_\mathrm{t}, x_\mathrm{t}', \tilde{k}_\mathrm{th}), \tag{5.10a}$$

$$H(x_\mathrm{t}, x_\mathrm{t}', \tilde{k}_\mathrm{th}) = \frac{1}{x_\mathrm{t}^2}\left[\frac{1}{1 - \mathrm{i}x_\mathrm{t}} - \frac{1}{\tilde{k}_\mathrm{th}}\frac{\tan x_\mathrm{t}'}{\tan x_\mathrm{t}' - x_\mathrm{t}'}\right]^{-1}. \tag{5.10b}$$

Epstein and Carhart obtained the above result written on a different form but with a sign-error in the thermal correction term, which however, did not show up in their final expression for the attenuation [8, 9]. Allegra and Hawley following a similar method obtained a result in agreement with what we present here [9].

The classical result for a compressible particle in an ideal fluid is $f_0^\mathrm{ideal} = 1 - \tilde{\kappa}_s$ as given by Gorkov [41]. Comparing the two we find that the inclusion of heat conduction adds a correction term which has both a real and an imaginary part. The thermal correction term may vanish in three distinct cases, namely if $\gamma = 1$, if $\tilde{\alpha}_p/\tilde{\rho}_0\tilde{C}_p = 1$, or if the function H vanishes. $\gamma = C_p/C_V = 1$ implies that thermal energy does not influence the volume of the fluid medium, such that heating does not do any mechanical work, or alternatively that the mechanical pressure waves do not lead to heating. The factor $(\gamma - 1)$ then gives a number for the influence of thermal effects on the mechanical pressure waves. This is multiplied by $(1 - \tilde{\alpha}_p/\tilde{\rho}_0\tilde{C}_p)^2$, and only the relative value between the medium and the particle are important for this factor. Note that $\chi_p = \alpha_p/\rho_0 C_p$ has units of m^3/J and it may be thought of as an isobaric expansion coefficient per added heat energy,

$$\chi_p = \frac{\alpha_p}{\rho_0 C_p} = \frac{-\frac{1}{\rho_0}\left(\frac{\partial\rho}{\partial T}\right)_p}{\rho_0 T_0 \left(\frac{\partial s}{\partial p}\right)_p} = -\frac{1}{\rho_0}\left(\frac{\partial\rho}{\partial q}\right)_p, \quad \text{with} \quad q = \rho_0 T_0 s, \tag{5.11}$$

with the expansion happening around the equilibrium values ρ_0, T_0 and with the heat q defined as an energy per volume. When the particle and the medium have the same value of χ_p they expand and contract in phase when subject to the periodic heating and cooling caused by the incident wave and thus the thermal correction vanishes. If $\tilde{\chi}_p \neq 1$ the particle expands more or less per added heat when compared to the medium which gives rise to monopole radiation described by the correction term.

Finally we expect the thermal correction term to vanish in the limit where the particle becomes much larger than the thermal boundary layer thickness. To see that this is true note that $x_\mathrm{t} = (1+\mathrm{i})a/\delta_\mathrm{t}$ and that $x_\mathrm{t}' = x_\mathrm{t}/\tilde{D}_\mathrm{th}^{1/2}$. Since $\tan[(1+\mathrm{i})x] \simeq \mathrm{i}$ for large x we see that $H \sim 1/x_\mathrm{t} \sim \delta_\mathrm{t}/a$ for large particles $a/\delta_\mathrm{t} \gg 1$. In the limit of $a/\delta_\mathrm{t} \to \infty$ the correction term thus vanishes as expected.

The opposite limit of $a/\delta_\mathrm{t} \to 0$, where the particle becomes essentially a point particle, implies that $x_\mathrm{t}, x_\mathrm{t}' \ll 1$ and we may expand the tangents in the function H. To lowest order we find $H \simeq -(1/3)\tilde{k}_\mathrm{th} x_\mathrm{t}'^2/x_\mathrm{t}^2$ and the asymptotic expressions for the monopole coefficient are thus

$$f_0(a/\delta_\mathrm{t} \to \infty) = f_0^\mathrm{ideal} = 1 - \tilde{\kappa}_s, \qquad \text{(Large particle limit)} \quad (5.12a)$$

$$f_0(a/\delta_\mathrm{t} \to 0) = 1 - \tilde{\kappa}_s - (\gamma - 1)\tilde{\rho}_0 \tilde{C}_p \left(1 - \frac{\tilde{\alpha}_p}{\tilde{\rho}_0\, \tilde{C}_p}\right)^2, \qquad \text{(Small particle limit)} \quad (5.12b)$$

where we have used that $D_\mathrm{th} = k_\mathrm{th}/\rho_0 C_p$. With $\gamma > 1$ the correction from thermal effects in the small particle limit is negative and consequently amplifies the magnitude of the coefficient for acoustically soft particles ($\tilde{\kappa}_s > 1$), while it reduces the magnitude of the coefficient for acoustically hard particles ($\tilde{\kappa}_s < 1$), unless the response becomes stronger with the opposite sign.

We note that within our approximations the parameter of viscosity does not enter the monopole scattering coefficient in Eq. (5.10) and consequently viscosity is negligible in the monopole mode. This might be anticipated because the monopole mode describes compression and expansion and thus a strong coupling to thermal effects is expected. Note also that because the thermal correction is proportional to $(\gamma - 1)$ one may expect the correction to become important especially in a gas medium. For a monatomic ideal gas for example, the heat capacity ratio is $\gamma = 5/3$, while for water at room temperature $\gamma = 1.01$. With our focus on microchannel acoustophoresis we will consider the case of liquids where significant corrections may still be found.

In order to analyze the monopole scattering coefficient graphically we must choose a value for the heat capacity ratio of the fluid medium γ. Moreover we need ratios of fluid parameters between the droplet and the medium. A standard example is that of a vegetable oil in water and we will choose the fixed parameters typical of such a configuration. Referring to Table 1 of Ref. [53] we will fix the following parameters using the rough estimates

$$\gamma = 1.01, \quad \tilde{\rho}_0 = 0.9, \quad \tilde{C}_p = 0.5, \quad \tilde{\alpha}_p = 3.5. \qquad (5.13)$$

The compressibility ratio $\tilde{\kappa}_s$ as well as the ratio of thermal diffusivities $\tilde{D}_\mathrm{th}$ will be varied in order to illustrate the general dependence of the monopole coefficient on these two

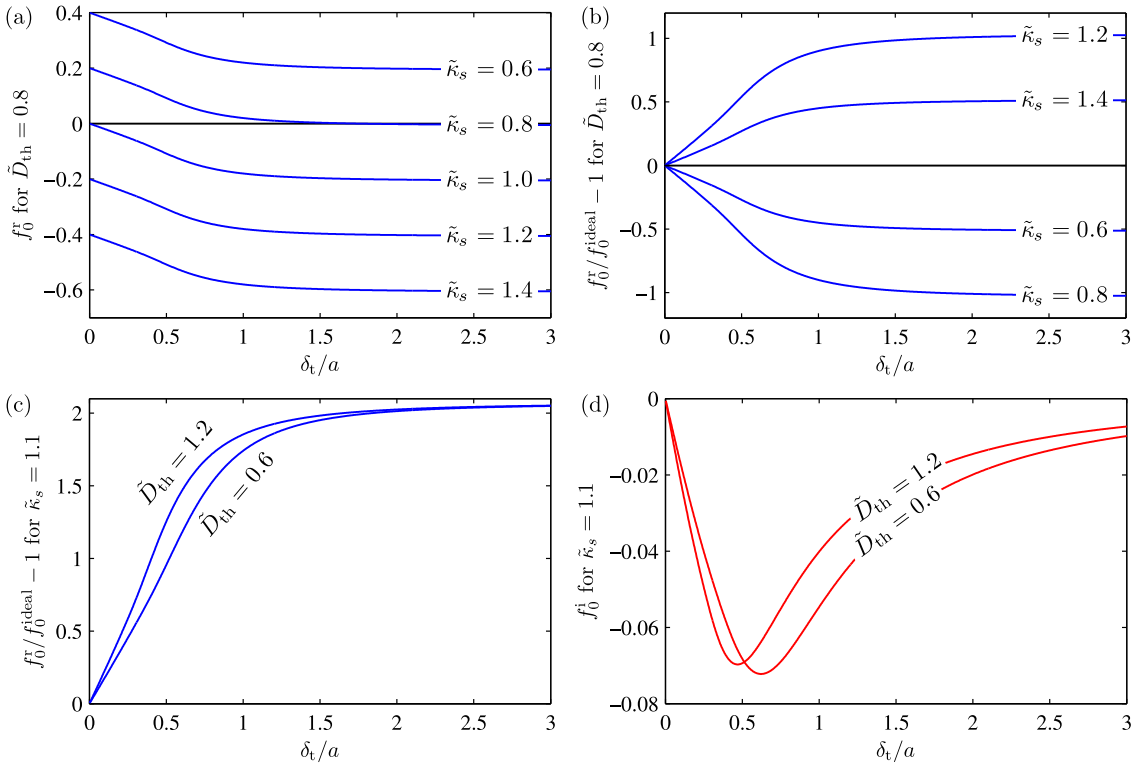

Figure 5.3: Monopole scattering coefficient plotted against the normalized thermal boundary layer thickness for various parameter values of $\tilde{\kappa}_s = \kappa_s'/\kappa_s$ and $\tilde{D}_{\rm th} = D_{\rm th}'/D_{\rm th}$ with other parameters typical for vegetable oil in water as discussed in the text. (a) Real part $f_0^{\rm r}$ for different values of $\tilde{\kappa}_s$. (b)-(c) Real part $f_0^{\rm r}$ relative to the monopole coefficient of an ideal fluid $f_0^{\rm ideal}$ for different values of $\tilde{\kappa}_s$ and $\tilde{D}_{\rm th}$, respectively. (d) Imaginary part $f_0^{\rm i}$ of the monopole scattering coefficient for different values of $\tilde{D}_{\rm th} = D_{\rm th}'/D_{\rm th}$. For an ideal fluid the imaginary part of the scattering coefficient is zero.

parameter ratios. Typical values for oil in water for the compressibility and the thermal diffusivity are $\tilde{\kappa}_s = 1.1$ and $\tilde{D}_{\rm th} = 0.8$. Note that with the above estimates $\tilde{\chi}_p = 7$.

Fig. 5.3 shows plots of the real part $f_0^{\rm r}$ and the imaginary part $f_0^{\rm i}$ of the monopole scattering coefficient plotted against the normalized thermal boundary layer thickness for various parameter values of $\tilde{\kappa}_s$ and $\tilde{D}_{\rm th}$. We find that the thermal corrections may be as large as 100% when the thermal boundary layer thickness becomes comparable to the particle radius.

5.5 Dipole scattering coefficient

We obtain the dipole scattering coefficient f_1 by solving for the expansion coefficient A_1 in the partial wave expansion for the propagating scattered wave and then use that $A_1 = (\mathrm{i}/6)x_{\rm c}^3 f_1$ to match the convention of Gorkov [41]. Setting $n = 1$ in Eq. (5.9) we

obtain the inhomogeneous system of equations written out in Eq. (C.27) of Section C.5. As shown in that section, terms involving the coefficients B_1 and B_1' are of negligible order and may be omitted within the general scheme of approximation, namely by neglecting terms of order $(k_0\delta_\mathrm{t})^2$ relative to 1. This reduces the system to 4 equations with 4 unknowns which are solved in Section C.5 with a fair amount of algebraic details not relevant to the treatment in this section.

Physically, the smallness of terms involving B_1 and B_1' means that thermal effects are negligible in the dipole mode in the long wavelength limit as compared to viscous effects. This is consistent with the dipole mode described as an oscillating back-and-forth motion of the undeformed particle relative to the fluid, for which we expect viscous effects to be important. As shown in the last section the thermal coupling is dominant in the monopole mode, where viscous effects on the other hand are negligible. Thus the two effects separate with the thermal effects coupling to the compressional mode of the monopole and the viscous effects dominant in the oscillating dipole mode, which is in good agreement with physical intuition.

The result of the calculations in Section C.5 is derived with terms of order $(k_0\delta_\mathrm{s})^2, (k_0\delta_\mathrm{t})^2$ and $(k_0 a)^2$ neglected relative to 1 and likewise for primed variables, which is consistent with our general scheme of approximation. The result for A_1 obtained in Eq. (C.35) was given by Allegra and Hawley [9] and with a misprint by Epstein and Carhart [8] in the context of attenuation of sound in emulsions and suspensions. We write the result for the dipole scattering coefficient f_1 on a different form more suitable for comparison to the theory for acoustic radiation forces as presented by Gorkov [41] and Settnes and Bruus [15],

$$f_1 = \frac{2\left[\tilde{\rho}_0 - 1\right]\left[1 + F(x_\mathrm{s}, x_\mathrm{s}', \tilde{\eta}_0) - G(x_\mathrm{s})\right]}{\left[2\tilde{\rho}_0 + 1\right]\left[1 + F(x_\mathrm{s}, x_\mathrm{s}', \tilde{\eta}_0)\right] - 3G(x_\mathrm{s})}, \tag{5.14a}$$

$$F(x_\mathrm{s}, x_\mathrm{s}', \tilde{\eta}_0) = (1 - \mathrm{i}x_\mathrm{s})\left[\frac{\tilde{\eta}_0 x_\mathrm{s}'^2(\tan x_\mathrm{s}' - x_\mathrm{s}')}{(3 - x_\mathrm{s}'^2)\tan x_\mathrm{s}' - 3x_\mathrm{s}'} - 2(\tilde{\eta}_0 - 1)\right]^{-1}, \tag{5.14b}$$

$$G(x_\mathrm{s}) = \frac{3}{x_\mathrm{s}}\left(\frac{1}{x_\mathrm{s}} - \mathrm{i}\right). \tag{5.14c}$$

In the limit of $\tilde{\eta}_0 \to \infty$ the function F vanishes and the result reduces to that obtained by Settnes and Bruus considering a compressible particle in a viscous fluid without thermal effects and without describing stresses and waves inside the particle. One finds

$$f_1(\tilde{\eta}_0 \to \infty) = \frac{2\left[\tilde{\rho}_0 - 1\right]\left[1 - G(x_\mathrm{s})\right]}{2\tilde{\rho}_0 + 1 - 3G(x_\mathrm{s})}. \tag{5.15}$$

This result, though written very differently, was obtained also by Allegra and Hawley in the context of attenuation of sound in suspensions and is valid for a solid elastic particle [9].

Considering the limit where the particle becomes much larger than the viscous boundary layer thicknesses we expect the result in Eq. (5.14) to reduce to the classical result for a particle in an ideal fluid. This is easily confirmed because in this limit $x_\mathrm{s} \to \infty$ and

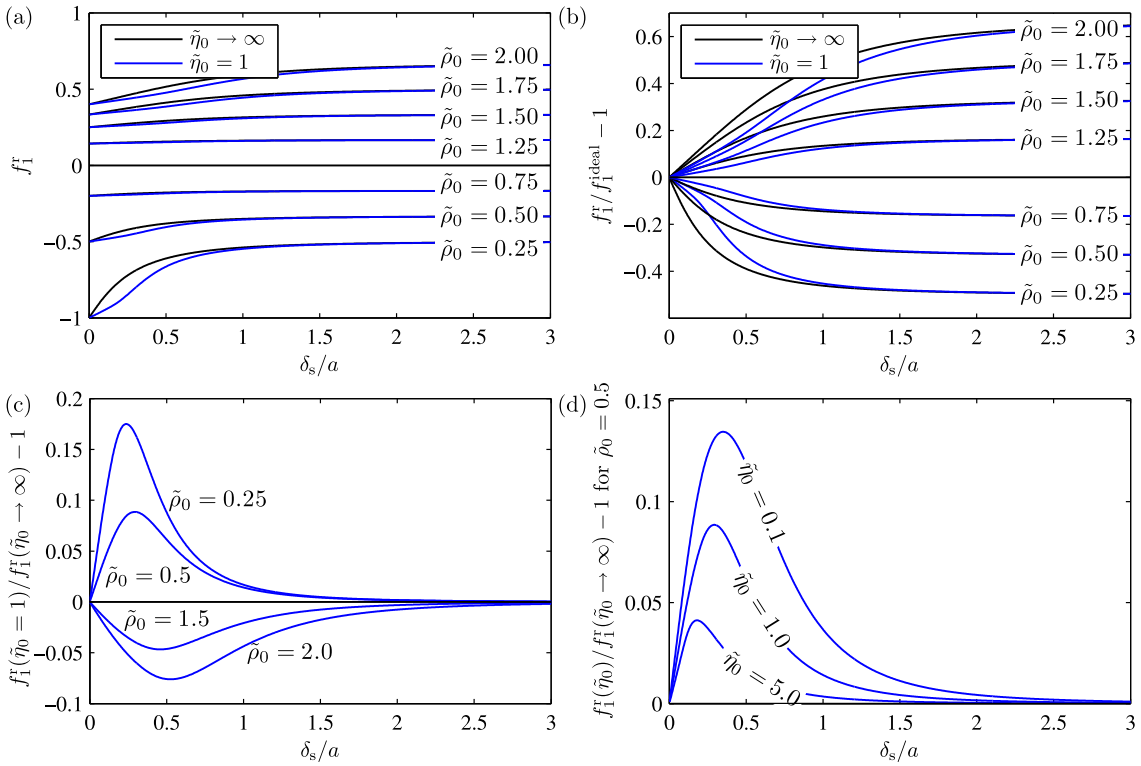

Figure 5.4: Real part f_1^{r} of the dipole scattering coefficient plotted against the normalized viscous boundary layer thickness for various parameter values of $\tilde{\rho}_0 = \rho_0'/\rho_0$ and $\tilde{\eta}_0 = \eta_0'/\eta_0$. (a) Real part f_1^{r} for different values of $\tilde{\rho}_0$. (b) Real part f_1^{r} relative to the dipole coefficient of an ideal fluid f_1^{ideal} for different values of $\tilde{\rho}_0$. (c)-(d) Real part $f_1^{\mathrm{r}}(\tilde{\eta}_0)$ relative to $f_1^{\mathrm{r}}(\tilde{\eta}_0 \to \infty)$ for different values of $\tilde{\rho}_0$ and $\tilde{\eta}_0$, respectively.

consequently $G(x_{\mathrm{s}})$ vanishes such that the factor $(1+F)$ drops out of the numerator and denominator thus reducing the fraction to the classical result for a particle in an ideal fluid [41]. In the opposite limit of a small particle, $x_{\mathrm{s}}, x_{\mathrm{s}}' \to 0$, we must expand the tangents in F to fifth order to get the correct limiting value of $F(x_{\mathrm{s}}' \to 0) = 1/(2+3\tilde{\eta}_0)$. With F finite the second bracket in the numerator of Eq. (5.14a) is dominated by the term with $G(x_{\mathrm{s}}) \to \infty$, and in the denominator only the term with $G(x_{\mathrm{s}})$ is important, and it may thus be divided out of the fraction. Hence, the asymptotic expressions for the dipole scattering coefficient are

$$f_1(a/\delta_{\mathrm{s}} \to \infty) = f_1^{\mathrm{ideal}} = \frac{2(\tilde{\rho}_0 - 1)}{2\tilde{\rho}_0 + 1}, \qquad \text{(Large particle limit)} \tag{5.16a}$$

$$f_1(a/\delta_{\mathrm{s}} \to 0) = \frac{2}{3}(\tilde{\rho}_0 - 1), \qquad \text{(Small particle limit)}. \tag{5.16b}$$

These asymptotic limits were also found by Settnes and Bruus [15], and by Doinikov though with a misprint in the sign for the small particle limit [43].

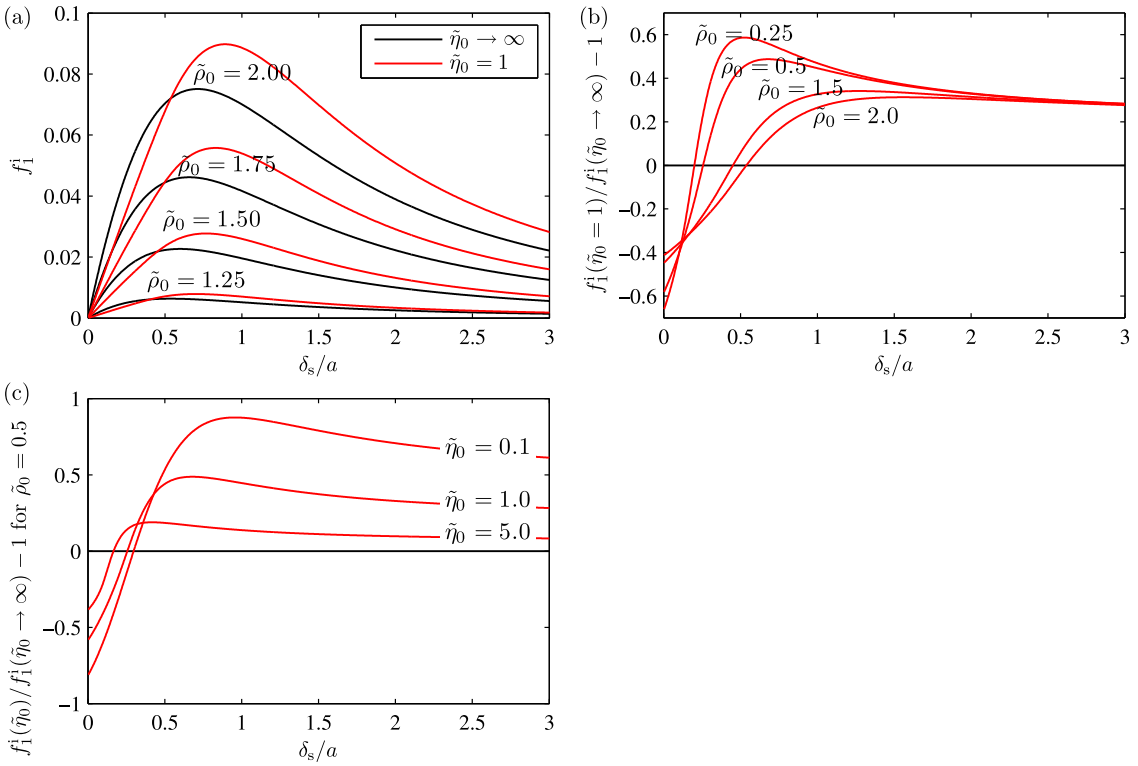

Figure 5.5: Imaginary part f_1^{i} of the dipole scattering coefficient plotted against the normalized viscous boundary layer thickness for various parameter values of $\tilde{\rho}_0 = \rho_0'/\rho_0$ and $\tilde{\eta}_0 = \eta_0'/\eta_0$. (a) Imaginary part f_1^{i} for different values of $\tilde{\rho}_0$. (b)-(c) Imaginary part $f_1^{\mathrm{i}}(\tilde{\eta}_0)$ relative to $f_1^{\mathrm{r}}(\tilde{\eta}_0 \to \infty)$ for different values of $\tilde{\rho}_0$ and $\tilde{\eta}_0$, respectively. For an ideal fluid the imaginary part of the scattering coefficient is zero.

Fig. 5.4 and Fig. 5.5 presents plots of the real part f_1^{r} and the imaginary part f_1^{i}, respectively, of the dipole scattering coefficient as functions of δ_{s}/a. We see that the greater the density contrast between the particle and the medium, the greater the deviation from classical ideal theory as expected. The plots also compare the expression for a viscous fluid droplet Eq. (5.14) with that of an elastic solid particle obtained in the limit of $\tilde{\eta}_0 \to \infty$ as given in Eq. (5.15). For the real part the two results differ significantly only for $\delta_{\mathrm{s}}/a \lesssim 2$, while for the imaginary part convergence with increasing δ_{s}/a is slower. In the limit of $\delta_{\mathrm{s}}/a \gg 1$ the two are equal with vanishing imaginary part as given in Eq. (5.16b).

5.6 Results for the acoustic radiation force

We investigate how the thermoviscous corrections affect the radiation force on a small particle in a standing wave field. Settnes and Bruus calculated the radiation force $\boldsymbol{F}^{\mathrm{rad}}$ on a particle by integrating the time-averaged second-order forces acting on a fixed surface encompassing the particle [15]. The general result is valid for ideal, viscous and thermovis-

cous theories because the integration is carried out in the far-field where the fluid medium may be considered ideal due to the smallness of Γ_s and Γ_t. The result of their calculation is

$$\boldsymbol{F}^\mathrm{rad} = -\pi a^3 \left[\frac{2\kappa_s}{3} \mathrm{Re}\left[f_0^* p_1^* \boldsymbol{\nabla} p_1 \right] - \rho_0 \mathrm{Re}\left[f_1^* \boldsymbol{v}_1^* \cdot \boldsymbol{\nabla} \boldsymbol{v}_1 \right] \right], \tag{5.17}$$

with p_1 and $\boldsymbol{v}_1$ evaluated at the particle position which is assumed to be away from walls, such that the boundary layers of the particle and of the walls do not overlap. This requirement is easily fulfilled in the limit relevant to microchannel acoustophoresis applications. In this limit the expressions for the first-order fields given in Eq. (3.43) evaluated in the bulk equals that of a horizontal pressure half-wave resonance to a very good approximation.

We consequently consider a horizontal pressure half-wave resonance, $p_1 = p_\mathrm{a} \sin(ky)$, $\boldsymbol{v}_1 = -(\mathrm{i}/\rho_0 c) p_\mathrm{a} \cos(ky) \mathbf{e}_y$, with channel width w and wavenumber $k = \pi/w$, for which the acoustic energy density is $E_\mathrm{ac} = (1/4)\kappa_s p_\mathrm{a}^2 = (1/4)\rho_0 v_\mathrm{a}^2$, where p_a and v_a are the pressure and velocity amplitudes, respectively. The expression for the radiation force then simplifies to

$$\boldsymbol{F}_\mathrm{1D}^\mathrm{rad} = -4\pi \Phi_\mathrm{ac} a^3 k E_\mathrm{ac} \sin(2ky) \mathbf{e}_y, \tag{5.18a}$$

$$\Phi_\mathrm{ac} = \frac{1}{3}\mathrm{Re}\left[f_0\right] + \frac{1}{2}\mathrm{Re}\left[f_1\right], \tag{5.18b}$$

where Φ_ac is the so-called acoustic contrast factor. The thermoviscous corrections to the radiation force are thus incorporated into Φ_ac and with the radiation force proportional to Φ_ac it is the relevant quantity to investigate further. Note that if the acoustic contrast factor is positive $\Phi_\mathrm{ac} > 0$ the particles will experience a force towards the nodes of the standing pressure wave, while the case of negative acoustic contrast factors $\Phi_\mathrm{ac} < 0$ leads to a force directed towards the anti-nodes.

In Fig. 5.6 we have plotted the acoustic contrast factor Φ_ac as a function of the viscous boundary layer thickness normalized by the particle radius δ_s/a. We have used parameters and parameter ratios typical of a vegetable oil droplet immersed in water at room temperature, namely

$$\begin{aligned} \gamma = 1.01, \quad \mathrm{Pr} = 6.1, \quad \tilde{\rho}_0 = 0.9, \quad \tilde{\kappa}_s = 1.1, \\ \tilde{D}_\mathrm{th} = 0.8, \quad \tilde{\alpha}_p = 3.5, \quad \tilde{C}_p = 0.5, \quad \tilde{\eta}_0 = 50, \end{aligned} \tag{5.19}$$

where only γ and Pr are absolute parameters for water, while the parameters with a tilde are parameter ratios typical to those of a vegetable oil such as sunflower oil [53] to those of water, e.g. $\tilde{\rho}_0 = \rho_0'/\rho_0 = 0.9$. The plots were generated by expressing x_s, x_s', x_t, and x_t' as functions of δ_s/a by using that $\delta_\mathrm{t} = \delta_\mathrm{s}/\mathrm{Pr}^{1/2}$, which leads to

$$x_\mathrm{s} = (1+\mathrm{i})\frac{a}{\delta_\mathrm{s}}, \qquad x_\mathrm{s}' = (1+\mathrm{i})\frac{\tilde{\rho}_0^{1/2}}{\tilde{\eta}_0^{1/2}}\frac{a}{\delta_\mathrm{s}}, \tag{5.20a}$$

$$x_\mathrm{t} = (1+\mathrm{i})\mathrm{Pr}^{1/2}\frac{a}{\delta_\mathrm{s}}, \quad x_\mathrm{t}' = (1+\mathrm{i})\frac{\mathrm{Pr}^{1/2}}{\tilde{D}_\mathrm{th}^{1/2}}\frac{a}{\delta_\mathrm{s}}. \tag{5.20b}$$

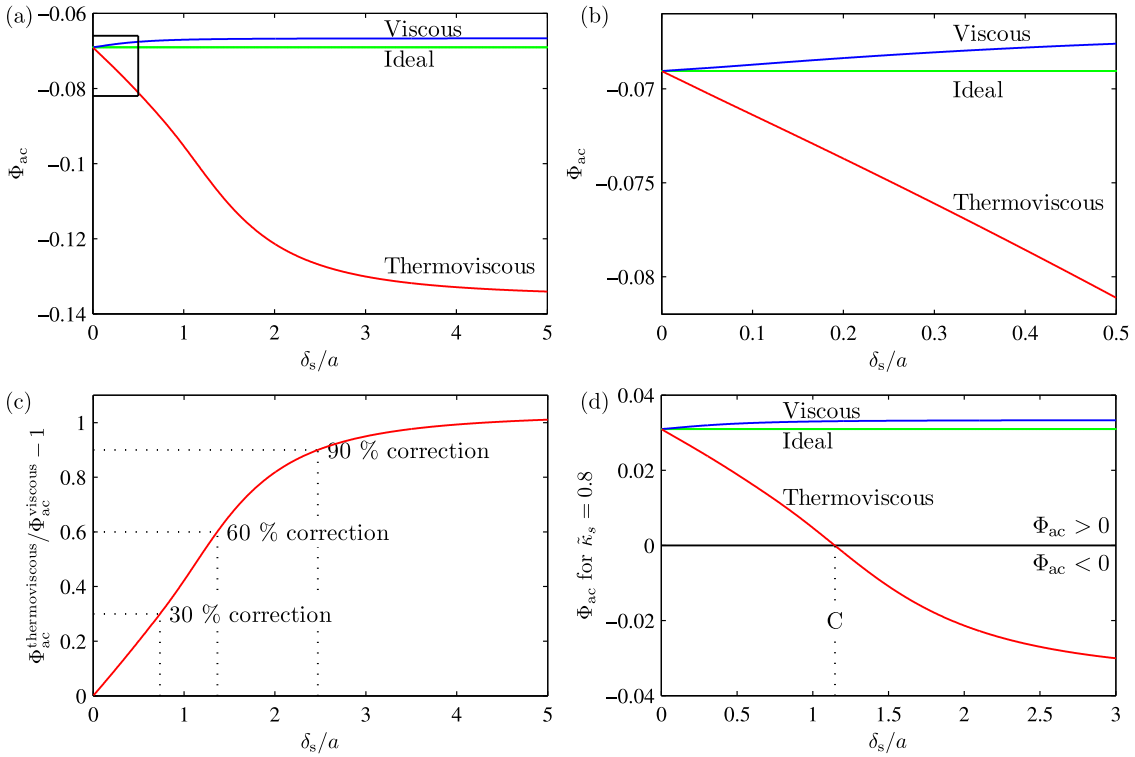

Figure 5.6: Acoustic contrast factor Φ_{ac} for typical parameters of a vegetable oil droplet immersed in water in a horizontal standing wave field. Ideal fluid theory, viscous theory, and thermoviscous theory are compared. (a) The acoustic contrast factor Φ_{ac} plotted as a function of the viscous boundary layer thickness δ_s divided by the particle radius a. (b) Zoom of the window indicated in (a) for small values of δ_s/a. (c) Relative comparison of viscous and thermoviscous theory. The thermoviscous theory introduces corrections of more than 100% compared to the viscous theory. (d) Same as in (a) but with $\tilde{\kappa}_s = 0.8$ instead of $\tilde{\kappa}_s = 1.1$. For these parameters the acoustic contrast factor Φ_{ac} changes sign at a critical value of δ_s/a indicated by the point C. This prediction is discussed in more detail in the text.

Fig. 5.6 shows that for the configuration of a typical vegetable oil droplet in water the acoustic contrast factor is negative such that the droplets will be focused at the anti-nodes of the pressure wave. The viscous correction arising from the corrected dipole scattering coefficient is small in comparison to the thermal corrections from the monopole scattering coefficient and we observe that the thermoviscous theory results in corrections to the viscous theory of more than 100% for sufficiently small particles.

One consequence of the relatively large correction from thermal effects in the monopole scattering coefficient is that we may think of systems for which the acoustic contrast factor changes sign as the frequency is varied. This is illustrated in Fig. 5.6(d) for the same parameters as those of Eq. (5.19) except with $\tilde{\kappa}_s = 0.8$, which means that the droplet

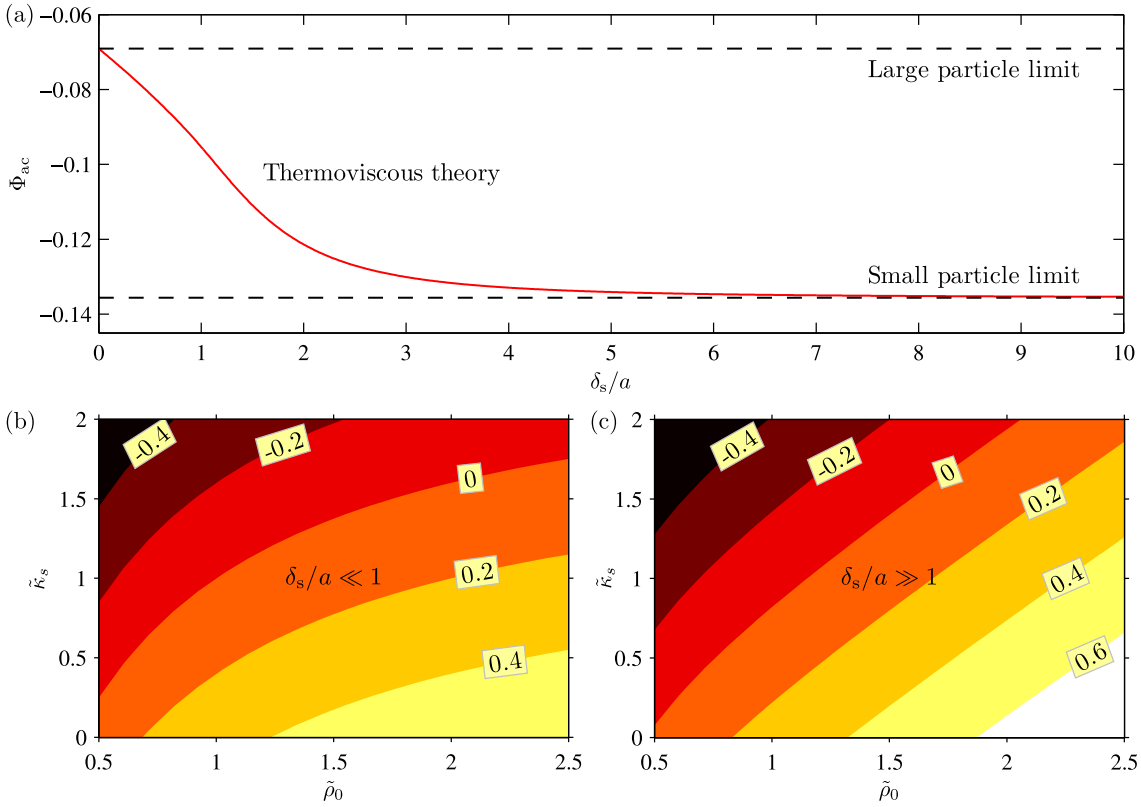

Figure 5.7: Acoustic contrast factor Φ_{ac} for typical parameters of a vegetable oil droplet immersed in water in a horizontal standing wave field. (a) Φ_{ac} plotted against the viscous boundary layer thickness δ_s divided by the particle radius a with the asymptotic limits for large and small particles indicated. (b)-(c) Contours of Φ_{ac} in the $(\tilde{\rho}_0, \tilde{\kappa}_s)$-plane in the asymptotic limit of large and small particles, respectively.

is less compressible than water. For a system with $\tilde{\kappa}_s = 0.8$ the figure shows that with thermoviscous corrections accounted for, the acoustic contrast factor changes sign at some critical value when δ_s/a is increased, which may be achieved for example by decreasing the frequency or increasing the particle size. The frequency corresponding to a given value of δ_s/a may be calculated as $f = \nu_0/[\pi a^2(\delta_s/a)^2]$. For a particle of radius $a = 1$ μm this gives a critical frequency of $f_C = 0.2$ MHz, at which the acoustic contrast factor changes sign as indicated in the figure.

It should be possible to design a microfluidic experiment where this prediction of positive and negative acoustic contrast factors can be tested. By varying the relative compressibility $\tilde{\kappa}_s$ the curve for Φ_{ac} in Fig. 5.6(d) may be shifted vertically and the crossing frequency changed. Another possibility is to change the viscosity of the water by adding glycerol or to consider particles of different sizes a at the same resonance frequency, which is perhaps the most promising experimental method considering a single resonant microchannel can be used. An experimental observation of the change of sign in the acoustic

contrast factor at some critical frequency, particle size, or viscosity would provide direct experimental verification of the importance of the thermal correction to the monopole scattering coefficient and would be well worth pursuing experimentally.

Combining the derived asymptotic expressions for the monopole and the dipole coefficients in Eq. (5.12) and Eq. (5.16) with the expression for the acoustic contrast factor in Eq. (5.18), one may derive expressions for the acoustic contrast factor in the limits of large and small particle sizes relative to the boundary layer thicknesses. In Fig. 5.7(a) the acoustic contrast factor $\Phi_{\rm ac}$ is plotted for the parameters of oil in water, Eq. (5.19), together with the asymptotic expressions in the limits of large and small particle sizes. The two limits are investigated further in Fig. 5.7(b) and (c) where contours of the acoustic contrast factor $\Phi_{\rm ac}$ are shown in the $(\tilde{\rho}_0, \tilde{\kappa}_s)$-plane with the other parameters kept fixed at the values of Eq. (5.19). The plots provide a general trend showing how thermoviscous corrections affect the radiation force for different values of $\tilde{\rho}_0$ and $\tilde{\kappa}_s$. In any particular case of interest we expect that most parameter values have some degree of interdependence and one must use the actual parameter ratios in order to get accurate estimates for the acoustic contrast factor. The plots show quite clearly, however, that for particles comparable to and smaller than the boundary layer thicknesses the thermoviscous corrections cannot be neglected without making errors that might be well above 10%, such as in the case of a vegetable oil in water where the thermoviscous theory leads to corrections of more than 100%.

5.7 Outlook on the acoustic radiation force

With much ongoing experimental research in acoustophoresis aimed at focusing still smaller particles such as submicrometer-sized bacteria and vira [54] the thermoviscous corrections to the radiation force can no longer be ignored, and we find that there is a need to tell the story of acoustic radiation forces on small particles, and to gather a collection of scattering coefficients f_0 and f_1 for a few important cases such as the rigid sphere, the solid elastic sphere, and the fluid droplet. Having once solved the thermoviscous scattering problem for a given scatterer Eq. (5.17) provides a way of evaluating acoustic radiation forces regardless of the incident field. This provides an easy and accessible formalism for evaluating acoustic radiation forces in experimental systems and an important step in bridging theory and experiment not achieved in past theoretical works on the thermoviscous radiation force problem.

A numerical finite-element model for calculating acoustic radiation forces on particles in a thermoviscous fluid medium is currently under development in a collaboration between the Theoretical Microfluidics group and COMSOL Multiphysics. The model will provide a direct means for numerical evaluation of the analytical theory presented in this thesis.

The theoretical prediction made in this thesis that thermoviscous corrections to the radiation force on small particles allow for a change in sign in the acoustic contrast factor at some critical frequency, particle size, or viscosity should be investigated further and if possible tested experimentally. The Theoretical Microfluidics group has a close collaboration with the Laurell group at Lund university possessing a high level of expertise in

experimental acoustophoresis. We may be able to design an experiment that can test the theoretical prediction.

Chapter 6

Conclusion and outlook

In this thesis we have studied acoustofluidics in microsystems under the unifying theme of *thermoviscous effects*. Until this work thermal effects have been neglected in most analytical theories of acoustofluidics [12, 13, 14, 15], except in the study of acoustic streaming [22]. Reviewing the literature from other fields we found that the framework of Epstein and Carhart [8] provides a theory of thermoviscous acoustics well suited for the study of microsystem acoustophoresis. The theory was developed in Chapter 2 with the main result being the derivation of three distinct wave equations corresponding to the longitudinal compressional mode, the longitudinal thermal mode, and the transverse shear mode. The thermal mode and the shear mode are highly damped waves describing thermal and viscous boundary layers emerging at interfaces between materials with different thermoacoustic properties such as density, compressibility, and heat conductivity. The description of thermoviscous acoustics utilizing these modes provides a mathematically rigorous and physically intuitive description of thermoviscous acoustofluidics.

The theoretical framework was further developed in Chapter 3 and applied to obtain a resonant field solution to the driven parallel-plate system. The solution is correct to first order in $k_0\delta_\mathrm{s}$, where $k_0 = 2\pi/\lambda$ is the wavenumber and δ_s is the viscous boundary layer thickness. It thus represents an improvement over classical Prandtl-Schlichting boundary layer theory approaches that are zeroth order in $k_0\delta_\mathrm{s}$ [12]. As a consequence, our theory describes variation of the acoustic fields perpendicular to walls, showing perfect agreement with numerical simulations in the full solution domain as described in Chapter 4. Interestingly, the analytical solution moreover describes the physics of the transition from low frequency shear flow solutions dominated by viscosity, with resonances completely suppressed, into the acoustic regime where the actuation results in a resonant field with large amplitudes. The resonant regime was investigated further in relation to microchannel acoustofluidics in Chapter 4 where we considered several measurable consequences of the theory. For example, the theory explains experimental values of quality-factors measured to 577 and 209 [33] as the consequence of viscous and thermal dissipation in the boundary layers near the walls.

Chapter 5 dealt with thermoviscous corrections to the acoustic radiation force. Reviewing the literature we found a need to treat thermoviscous effects in the limit relevant

to microparticle acoustophoresis, where the boundary layer thicknesses δ_s and δ_t are the same order of magnitude as the particle radius a but much less than the wavelength λ, i.e., $\delta_s \sim \delta_t \sim a \ll \lambda$. Following the treatment of Epstein and Carhart [8] we derived expressions for the monopole and dipole scattering coefficients for the case of a viscous, heat-conducting spherical droplet in a viscous, heat-conducting fluid medium. We found that thermal effects couple to the monopole mode of radial compression and expansion of the particle relative to the fluid medium, while viscous effects couple to the dipole mode describing an oscillating back-and-forth motion of the particle relative to the fluid medium. Using the derived scattering coefficients we evaluated the acoustic radiation force on the particle by applying the theory of Settnes and Bruus [15]. We found that thermal effects may lead to large corrections to the radiation force when the boundary layer thicknesses become comparable to the particle radius. For the case of a typical vegetable oil droplet in water we found corrections of more than 100%. With much ongoing experimental research in acoustofluidics aiming at focusing submicrometer-sized particles such as bacteria and vira [54] these corrections are interesting not only theoretically, but also from an engineering point of view.

Outlook

Acoustic radiation force

We wish to present the results of this thesis in a journal article including numerical results from the COMSOL Multiphysics model currently being developed. The analytical theory may be extended to include solid particles and a complete theory of thermoviscous acoustic radiation forces in the long-wavelength limit may be presented.
It should be possible to experimentally test the prediction made in this thesis that the thermoviscous corrections to the radiation force allow for a change in sign in the acoustic contrast factor at some critical frequency, particle size, or viscosity.

Chip design

The analytical parallel-plate theory may be extended to include acoustic impedance of the walls as well as sidewalls. One may consider investigating the effect of layered material on energy densities, quality-factors, and timescales of the system. Analytical estimates could prove valuable for assessing the possibilities and limitations of future low-cost chip design.

Acoustic streaming

Acoustic streaming has not been a main concern in this thesis. To our knowledge a solution that does not employ the boundary layer approximation has never been presented. Moreover, a complete theory describing the second-order velocity field must include perturbations of parameter values due to the first-order pressure and temperature fields. Preliminary studies show that such perturbations could be significant.

Appendix A

Appendix to Chapter 2

A.1 Thermodynamic identities

To derive the relations for $\gamma = C_p/C_V$ given in Eq. (2.15) we will employ the Jacobian determinant [26]

$$\frac{\partial(u,v)}{\partial(x,y)} = \left(\frac{\partial u}{\partial x}\right)_y \left(\frac{\partial v}{\partial y}\right)_x - \left(\frac{\partial u}{\partial y}\right)_x \left(\frac{\partial v}{\partial x}\right)_y, \tag{A.1}$$

which has several useful properties for performing change of variables in multi-variable calculus, such as

$$\frac{\partial(u,v)}{\partial(x,y)} = \frac{\partial(u,v)}{\partial(a,b)}\frac{\partial(a,b)}{\partial(x,y)}, \text{ and } \frac{\partial(u,v)}{\partial(x,v)} = \left(\frac{\partial u}{\partial x}\right)_v. \tag{A.2}$$

Using Eq. (A.2) we obtain the ratio κ_T over κ_s

$$\frac{\kappa_T}{\kappa_s} = \frac{\frac{1}{\rho}\frac{\partial(\rho,T)}{\partial(p,T)}}{\frac{1}{\rho}\frac{\partial(\rho,s)}{\partial(p,s)}} = \frac{\frac{\partial(p,s)}{\partial(p,T)}}{\frac{\partial(\rho,s)}{\partial(\rho,T)}} = \frac{T\frac{\partial(s,p)}{\partial(T,p)}}{T\frac{\partial(s,V)}{\partial(T,V)}} = \frac{C_p}{C_V} = \gamma, \tag{A.3}$$

while we can rewrite C_V into quantities depending on T and p without references to V as follows

$$\begin{aligned} C_V &= T\left(\frac{\partial s}{\partial T}\right)_V = T\,\frac{\partial(s,V)}{\partial(T,V)} = T\,\frac{\partial(s,V)}{\partial(T,p)}\,\frac{\partial(T,p)}{\partial(T,V)} \\ &= T\left[\left(\frac{\partial s}{\partial T}\right)_p\left(\frac{\partial V}{\partial p}\right)_T - \left(\frac{\partial s}{\partial p}\right)_T\left(\frac{\partial V}{\partial T}\right)_p\right]\left(\frac{\partial V}{\partial p}\right)_T^{-1} \\ &= T\left(\frac{\partial s}{\partial T}\right)_p - T\left(\frac{\partial s}{\partial p}\right)_T\left(\frac{\partial \rho}{\partial T}\right)_p\left(\frac{\partial \rho}{\partial p}\right)_T^{-1} \\ &= C_p - T\,\frac{\alpha_p}{\rho}\alpha_p\,\frac{1}{\kappa_T} = C_p - \frac{\alpha_p^2 T}{\kappa_T \rho}, \end{aligned} \tag{A.4}$$

Consequently, using $\gamma = C_p/C_V$ with Eq. (A.3) and Eq. (A.4), we obtain

$$\gamma - 1 = \frac{C_p - C_V}{C_V} = \frac{\alpha_p^2 T}{\kappa_T \rho C_V} = \frac{\alpha_p^2 T}{\kappa_s \rho C_p}. \tag{A.5}$$

Appendix B

Appendix to Chapter 4

B.1 Acoustic energy density: Calculations

This section has been included to show the details of the calculation going from Eq. (4.7) to Eq. (4.8) in section Section 4.1.4 concerning the energy lineshape function of the acoustic resonance in the parallel-plate system. The starting point is Eq. (4.7)

$$E_{\mathrm{ac}} \simeq \frac{1}{4}\rho_0 v_{\mathrm{bc}}^2 \frac{1}{|\cos\left(k_y w/2\right)|^2}. \tag{B.1}$$

We will write the wavenumber with real and imaginary parts as $k_y = k_y^{\mathrm{r}} + \mathrm{i}k_y^{\mathrm{i}}$, with $k_y^{\mathrm{r}}, k_y^{\mathrm{i}} \in \mathbb{R}$. Moreover, we will indicate the wavenumber calculated at resonance frequency with a hat, i.e. $\hat{k}_y^{\mathrm{r}}$ is the real part of wavenumber k_y calculated at resonance frequency ω_{res}.

Expanding $\cos(k_y w/2)$ around resonance conditions $\hat{k}_y w/2$ yields

$$\begin{aligned}\cos\left(k_y w/2\right) &\simeq \cos\left(\hat{k}_y w/2\right) - \sin\left(\hat{k}_y w/2\right)\frac{w}{2}\left(k_y - \hat{k}_y\right), \\ &\simeq -\frac{w}{2}\left(k_y^{\mathrm{r}} - \hat{k}_y^{\mathrm{r}} + \mathrm{i}k_y^{\mathrm{i}}\right),\end{aligned} \tag{B.2}$$

where we wrote out the complex arguments with explicit real and imaginary parts and evaluated to first order the resulting expressions noting that $\sin(\hat{k}_y^{\mathrm{r}} w/2) = 1$, $\cos(\hat{k}_y^{\mathrm{r}} w/2) = 0$, and $\hat{k}_y^{\mathrm{i}} w/2 \ll 1$.

When close to resonance, $\omega \simeq \omega_{\mathrm{res}}$, it is a good approximation to replace $k_y^{\mathrm{i}} \simeq \hat{k}_y^{\mathrm{i}}$ in the last term, thus writing

$$\cos\left(k_y w/2\right) \simeq -\frac{w}{2}\left(k_y^{\mathrm{r}} - \hat{k}_y^{\mathrm{r}} + \mathrm{i}\hat{k}_y^{\mathrm{i}}\right). \tag{B.3}$$

Using the expressions for the wavenumbers Eq. (4.1) to go from wavenumbers to frequencies and moreover taking the absolute square gives

$$|\cos\left(k_y w/2\right)|^2 \simeq \frac{w^2}{4c^2}\left[\left(\omega - \omega_{\mathrm{res}}\right)^2 + \Gamma_{\mathrm{sys}}^2 \omega_{\mathrm{res}}^2\right], \tag{B.4}$$

where we have defined the complete thermoviscous damping factor Γ_{sys} as

$$\Gamma_{\mathrm{sys}} = \frac{1}{2h}\left[\delta_{\mathrm{s}} + (\gamma - 1)\delta_{\mathrm{t}}\right]. \tag{B.5}$$

Inserting in Eq. (B.1) for E_{ac} and using that $\omega_{\mathrm{res}} \simeq \pi c/w$ then gives the final Lorentzian line shape as a function of frequency,

$$E_{\mathrm{ac}} = \frac{\rho_0 v_{\mathrm{bc}}^2}{\pi^2} \frac{\omega_{\mathrm{res}}^2}{\left(\omega - \omega_{\mathrm{res}}\right)^2 + \Gamma_{\mathrm{sys}}^2 \omega_{\mathrm{res}}^2}, \quad \omega \simeq \omega_{\mathrm{res}}. \tag{B.6}$$

B.2 Higher modes: Calculations

B.2.1 Auxiliary functions G^{r} and G^{i}

The functions G^{r} and G^{i} used in Eq. (4.26) derive from

$$\tan[(\tilde{k}_z^{\mathrm{r}} + \mathrm{i}\tilde{k}_z^{\mathrm{i}})/2] = G^{\mathrm{r}} + \mathrm{i}G^{\mathrm{i}}, \quad G^{\mathrm{r}}, G^{\mathrm{i}} \in \mathbb{R}. \tag{B.7}$$

Written out explicitly G^{r} and G^{i} are given as

$$G^{\mathrm{r}} = \frac{\tan\left(\tilde{k}_z^{\mathrm{r}}/2\right)\left[1 - \tanh^2\left(\tilde{k}_z^{\mathrm{i}}/2\right)\right]}{1 + \tan^2\left(\tilde{k}_z^{\mathrm{r}}/2\right)\tanh^2\left(\tilde{k}_z^{\mathrm{i}}/2\right)}, \tag{B.8a}$$

$$G^{\mathrm{i}} = \frac{\tanh\left(\tilde{k}_z^{\mathrm{i}}/2\right)\left[1 + \tan^2\left(\tilde{k}_z^{\mathrm{r}}/2\right)\right]}{1 + \tan^2\left(\tilde{k}_z^{\mathrm{r}}/2\right)\tanh^2\left(\tilde{k}_z^{\mathrm{i}}/2\right)}, \tag{B.8b}$$

B.2.2 Expansion coefficients C_n

The expansion coefficients of Eq. (4.31) are

$$C_n = \frac{2A_0}{h}\int_{-h/2}^{h/2}\left[\sin\left(k_z^0 z\right) - B_0 \sinh\left[(1 - \mathrm{i})z/\delta_{\mathrm{s}}\right]\right]\sin\left(2\pi n\frac{z}{h}\right)\mathrm{d}z. \tag{B.9}$$

To simplify matters note that

$$\sinh\left[(1 - \mathrm{i})z/\delta_{\mathrm{s}}\right] = \sinh\left(-\mathrm{i}k_{\mathrm{s}}z\right) = -\mathrm{i}\sin\left(k_{\mathrm{s}}z\right), \tag{B.10}$$

with $k_{\mathrm{s}} = (1 + i)/\delta_{\mathrm{s}}$ the usual shear wavenumber. Then the expansion coefficients are written as

$$C_n = \frac{2A_0}{h}\int_{-h/2}^{h/2}\left[\sin\left(k_z^0 z\right) + \mathrm{i}B_0 \sin\left(k_{\mathrm{s}}z\right)\right]\sin\left(2\pi n\frac{z}{h}\right)\mathrm{d}z. \tag{B.11}$$

The integrals are evaluated as

$$\int_{-h/2}^{h/2}\sin\left(Kz\right)\sin\left(2\pi n\frac{z}{h}\right)\mathrm{d}z = \frac{4\pi n h(-1)^n}{K^2h^2 - (2\pi n)^2}\sin\left(\frac{Kh}{2}\right). \tag{B.12}$$

Consequently, we find

$$C_n = (-1)^n 8\pi n A_0 \left[\frac{\sin\left(k_z^0 h/2\right)}{(k_z^0)^2 h^2 - (2\pi n)^2} + \mathrm{i} B_0 \frac{\sin\left(k_\mathrm{s} h/2\right)}{k_\mathrm{s}^2 h^2 - (2\pi n)^2} \right], \tag{B.13}$$

as given in Eq. (4.32).

B.3 Acoustic streaming: Calculations

B.3.1 Scaling arguments in the boundary layer region

To simplify the treatment of the second-order equations for the streaming velocity field we consider several approximations valid in the boundary layer region.

The first-order fields in the isentropic limit are obtained from Eq. (3.43) of Chapter 3,

$$p_1 = \mathrm{i}\omega\rho_0 \frac{v_\mathrm{bc}}{k_y} \frac{\sin\left(k_y y\right)}{\cos\left(k_y w/2\right)} \cos\left(k_z z\right), \tag{B.14a}$$

$$v_{1y} = v_\mathrm{bc} \frac{\cos\left(k_y y\right)}{\cos\left(k_y w/2\right)} \left[\cos\left(k_z z\right) - \cos\left(\frac{k_z h}{2}\right) \frac{\cosh\left[(1-\mathrm{i})z/\delta_\mathrm{s}\right]}{\cosh\left[(1-\mathrm{i})h/2\delta_\mathrm{s}\right]} \right], \tag{B.14b}$$

$$v_{1z} = -v_\mathrm{bc} \frac{k_z}{k_y} \frac{\sin\left(k_y y\right)}{\cos\left(k_y w/2\right)} \left[\sin\left(k_z z\right) - \sin\left(\frac{k_z h}{2}\right) \frac{\sinh\left[(1-\mathrm{i})z/\delta_\mathrm{s}\right]}{\sinh\left[(1-\mathrm{i})h/2\delta_\mathrm{s}\right]} \right]. \tag{B.14c}$$

In the boundary layers near the walls we see that derivatives of the first-order velocity scale as

$$\partial_y \sim k_y, \quad \partial_z \sim 1/\delta_\mathrm{s}. \tag{B.15}$$

Moreover from Eq. (3.48) in the isentropic limit

$$k_y = \frac{\omega}{c}\left[1 + (1+\mathrm{i})\frac{\delta_\mathrm{s}}{2h}\right], \quad k_z = -i\frac{\omega}{c}\sqrt{(1+\mathrm{i})\frac{\delta_\mathrm{s}}{h}}, \tag{B.16}$$

and consequently

$$k_z \sim \sqrt{\frac{\delta_\mathrm{s}}{h}} k_y. \tag{B.17}$$

From the expression for the first-order fields and this relation we find that v_{1z} is an order $k_y\delta_\mathrm{s}$ smaller than v_{1y}. Indeed

$$v_{1z} \sim \frac{k_z^2 h}{k_y} v_{1y} \sim k_y \delta_\mathrm{s} v_{1y}. \tag{B.18}$$

These considerations allow a great simplification of the theory when considering the streaming velocity field in the boundary layer and leads to the approximate equations that will be used to derive the effective streaming boundary condition on the bulk velocity field.

B.3.2 Approximation of the potential equations

In this section we will derive approximations of the potential equations Eq. (4.42) for $\langle\phi_2\rangle$ and $\langle\psi_2\rangle$ in the boundary layer. For convenience the equations are given below

$$\nabla^2\langle\phi_2\rangle = -\frac{1}{\rho_0}\boldsymbol{\nabla}\cdot\langle\rho_1\boldsymbol{v}_1\rangle\,, \tag{B.19a}$$

$$\nu_0\nabla^2\nabla^2\langle\psi_2\rangle = -\langle S\rangle\,. \tag{B.19b}$$

We will approximate the bi-harmonic operator as well as the Laplace operator noting that the variation of the first-order fields will be inherited by the two potentials. Consequently $\partial_y \sim k_y$ and $\partial_z \sim 1/\delta_\mathrm{s}$, and we write

$$\nabla^2\nabla^2 = \partial_y^4 + \partial_z^4 + 2\partial_y^2\partial_z^2 = \partial_z^4 + \mathcal{O}\left(k_y^2\delta_\mathrm{s}^2\right), \tag{B.20a}$$

$$\nabla^2 = \partial_y^2 + \partial_z^2 = \partial_z^2 + \mathcal{O}\left(k_y^2\delta_\mathrm{s}^2\right). \tag{B.20b}$$

Then the potential equations become

$$\partial_z^2\langle\phi_2\rangle = -\frac{1}{\rho_0}\boldsymbol{\nabla}\cdot\langle\rho_1\boldsymbol{v}_1\rangle + \mathcal{O}\left(k_y^2\delta_\mathrm{s}^2\right), \tag{B.21a}$$

$$\nu_0\partial_z^4\langle\psi_2\rangle = -\langle S\rangle + \mathcal{O}\left(k_y^2\delta_\mathrm{s}^2\right). \tag{B.21b}$$

From these two equations and the expression for the source in Eq. (4.37b) we may approximate the order of magnitude of the two potentials in the boundary layer

$$\langle\phi_2\rangle \sim \delta_\mathrm{s}^2\frac{\rho_1}{\rho_0}k_y u_0 \sim \delta_\mathrm{s}^2 k_y\frac{u_0^2}{c}, \tag{B.22a}$$

$$\langle\psi_2\rangle \sim \frac{1}{\delta_\mathrm{s}^2\omega}\delta_\mathrm{s}^4 k_y\frac{1}{\delta_\mathrm{s}}u_0^2 \sim \delta_\mathrm{s}\frac{u_0^2}{c}, \tag{B.22b}$$

where u_0 is the magnitude of $\boldsymbol{v}_1$, and we have used that $\nu_0 = \delta_\mathrm{s}^2\omega/2$ and that $k_y \simeq \omega/c$. Consequently we have found that

$$\langle\phi_2\rangle \sim k_y\delta_\mathrm{s}\langle\psi_2\rangle\,, \tag{B.23}$$

which means that

$$\langle v_{2y}\rangle = \partial_y\langle\phi_2\rangle + \partial_z\langle\psi_2\rangle \sim k_y^2\delta_\mathrm{s}\langle\psi_2\rangle + \frac{1}{\delta_\mathrm{s}}\langle\psi_2\rangle\,, \tag{B.24}$$

and hence

$$\langle v_{2y}\rangle = \partial_z\langle\psi_2\rangle + \mathcal{O}\left(k_y^2\delta_\mathrm{s}^2\right). \tag{B.25}$$

Combining this with Eq. (B.21b) for $\langle\psi_2\rangle$ we get an equation for $\langle v_{2y}\rangle$

$$\nu_0\partial_z^3\langle v_{2y}\rangle = -\langle S\rangle + \mathcal{O}\left(k_y^2\delta_\mathrm{s}^2\right). \tag{B.26}$$

This equation is the final result of our approximations, correct to order $\mathcal{O}\left(k_y^2\delta_\mathrm{s}^2\right)$.

To get the z-component of the velocity $\langle v_{2z}\rangle$ one would need to calculate the potentials $\langle\phi_2\rangle$ and $\langle\psi_2\rangle$ from Eq. (B.21). However, from Eq. (B.23) and the decomposition

$$\langle v_{2z}\rangle = \partial_z\langle\phi_2\rangle - \partial_y\langle\psi_2\rangle \sim k_y\langle\psi_2\rangle\,, \tag{B.27}$$

and consequently

$$\langle v_{2z}\rangle \sim k_y\delta_\mathrm{s}\left\langle v_{2y}\right\rangle, \tag{B.28}$$

which means that in the boundary layer region the z-component of the second-order streaming velocity may be neglected to order $\mathcal{O}\left(k_y\delta_\mathrm{s}\right)$ relative to the y-component.

B.3.3 Approximation of the vorticity source terms

Writing out the full expression for the vorticity source terms in Eq. (4.37b) we have

$$\begin{aligned}\langle S\rangle = \partial_y\left\{\frac{1}{\rho_0}\langle\rho_1\partial_t v_{1z}\rangle + \left\langle v_{1y}(\partial_y v_{1z})\right\rangle + \langle v_{1z}(\partial_z v_{1z})\rangle\right\}\\ - \partial_z\left\{\frac{1}{\rho_0}\left\langle\rho_1\partial_t v_{1y}\right\rangle + \left\langle v_{1y}(\partial_y v_{1y})\right\rangle + \left\langle v_{1z}(\partial_z v_{1y})\right\rangle\right\}.\end{aligned} \tag{B.29}$$

Considering the complex first-order fields it is not a pleasant outlook to have to evaluate all these terms. Some terms are more important than others, however, and with the approximations introduced in the last section we will find out which.

Assign to the terms in Eq. (B.29) from left to right numbers 1-6. To evaluate terms 1 and 4 we will use the first-order continuity equation in time-domain

$$\partial_t\rho_1 = -\rho_0\boldsymbol{\nabla}\cdot\boldsymbol{v}_1 = -\rho_0\left(\partial_y v_{1y} + \partial_z v_{1z}\right). \tag{B.30}$$

In the boundary layer both terms of the divergence are the same order of magnitude, as is easily verified

$$\partial_t\rho_1 \sim -\rho_0\left(k_y v_{1y} + \frac{1}{\delta_\mathrm{s}}v_{1z}\right) \sim -\rho_0\left(k_y v_{1y} + k_y v_{1y}\right). \tag{B.31}$$

We may then approximate the relative size of the source terms in Eq. (B.29) using the approximations appropriate in the boundary layer. With the terms arranged left to right from 1-6 as in Eq. (B.29) we find the orders of magnitude

$$\langle S\rangle \sim k_y^3\delta_\mathrm{s}\left\langle v_{1y}^2\right\rangle + k_y^3\delta_\mathrm{s}\left\langle v_{1y}^2\right\rangle + k_y^3\delta_\mathrm{s}\left\langle v_{1y}^2\right\rangle - \frac{k_y}{\delta_\mathrm{s}}\left\langle v_{1y}^2\right\rangle - \frac{k_y}{\delta_\mathrm{s}}\left\langle v_{1y}^2\right\rangle - \frac{k_y}{\delta_\mathrm{s}}\left\langle v_{1y}^2\right\rangle. \tag{B.32}$$

Consequently the first three terms are an order $k_y^2\delta_\mathrm{s}^2$ smaller than the last three, and we choose to neglect them and write

$$\langle S\rangle = -\partial_z\left\{\frac{1}{\rho_0}\left\langle\rho_1\partial_t v_{1y}\right\rangle + \left\langle v_{1y}(\partial_y v_{1y})\right\rangle + \left\langle v_{1z}(\partial_z v_{1y})\right\rangle\right\} + \mathcal{O}\left(k_y^2\delta_\mathrm{s}^2\right). \tag{B.33}$$

We may use the continuity equation to express the first term above in terms of the velocity fields only. We write

$$-\frac{1}{\rho_0}\partial_z\left\langle\rho_1\partial_t v_{1y}\right\rangle = \frac{1}{\rho_0}\partial_z\left\langle(\partial_t\rho_1)v_{1y}\right\rangle = -\partial_z\left\langle(\partial_y v_{1y})v_{1y}\right\rangle - \partial_z\left\langle(\partial_z v_{1z})v_{1y}\right\rangle. \tag{B.34}$$

Here a minus sign was introduced when moving $\partial_t = -\mathrm{i}\omega$ from one component to the other inside the time-average operator. Using the above identity the source becomes

$$\langle S\rangle = -2\partial_z\left\langle(\partial_y v_{1y})v_{1y}\right\rangle - \partial_z\left\langle(\partial_z v_{1z})v_{1y}\right\rangle - \partial_z\left\langle(\partial_z v_{1y})v_{1z}\right\rangle. \tag{B.35}$$

Now

$$-2\partial_z\left\langle(\partial_y v_{1y})v_{1y}\right\rangle = -\partial_z\left\langle\partial_y\left\{v_{1y}^2\right\}\right\rangle = -\partial_z\partial_y\left\langle v_{1y}^2\right\rangle = -\frac{1}{2}\partial_z\partial_y\left\{|v_{1y}|^2\right\}, \tag{B.36a}$$

$$-\partial_z\left\langle(\partial_z v_{1z})v_{1y}\right\rangle - \partial_z\left\langle(\partial_z v_{1y})v_{1z}\right\rangle = -\partial_z^2\left\langle v_{1y}v_{1z}\right\rangle = -\frac{1}{2}\partial_z^2\left\{\mathrm{Re}\left[v_{1y}^* v_{1z}\right]\right\}, \tag{B.36b}$$

where we have used that the time-average of a product of two time-harmonic fields may be calculated as $\langle A(t)B(t)\rangle = \mathrm{Re}[A_0^* B_0]/2$. Consequently the final expression for the approximated vorticity source is

$$\langle S\rangle = -\frac{1}{2}\partial_z\partial_y\left\{|v_{1y}|^2\right\} - \frac{1}{2}\partial_z^2\left\{\mathrm{Re}\left[v_{1y}^* v_{1z}\right]\right\} + \mathcal{O}\left(k_y^2\delta_\mathrm{s}^2\right). \tag{B.37}$$

We will not need to evaluate the source terms explicitly when solving only for the y-component of the second-order streaming velocity since a particlar solution is obtained from Eq. (4.46).

B.3.4 Evaluation of the vorticity source terms

Using the first-order fields of Eq. (3.43) in the isentropic limit as given in Eq. (B.14) we evaluate the vorticity source terms of Eq. (B.37). To evaluate the particular solution of Eq. (4.46) which will give the effective boundary condition for the bulk streaming velocity, we must evaluate $\partial_y\{|v_{1y}|^2\}$ and $\mathrm{Re}[v_{1y}^* v_{1z}]$ in the boundary layer. To do so we will work in the boundary layer at the bottom of the channel.

To simplify calculations we first make a coordinate transformation. Let us denote the symmetric coordinate system used in Eq. (B.14) as the (y, z')-coordinate system, *i.e.* let $z \to z'$ in Eq. (B.14). Then z' represents the symmetric coordinate system for which $z' \in [-h/2, h/2]$. To simplify matters we then make the coordinate transformation

$$z' = z - h/2, \tag{B.38}$$

and consequently work in the asymmetric coordinatesystem where $z \in [0, h]$. In the first-order fields we then expand the sine and cosine around $z = 0$ to first order to get

$$\cos\left(k_z z'\right) = \cos\left(k_z z - \frac{k_z h}{2}\right) \simeq \cos\left(\frac{k_z h}{2}\right), \tag{B.39a}$$

$$\sin\left(k_z z'\right) = \sin\left(k_z z - \frac{k_z h}{2}\right) \simeq -\sin\left(\frac{k_z h}{2}\right) + \cos\left(\frac{k_z h}{2}\right) k_z z. \tag{B.39b}$$

Furthermore the hyperbolic functions reduce to simple exponentials

$$\frac{\cosh\left[\frac{(1-\mathrm{i})z'}{\delta_\mathrm{s}}\right]}{\cosh\left[\frac{(1-\mathrm{i})h}{2\delta_\mathrm{s}}\right]} = \frac{\cosh\left[\frac{(1-\mathrm{i})(z-h/2)}{\delta_\mathrm{s}}\right]}{\cosh\left[\frac{(1-\mathrm{i})h}{2\delta_\mathrm{s}}\right]} = \frac{\mathrm{e}^{(1-\mathrm{i})z/\delta_\mathrm{s}}\mathrm{e}^{-(1-\mathrm{i})h/2\delta_\mathrm{s}} + \mathrm{e}^{-(1-\mathrm{i})z/\delta_\mathrm{s}}\mathrm{e}^{(1-\mathrm{i})h/2\delta_\mathrm{s}}}{\mathrm{e}^{(1-\mathrm{i})h/2\delta_\mathrm{s}} + \mathrm{e}^{-(1-\mathrm{i})h/2\delta_\mathrm{s}}}$$
$$\simeq \mathrm{e}^{-(1-\mathrm{i})z/\delta_\mathrm{s}}, \tag{B.40a}$$

$$\frac{\sinh\left[\frac{(1-\mathrm{i})z'}{\delta_\mathrm{s}}\right]}{\sinh\left[\frac{(1-\mathrm{i})h}{2\delta_\mathrm{s}}\right]} = \frac{\sinh\left[\frac{(1-\mathrm{i})(z-h/2)}{\delta_\mathrm{s}}\right]}{\sinh\left[\frac{(1-\mathrm{i})h}{2\delta_\mathrm{s}}\right]} = \frac{\mathrm{e}^{(1-\mathrm{i})z/\delta_\mathrm{s}}\mathrm{e}^{-(1-\mathrm{i})h/2\delta_\mathrm{s}} - \mathrm{e}^{-(1-\mathrm{i})z/\delta_\mathrm{s}}\mathrm{e}^{(1-\mathrm{i})h/2\delta_\mathrm{s}}}{\mathrm{e}^{(1-\mathrm{i})h/2\delta_\mathrm{s}} - \mathrm{e}^{-(1-\mathrm{i})h/2\delta_\mathrm{s}}}$$
$$\simeq -\mathrm{e}^{-(1-\mathrm{i})z/\delta_\mathrm{s}}. \tag{B.40b}$$

We further use that $k_z h/2 \ll 1$ and approximate to first order

$$\sin\left(\frac{k_z h}{2}\right) \simeq \frac{k_z h}{2}, \quad \cos\left(\frac{k_z h}{2}\right) \simeq 1. \tag{B.41}$$

The first-order fields in Eq. (B.14) written in the asymmetric coordinate system then reduce to

$$v_{1y} = v_\mathrm{bc}\frac{\cos\left(k_y y\right)}{\cos\left(k_y w/2\right)}\left[1 - \mathrm{e}^{-(1-\mathrm{i})z/\delta_\mathrm{s}}\right], \tag{B.42a}$$

$$v_{1z} = -v_\mathrm{bc} h\frac{k_z^2}{k_y}\frac{\sin\left(k_y y\right)}{\cos\left(k_y w/2\right)}\left[-\frac{1}{2} + \frac{z}{h} + \frac{1}{2}\mathrm{e}^{-(1-\mathrm{i})z/\delta_\mathrm{s}}\right], \tag{B.42b}$$

which naturally resembles the structure of the first-order fields used in the Landau-Lifshitz solution utilizing boundary layer theory [12]. With these expressions for v_{1y} and v_{1z} we may then proceed and evaluate $\partial_y\{|v_{1y}|^2\}$ and $\mathrm{Re}[v_{1y}^* v_{1z}]$.

To do so the complex wavenumbers are written explicitly with real and imaginary parts as

$$k_y = k_y^\mathrm{r} + \mathrm{i}k_y^\mathrm{i}, \quad k_y^\mathrm{r}, k_y^\mathrm{i} \in \mathbb{R}, \tag{B.43a}$$

$$k_z = k_z^\mathrm{r} + \mathrm{i}k_z^\mathrm{i}, \quad k_z^\mathrm{r}, k_z^\mathrm{i} \in \mathbb{R}. \tag{B.43b}$$

Expressing the complex functions of the first-order fields in their exponential form we are then able to calculate explicitly the complex conjugate of the fields and to evaluate

$\partial_y\{|v_{1y}|^2\}$ and $\mathrm{Re}[v_{1y}^* v_{1z}]$. Straight forward calculations give

$$\partial_y\{|v_{1y}|^2\} = -2v_{\mathrm{bc}}^2 \frac{k_y^{\mathrm{r}} \sin\left(2k_y^{\mathrm{r}} y\right) - k_y^{\mathrm{i}} \sinh\left(2k_y^{\mathrm{i}} y\right)}{\cos\left(k_y^{\mathrm{r}} w\right) + \cosh\left(k_y^{\mathrm{i}} w\right)} \left[\mathrm{e}^{-2z/\delta_{\mathrm{s}}} - 2\mathrm{e}^{-z/\delta_{\mathrm{s}}} \cos\left(\frac{z}{\delta_{\mathrm{s}}}\right)\right] + C_1(y), \tag{B.44a}$$

$$\begin{aligned}\mathrm{Re}[v_{1y}^* v_{1z}] = \frac{-v_{\mathrm{bc}}^2 h}{|k_y|^2} \frac{1}{\cos\left(k_y^{\mathrm{r}} w\right) + \cosh\left(k_y^{\mathrm{i}} w\right)} \Big\{ &\left[K^{\mathrm{r}} \sin\left(2k_y^{\mathrm{r}} y\right) - K^{\mathrm{i}} \sinh\left(2k_y^{\mathrm{i}} y\right)\right] \\ &\times \left[\frac{z}{h} - \frac{1}{2}\mathrm{e}^{-2z/\delta_{\mathrm{s}}} + \mathrm{e}^{-z/\delta_{\mathrm{s}}} \cos\left(\frac{z}{\delta_{\mathrm{s}}}\right) - \frac{z}{h}\mathrm{e}^{-z/\delta_{\mathrm{s}}} \cos\left(\frac{z}{\delta_{\mathrm{s}}}\right)\right] \\ &- \left[K^{\mathrm{r}} \sinh\left(2k_y^{\mathrm{i}} y\right) + K^{\mathrm{i}} \sin\left(2k_y^{\mathrm{r}} y\right)\right] \frac{z}{h}\mathrm{e}^{-z/\delta_{\mathrm{s}}} \sin\left(\frac{z}{\delta_{\mathrm{s}}}\right) \Big\} + C_2(y),\end{aligned} \tag{B.44b}$$

where $C_1(y)$ and $C_2(y)$ are functions that do not depend on z and consequently they are not interesting when finding the particular solution $\langle v_{2y} \rangle^{\mathrm{part}}$. The constants K^{r} and K^{i} have units of m^{-3} and are defined from the wavenumbers as

$$K^{\mathrm{r}} = (k_z^{\mathrm{r}})^2 k_y^{\mathrm{r}} - (k_z^{\mathrm{i}})^2 k_y^{\mathrm{r}} + 2k_z^{\mathrm{r}} k_z^{\mathrm{i}} k_y^{\mathrm{i}}, \tag{B.45a}$$

$$K^{\mathrm{i}} = (k_z^{\mathrm{i}})^2 k_y^{\mathrm{i}} - (k_z^{\mathrm{r}})^2 k_y^{\mathrm{i}} + 2k_z^{\mathrm{r}} k_z^{\mathrm{i}} k_y^{\mathrm{r}}. \tag{B.45b}$$

We will write the terms in Eq. (B.44) as

$$\partial_y\{|v_{1y}|^2\} = Y_1(y)Z_1(z) + C_1(y), \tag{B.46a}$$

$$\mathrm{Re}[v_{1y}^* v_{1z}] = Y_2(y)Z_2(y) + Y_3(y)Z_3(z) + C_2(y), \tag{B.46b}$$

where the Y-functions include all constants and y-dependence, and consequently the dimensionless Z-functions are given as

$$Z_1(z) = \mathrm{e}^{-2z/\delta_{\mathrm{s}}} - 2\mathrm{e}^{-z/\delta_{\mathrm{s}}} \cos\left(\frac{z}{\delta_{\mathrm{s}}}\right), \tag{B.47a}$$

$$Z_2(z) = \frac{z}{h} - \frac{1}{2}\mathrm{e}^{-2z/\delta_{\mathrm{s}}} + \mathrm{e}^{-z/\delta_{\mathrm{s}}} \cos\left(\frac{z}{\delta_{\mathrm{s}}}\right) - \frac{z}{h}\mathrm{e}^{-z/\delta_{\mathrm{s}}} \cos\left(\frac{z}{\delta_{\mathrm{s}}}\right), \tag{B.47b}$$

$$Z_3(z) = \frac{z}{h}\mathrm{e}^{-z/\delta_{\mathrm{s}}} \sin\left(\frac{z}{\delta_{\mathrm{s}}}\right), \tag{B.47c}$$

which then also defines $Y_1(y)$, $Y_2(y)$, and $Y_3(y)$ from the expressions given.

Eq. (4.46) may then be written as

$$\langle v_{2y} \rangle^{\mathrm{part}} = \frac{1}{2\nu_0} \left[Y_1(y)I_1(z) + Y_2(y)I_2(z) + Y_3(y)I_3(z)\right], \tag{B.48}$$

where the functions $I_1(z)$, $I_2(z)$, and $I_3(z)$ are given by the integrals

$$I_1(z) = \int \mathrm{d}z \int \mathrm{d}z \left\{Z_1(z)\right\} = \frac{\delta_\mathrm{s}^2}{4}\mathrm{e}^{-2z/\delta_\mathrm{s}}\left[1 + 4\mathrm{e}^{z/\delta_\mathrm{s}}\sin\left(\frac{z}{\delta_\mathrm{s}}\right)\right], \tag{B.49a}$$

$$\begin{aligned} I_2(z) &= \int \mathrm{d}z \left\{Z_2(z)\right\}, \\ &= \frac{1}{4h}\left[\delta_\mathrm{s} h\mathrm{e}^{-2z/\delta_\mathrm{s}} + 2z^2 + 2\delta_\mathrm{s}\mathrm{e}^{-z/\delta_\mathrm{s}}\left\{(z-h)\cos\left(\frac{z}{\delta_\mathrm{s}}\right) - (z+\delta_\mathrm{s}-h)\sin\left(\frac{z}{\delta_\mathrm{s}}\right)\right\}\right], \end{aligned} \tag{B.49b}$$

$$I_3(z) = \int \mathrm{d}z \left\{Z_3(z)\right\} = -\frac{\delta_\mathrm{s}}{2h}\mathrm{e}^{-z/\delta_\mathrm{s}}\left[(z+\delta_\mathrm{s})\cos\left(\frac{z}{\delta_\mathrm{s}}\right) + z\sin\left(\frac{z}{\delta_\mathrm{s}}\right)\right]. \tag{B.49c}$$

B.3.5 Evaluation of the bulk streaming boundary condition

In the previous section we found a particular solution of Eq. (4.36a) valid in the boundary layer under the given approximations. When the rotation of the source is zero or negligible in the bulk, which is true in the microchannel acoustofluidics limit considered in Chapter 4, the homogeneous equation corresponding to Eq. (4.36a) describes the bulk field. The sum of the particular solution (boundary layer solution) and the homogeneous solution (bulk solution) must fulfill the no-slip condition on the total velocity field. Consequently, the boundary condition on the bulk field at $z = 0$ is

$$\left\langle v_{2y}\right\rangle_{z=0}^{\mathrm{bulk}} = -\left\langle v_{2y}\right\rangle_{z=0}^{\mathrm{part}}. \tag{B.50}$$

In this section we evaluate this boundary condition. Consequently we must evaluate Eq. (B.48) at $z = 0$. Evaluating the I_{1-3} functions of Eq. (B.49) at $z = 0$ gives

$$I_1(0) = \frac{\delta_\mathrm{s}^2}{4}, \quad I_2(0) = -\frac{\delta_\mathrm{s}}{4}, \quad I_3(0) = -\frac{\delta_\mathrm{s}^2}{2h}. \tag{B.51}$$

Inserting these expressions into Eq. (B.48) evaluated at $z = 0$ and simplifying the result gives

$$\begin{aligned} \left\langle v_{2y}\right\rangle_{z=0}^{\mathrm{part}} = \frac{v_\mathrm{bc}^2}{2\nu_0}\frac{1}{\cos\left(k_y^\mathrm{r} w\right) + \cosh\left(k_y^\mathrm{i} w\right)}\Big\{ &- \frac{\delta_\mathrm{s}^2}{2}\left[k_y^\mathrm{r}\sin\left(2k_y^\mathrm{r} y\right) - k_y^\mathrm{i}\sinh\left(2k_y^\mathrm{i} y\right)\right] \\ &+ \frac{h\delta_\mathrm{s}}{4|k_y|^2}\left[K^\mathrm{r}\sin\left(2k_y^\mathrm{r} y\right) - K^\mathrm{i}\sinh\left(2k_y^\mathrm{i} y\right)\right] \\ &- \frac{\delta_\mathrm{s}^2}{2|k_y|^2}\left[K^\mathrm{i}\sin\left(2k_y^\mathrm{r} y\right) + K^\mathrm{r}\sinh\left(2k_y^\mathrm{i} y\right)\right]\Big\}. \end{aligned} \tag{B.52}$$

Except for a sign-change this is what we would interpret as the effective boundary condition on the bulk streaming velocity field. It looks quite complex and very different from the simple Rayleigh result [18]. However, in the microchannel acoustofluidics limit of Chapter 4 we will show that it does indeed compare to the Rayleigh result. Let us first

introduce a sign-change and change the focus to the effective boundary condition of the bulk streaming velocity field. Collecting terms we write the derived boundary condition as

$$\left\langle v_{2y}\right\rangle_{z=0}^{\text{bulk}} = -\frac{v_{\text{bc}}^2}{2\nu_0}\delta_{\text{s}}^2 k_y^{\text{r}} \frac{1}{\cos\left(k_y^{\text{r}}w\right)+\cosh\left(k_y^{\text{i}}w\right)} \left\{-\frac{1}{2}+\frac{h}{4\delta_{\text{s}}}\frac{K^{\text{r}}}{|k_y|^2 k_y^{\text{r}}}-\frac{1}{2}\frac{K^{\text{i}}}{|k_y|^2 k_y^{\text{r}}}\right\}\sin\left(2k_y^{\text{r}}y\right)$$
$$-\frac{v_{\text{bc}}^2}{2\nu_0}\delta_{\text{s}}^2 k_y^{\text{i}} \frac{1}{\cos\left(k_y^{\text{r}}w\right)+\cosh\left(k_y^{\text{i}}w\right)} \left\{\frac{1}{2}-\frac{h}{4\delta_{\text{s}}}\frac{K^{\text{i}}}{|k_y|^2 k_y^{\text{i}}}-\frac{1}{2}\frac{K^{\text{r}}}{|k_y|^2 k_y^{\text{i}}}\right\}\sinh\left(2k_y^{\text{i}}y\right). \tag{B.53}$$

For the parameters of Chapter 4, $k_y^{\text{i}}w/2 \sim 10^{-3}$, which makes the terms involving $\sinh(2k_y^{\text{i}}y)$ negligible in comparison to the terms involving $\sin(2k_y^{\text{r}}y)$ everywhere except at the domain ends at $y=\pm w/2$, where both functions are close to zero. Consequently we neglect the $\sinh(2k_y^{\text{i}}y)$ terms.

Now, at resonance we have

$$k_y^{\text{r}} = \frac{\omega_0}{c} = \frac{\pi}{w} \quad\Rightarrow\quad \cos\left(k_y^{\text{r}}w\right) = -1. \tag{B.54}$$

From the first-order fields one may also derive the max amplitude of v_{1y} in the bulk, which we will denote u_0. At resonance it becomes

$$u_0 = \frac{2v_{\text{bc}}}{\cosh\left(k_y^{\text{i}}\right)-1}\sinh\left(\frac{k_y^{\text{i}}w}{2}\right). \tag{B.55}$$

Then

$$u_0^2 = 4v_{\text{bc}}^2\frac{\sinh^2\left(k_y^{\text{i}}w/2\right)}{\left[\cos\left(k_y^{\text{i}}w\right)-1\right]^2} = 2v_{\text{bc}}^2\frac{\cosh\left(k_y^{\text{i}}w\right)-1}{\left[\cos\left(k_y^{\text{i}}w\right)-1\right]^2} = \frac{2v_{\text{bc}}^2}{\cosh\left(k_y^{\text{i}}w\right)-1}. \tag{B.56}$$

With these results we rewrite Eq. (B.53) to get

$$\left\langle v_{2y}\right\rangle_{z=0}^{\text{bulk}} = -\frac{\delta_{\text{s}}^2 k_y^{\text{r}}}{4\nu_0}u_0^2\left\{-\frac{1}{2}+\frac{h}{4\delta_{\text{s}}}\frac{K^{\text{r}}}{|k_y|^2 k_y^{\text{r}}}-\frac{1}{2}\frac{K^{\text{i}}}{|k_y|^2 k_y^{\text{r}}}\right\}\sin\left(2k_y^{\text{r}}y\right). \tag{B.57}$$

Now use that $\delta_{\text{s}}^2 = 2\nu_0/\omega_{\text{res}}$ and that $k_y^{\text{r}} = \omega_0/c$. Then

$$\left\langle v_{2y}\right\rangle_{z=0}^{\text{bulk}} = -\frac{u_0^2}{2c}\frac{\omega_0}{\omega_{\text{res}}}\left\{-\frac{1}{2}+\frac{h}{4\delta_{\text{s}}}\frac{K^{\text{r}}}{|k_y|^2 k_y^{\text{r}}}-\frac{1}{2}\frac{K^{\text{i}}}{|k_y|^2 k_y^{\text{r}}}\right\}\sin\left(2k_y^{\text{r}}y\right). \tag{B.58}$$

For the parameters of Chapter 4 we find the numerical values

$$K^{\text{r}} \sim K^{\text{i}} \sim 10^9\ \text{m}^{-3}, \tag{B.59a}$$
$$(k_z^{\text{r}})^2 k_y^{\text{r}} \sim 3\times 10^8\ \text{m}^{-3}, \quad (k_z^{\text{i}})^2 k_y^{\text{r}} \sim 2\times 10^9\ \text{m}^{-3}, \quad 2k_z^{\text{r}}k_z^{\text{i}}k_y^{\text{r}} \sim 1\times 10^6\ \text{m}^{-3}. \tag{B.59b}$$

Consequently the term involving K^{r} is a factor $h/\delta_{\mathrm{s}} \sim 420$ larger than the term involving K^{i} and we will consequently neglect the smaller term. Moreover we see that we may approximate K^{r} with only two terms

$$K^{\mathrm{r}} = (k_z^{\mathrm{r}})^2 k_y^{\mathrm{r}} - (k_z^{\mathrm{i}})^2 k_y^{\mathrm{r}}. \tag{B.60}$$

From Eq. (3.48) we have expressions for the wavenumbers at resonance

$$k_y = \frac{\omega_{\mathrm{res}}}{c}\left[1 + (1+\mathrm{i})\frac{\delta_{\mathrm{s}}}{2h}\right], \quad k_z = -\mathrm{i}\frac{\omega_{\mathrm{res}}}{c}\sqrt{(1+\mathrm{i})\frac{\delta_{\mathrm{s}}}{h}}. \tag{B.61}$$

Now,

$$(1+\mathrm{i})^{1/2} = \left(\sqrt{2}\mathrm{e}^{\mathrm{i}\pi/4}\right)^{1/2} = 2^{1/4}\mathrm{e}^{\mathrm{i}\pi/8}. \tag{B.62}$$

Consequently,

$$k_z = -\frac{\omega_{\mathrm{res}}}{c}\sqrt{\frac{\delta_{\mathrm{s}}}{h}}2^{1/4}\left[\cos\left(\frac{5\pi}{8}\right) + \mathrm{i}\sin\left(\frac{5\pi}{8}\right)\right]. \tag{B.63}$$

We may then evaluate the last term, namely

$$\frac{K^{\mathrm{r}}}{|k_y|^2 k_y^{\mathrm{r}}} = \frac{(k_z^{\mathrm{r}})^2 - (k_z^{\mathrm{i}})^2}{|k_y|^2} \simeq \frac{(k_z^{\mathrm{r}})^2 - (k_z^{\mathrm{i}})^2}{(k_y^{\mathrm{r}})^2} \simeq \frac{\delta_{\mathrm{s}}}{h}\sqrt{2}\left[\cos^2\left(\frac{5\pi}{8}\right) - \sin^2\left(\frac{5\pi}{8}\right)\right] = -\frac{\delta_{\mathrm{s}}}{h}. \tag{B.64}$$

The boundary condition Eq. (B.58) then finally reduces quite beautifully to give

$$\left\langle v_{2y}\right\rangle_{z=0}^{\mathrm{bulk}} = \frac{3}{8}\frac{u_0^2}{c}\sin\left(2k_y^{\mathrm{r}}y\right). \tag{B.65}$$

Considering that we came from the expression in Eq. (B.53) this is quite a beautiful result in agreement with Rayleigh [18]. The solution of Rayleigh assumes a horizontal bulk wave with a real wavenumber k, while our solution for the first-order fields has complex wavenumbers k_y and k_z. To go from the Rayleigh result to our result one quite naturally has to let $k \to k_y^{\mathrm{r}}$ because our solution comes from a complete description of the first-order fields which includes damping and variation in the z-direction.

Appendix C

Appendix to Chapter 5

C.1 Vector wave equation in spherical coordinates

Consider the Helmholtz vector wave equation encountered when describing transverse waves such as electromagnetic waves or shear waves in a fluid

$$\nabla^2 \boldsymbol{A} + k^2 \boldsymbol{A} = \boldsymbol{0}. \tag{C.1}$$

In spherical coordinates the components do not separate due to the spatial dependence of the unit vectors. The spherical vector wave functions $\boldsymbol{A}$ are obtained from generating functions A solving the corresponding scalar equation. Let

$$\nabla^2 A + k^2 A = 0. \tag{C.2}$$

Then $\boldsymbol{A}_0$, $\boldsymbol{A}_1$, and $\boldsymbol{A}_2$ given as

$$\begin{array}{lll} \boldsymbol{A}_0 = \boldsymbol{\nabla} A, & \boldsymbol{A}_1 = \boldsymbol{A}_0 \times \boldsymbol{r}, & \boldsymbol{A}_2 = \dfrac{1}{k} \boldsymbol{\nabla} \times \boldsymbol{A}_1, \\ \boldsymbol{\nabla} \cdot \boldsymbol{A}_0 \neq 0, & \boldsymbol{\nabla} \cdot \boldsymbol{A}_1 = 0, & \boldsymbol{\nabla} \cdot \boldsymbol{A}_2 = 0, \end{array} \tag{C.3}$$

are solutions of the vector wave equation Eq. (C.1). It is assumed that $\boldsymbol{A}_1$ and $\boldsymbol{A}_2$ form a complete basis for divergence-free solutions of the vector wave equation Eq. (C.1).

C.2 Expansion for the vector potential $\boldsymbol{\Psi}$

We find the correct expansion that solves Eq. (2.32c). The problem is expressed as

$$\nabla^2 \boldsymbol{\Psi} + k_\mathrm{s}^2 \boldsymbol{\Psi} = \boldsymbol{0}, \text{ with } \boldsymbol{\nabla} \cdot \boldsymbol{\Psi} = 0, \tag{C.4}$$

and moreover exhibits azimuthal symmetry. Let $F = F(r, \theta)$ solve the corresponding scalar wave equation

$$\nabla^2 F + k_\mathrm{s}^2 F = 0. \tag{C.5}$$

For an outgoing wave it is solved by the expansion

$$F = \sum_{n=0}^{\infty} F_n = \sum_{n=0}^{\infty} K_n h_n^{(1)}(k_\mathrm{s} r) P_n(\cos\theta), \tag{C.6}$$

where K_n are the expansion coefficients. Seeking only the divergence-free solutions of the vector wave equation we can write the two possible solutions according to Eq. (C.3),

$$\boldsymbol{\Psi}_1 = \sum_{n=0}^{\infty} \boldsymbol{\Psi}_{1n}, \quad \boldsymbol{\Psi}_{1n} = \boldsymbol{\nabla} F_n \times \boldsymbol{r}, \tag{C.7a}$$

$$\boldsymbol{\Psi}_2 = \sum_{n=0}^{\infty} \boldsymbol{\Psi}_{2n}, \quad \boldsymbol{\Psi}_{2n} = \frac{1}{k_\mathrm{s}} \boldsymbol{\nabla} \times \boldsymbol{\Psi}_{1n}. \tag{C.7b}$$

One finds

$$\boldsymbol{\Psi}_{1n} = f(r,\theta)\mathbf{e}_\phi, \tag{C.8a}$$

$$\boldsymbol{\Psi}_{2n} = g(r,\theta)\mathbf{e}_r + h(r,\theta)\mathbf{e}_\theta, \tag{C.8b}$$

where for simplicity we have written the functional dependencies as arbitrary functions f, g, and h.

The velocity field arising from $\boldsymbol{\Psi}$ is given as the rotation $\boldsymbol{\nabla} \times \boldsymbol{\Psi}$. Due to the azimuthal symmetry it cannot depend on ϕ and the ϕ-component must be zero. Considering the forms of $\boldsymbol{\Psi}_{1n}$ and $\boldsymbol{\Psi}_{2n}$ in Eq. (C.8) one finds for the ϕ-components

$$[\boldsymbol{\nabla} \times \boldsymbol{\Psi}_{1n}]_\phi = 0, \tag{C.9a}$$

$$[\boldsymbol{\nabla} \times \boldsymbol{\Psi}_{2n}]_\phi \neq 0. \tag{C.9b}$$

Consequently the only divergence-free solution of $\boldsymbol{\Psi}$ which gives the correct azimuthal symmetry of the velocity field is $\boldsymbol{\Psi}_1$ given from Eq. (C.7a). Since the only non-vanishing component of the vector potential is the ϕ-component we write

$$\boldsymbol{\Psi} = \psi_\mathrm{s}\, \mathbf{e}_\phi, \tag{C.10}$$

and we have from Eq. (C.7a) and Eq. (C.6)

$$\psi_\mathrm{s} = \sum_{n=0}^{\infty} K_n h_n^{(1)}(k_\mathrm{s} r) \sin\theta\, P_n'(\cos\theta), \tag{C.11}$$

where prime denotes differentiation with respect to the argument. The definition of the associated Legendre polynomials ($m = 1$) from the ordinary Legendre polynomials is

$$P_n^1(\cos\theta) = \sin\theta\, P_n'(\cos\theta). \tag{C.12}$$

Making this substitution in Eq. (C.11) we find the expansion which was used in Chapter 5,

$$\psi_\mathrm{s} = \phi_0 \sum_{n=0}^{\infty} \mathrm{i}^n (2n+1) C_n h_n^{(1)}(k_\mathrm{s} r) P_n^1(\cos\theta), \tag{C.13}$$

where we have redefined the expansion coefficient $K_n = \phi_0\, \mathrm{i}^n (2n+1) C_n$.

C.3 Stress tensor components in spherical coordinates

In coordinate free form the symmetric stress tensor is given as

$$\boldsymbol{\sigma} = -p\mathbf{I} + \eta\left[\boldsymbol{\nabla}\boldsymbol{v} + (\boldsymbol{\nabla}\boldsymbol{v})^{\mathrm{T}}\right] + (\beta-1)\eta\,(\boldsymbol{\nabla}\cdot\boldsymbol{v})\,\mathbf{I}. \tag{C.14}$$

The stress tensor components in spherical coordinates for an incompressible fluid are given in Landau and Lifshitz [12]. Considering here a compressible fluid we add the divergence term in the diagonal according to the above. The components of interest for the calculation in Chapter 5 with azimuthal symmetry are then given in spherical coordinates (r, θ, ϕ) as

$$\sigma_{rr}^{(1)} = -p_1 + 2\eta_0\partial_r v_{1r} + (\beta-1)\eta_0\boldsymbol{\nabla}\cdot\boldsymbol{v}_1, \tag{C.15a}$$

$$\sigma_{r\theta}^{(1)} = \eta_0\left(\frac{1}{r}\partial_\theta v_{1r} + \partial_r v_{1\theta} - \frac{v_{1\theta}}{r}\right). \tag{C.15b}$$

The velocity components follow directly from writing the gradient and the rotation of the Helmholtz decomposition $\boldsymbol{v}_1 = -\boldsymbol{\nabla}\Phi + \boldsymbol{\nabla}\times\boldsymbol{\Psi}$ in spherical coordinates, remembering that $\boldsymbol{\Psi} = \psi_{\mathrm{s}}\,\mathbf{e}_\phi$. Inserting into the above expression gives the final form of $\sigma_{r\theta}^{(1)}$ as given in Eq. (5.5). For $\sigma_{rr}^{(1)}$ one finds

$$\sigma_{rr}^{(1)} = -p_1 + 2\eta_0\left[-\partial_r^2\Phi + \frac{1}{\sin\theta}\partial_\theta\left\{\sin\theta\left(-\frac{1}{r^2}\psi_{\mathrm{s}} + \frac{1}{r}\partial_r\psi_{\mathrm{s}}\right)\right\}\right] - (\beta-1)\eta_0\nabla^2\Phi. \tag{C.16}$$

The pressure is given in terms of Φ according to Eq. (2.39). Using that expression together with the wave equations and wavenumbers of Eq. (2.32) and Eq. (2.33), and neglecting Γ_{s} and Γ_{t} relative to 1, one finds

$$-p_1 - (\beta-1)\eta_0\nabla^2\Phi = \mathrm{i}\omega\rho_0\left[\phi_{\mathrm{c}} + \left(1 - \frac{2\nu_0}{D_{\mathrm{th}}}\right)\phi_{\mathrm{t}}\right]. \tag{C.17}$$

Using this substitution in the above expression for $\sigma_{rr}^{(1)}$ then gives the final form written in Eq. (5.5).

C.4 Monopole scattering coefficient: Calculations

From the partial wave expansion Eq. (5.1) and the boundary conditions Eq. (5.3) one obtains the equations of order $n = 0$ similar to those given in Eq. (5.9) for $n \geq 1$. The boundary conditions for $v_{1\theta}$ and $\sigma_{r\theta}^{(1)}$ are trivially satisfied for the $n = 0$ equations because there is no angular dependence in the zeroth order Legendre and associated Legendre polynomials, $P_0(x) = 1$ and $P_0^1(x) = 0$. $P_0^1(x) = 0$ leads to $\psi_{\mathrm{s}} = 0$ at this order and the coefficients C_0 and C_0' drop out of the equations leaving 4 equations with 4 unknowns.

The resulting equations for the monopole term $n = 0$ are

$$x_{\rm c} j_0'(x_{\rm c}) + A_0 x_{\rm c} h_0'(x_{\rm c}) + B_0 x_{\rm t} h_0'(x_{\rm t}) = A_0' x_{\rm c}' j_0'(x_{\rm c}') + B_0' x_{\rm t}' j_0'(x_{\rm t}'), \tag{C.18a}$$

$$b_{\rm c} j_0(x_{\rm c}) + A_0 b_{\rm c} h_0(x_{\rm c}) + B_0 b_{\rm t} h_0(x_{\rm t}) = A_0' b_{\rm c}' j_0(x_{\rm c}') + B_0' b_{\rm t}' j_0(x_{\rm t}'), \tag{C.18b}$$

$$\begin{aligned} &k_{\rm th} b_{\rm c} x_{\rm c} j_0'(x_{\rm c}) + A_0 k_{\rm th} b_{\rm c} x_{\rm c} h_0'(x_{\rm c}) + B_0 k_{\rm th} b_{\rm t} x_{\rm t} h_0'(x_{\rm t}) \\ &\quad = A_0' k_{\rm th}' b_{\rm c}' x_{\rm c}' j_0'(x_{\rm c}') + B_0' k_{\rm th}' b_{\rm t}' x_{\rm t}' j_0'(x_{\rm t}'), \end{aligned} \tag{C.18c}$$

$$\begin{aligned} &\eta_0 \left[x_{\rm s}^2 j_0(x_{\rm c}) - 2x_{\rm c}^2 j_0''(x_{\rm c}) \right] + A_0 \eta_0 \left[x_{\rm s}^2 h_0(x_{\rm c}) - 2x_{\rm c}^2 h_0''(x_{\rm c}) \right] \\ &\qquad + B_0 \eta_0 \left[x_{\rm s}^2 M h_0(x_{\rm t}) - 2x_{\rm t}^2 h_0''(x_{\rm t}) \right] \\ &\quad = A_0' \eta_0' \left[x_{\rm s}'^2 j_0(x_{\rm c}') - 2x_{\rm c}'^2 j_0''(x_{\rm c}') \right] + B_0' \eta_0' \left[x_{\rm s}'^2 M' j_0(x_{\rm t}') - 2x_{\rm t}'^2 j_0''(x_{\rm t}') \right], \end{aligned} \tag{C.18d}$$

Considering the Rayleigh limit we will neglect terms of order $x_{\rm c}^2$ and $x_{\rm c}'^2$ relative to 1. This allows the use of the approximate expressions for the Bessel and Hankel functions when $x_{\rm c}$ or $x_{\rm c}'$ is the argument given in Eq. (C.37) of Section C.6.

Neglecting $x_{\rm c}^2$ and $x_{\rm c}'^2$ relative to 1 and moreover using the general relation that $f_0'(x) = -f_1(x)$ where f can be any spherical Bessel of Hankel function, Eq. (C.18) is written as

$$A_0 \frac{\mathrm{i}}{x_{\rm c}} + A_0' \frac{1}{3} x_{\rm c}'^2 - B_0 x_{\rm t} h_1(x_{\rm t}) + B_0' x_{\rm t}' j_1(x_{\rm t}') = \frac{1}{3} x_{\rm c}^2, \tag{C.19a}$$

$$A_0 b_{\rm c} \left(1 - \frac{\mathrm{i}}{x_{\rm c}} \right) - A_0' b_{\rm c}' + B_0 b_{\rm t} h_0(x_{\rm t}) - B_0' b_{\rm t}' j_0(x_{\rm t}') = -b_{\rm c}, \tag{C.19b}$$

$$A_0 k_{\rm th} b_{\rm c} \frac{\mathrm{i}}{x_{\rm c}} + A_0' \frac{1}{3} k_{\rm th}' b_{\rm c}' x_{\rm c}'^2 - B_0 k_{\rm th} b_{\rm t} x_{\rm t} h_1(x_{\rm t}) + B_0' k_{\rm th}' b_{\rm t}' x_{\rm t}' j_1(x_{\rm t}') = \frac{1}{3} k_{\rm th} b_{\rm c} x_{\rm c}^2, \tag{C.19c}$$

$$\begin{aligned} &A_0 \eta_0 \left[x_{\rm s}^2 - \left(x_{\rm s}^2 - 4 \right) \frac{\mathrm{i}}{x_{\rm c}} \right] - A_0' \eta_0' x_{\rm s}'^2 + B_0 \eta_0 \left[M x_{\rm s}^2 h_0(x_{\rm t}) - 2x_{\rm t}^2 h_0''(x_{\rm t}) \right] \\ &\qquad - B_0' \eta_0' \left[M' x_{\rm s}'^2 j_0(x_{\rm t}') - 2x_{\rm t}'^2 j_0''(x_{\rm t}') \right] = -\eta_0 x_{\rm s}^2. \end{aligned} \tag{C.19d}$$

Multiplying Eq. (C.19c) by $1/k_{\rm th} b_{\rm t}$ we see that the terms with B_0 and B_0' are the same order of magnitude as those same terms in Eq. (C.19a) while the remaining terms in Eq. (C.19c) are suppressed by the small factors $b_{\rm c}/b_{\rm t}$ and $b_{\rm c}'/b_{\rm t}$,

$$\frac{b_{\rm c}}{b_{\rm t}} = \frac{\mathrm{i}}{2} (\gamma - 1) \frac{\omega^2}{c^2} \delta_{\rm t}^2 \sim (k_0 \delta_{\rm t})^2. \tag{C.20}$$

Consequently, in accordance with our general scheme of approximation we neglect those terms and Eq. (C.19c) becomes

$$B_0' = \frac{\tilde{\alpha}_p}{\tilde{\rho}_0 \tilde{C}_p} \frac{x_{\rm t}}{x_{\rm t}'} \frac{h_1(x_{\rm t})}{j_1(x_{\rm t}')} B_0, \tag{C.21}$$

where we have used that $b_\mathrm{t} = -1/\alpha_p D_\mathrm{th}$ and $D_\mathrm{th} = k_\mathrm{th}/\rho_0 C_p$ and we note again that parameters with a tilde represent the parameter ratio between the droplet medium and the surrounding fluid, e.g. $\tilde{\rho}_0 = \rho_0'/\rho_0$.

Eliminating B_0' from the system of equations Eq. (C.19) the remaining three equations may be written on the form

$$A_0 \frac{\mathrm{i}}{x_\mathrm{c}} + A_0' \frac{1}{3} x_\mathrm{c}'^2 - B_0 S_1 = \frac{1}{3} x_\mathrm{c}^2, \tag{C.22a}$$

$$A_0 \frac{b_\mathrm{c}}{b_\mathrm{t}} \left(\frac{\mathrm{i}}{x_\mathrm{c}} - 1 \right) + A_0' \frac{b_\mathrm{c}'}{b_\mathrm{t}} - B_0 S_2 = \frac{b_\mathrm{c}}{b_\mathrm{t}}, \tag{C.22b}$$

$$A_0 \left[\left(x_\mathrm{s}^2 - 4 \right) \frac{\mathrm{i}}{x_\mathrm{c}} - x_\mathrm{s}^2 \right] + A_0' \tilde{\eta}_0 x_\mathrm{s}'^2 - B_0 S_3 = x_\mathrm{s}^2, \tag{C.22c}$$

where we have introduced the functions S_1, S_2, and S_3,

$$S_1 = \left(1 - \frac{\tilde{\alpha}_p}{\tilde{\rho}_0 \tilde{C}_p} \right) x_\mathrm{t} h_1(x_\mathrm{t}), \tag{C.23a}$$

$$S_2 = h_0(x_\mathrm{t}) - \frac{1}{\tilde{k}_\mathrm{th}} \frac{x_\mathrm{t}}{x_\mathrm{t}'} \frac{j_0(x_\mathrm{t}')}{j_1(x_\mathrm{t}')} h_1(x_\mathrm{t}), \tag{C.23b}$$

$$\begin{aligned} S_3 = {} & \left(M x_\mathrm{s}^2 + 2 x_\mathrm{t}^2 \right) h_0(x_\mathrm{t}) - 4 \left(1 - \frac{\tilde{\alpha}_p \tilde{\eta}_0}{\tilde{\rho}_0 \tilde{C}_p} \right) x_\mathrm{t} h_1(x_\mathrm{t}) \\ & - \left(M' x_\mathrm{s}'^2 + 2 x_\mathrm{t}'^2 \right) \frac{\tilde{\alpha}_p \tilde{\eta}_0}{\tilde{\rho}_0 \tilde{C}_p} \frac{x_\mathrm{t}}{x_\mathrm{t}'} \frac{j_0(x_\mathrm{t}')}{j_1(x_\mathrm{t}')} h_1(x_\mathrm{t}) \end{aligned} \tag{C.23c}$$

In obtaining the expression for S_3 we have used the general relation that $f_0''(x) = -f_0(x) + (2/x) f_1(x)$ where f can be any spherical Bessel or Hankel function.

We use Cramer's rule also known as solution by determinants to solve the inhomogeneous system of equations in Eq. (C.22). Let the determinant of the system matrix be defined as D and the determinant of the system matrix with the first column replaced by the column of the inhomogeneous righthand-side as $D(A_0)$. Then, according to Cramer's rule $A_0 = D(A_0)/D$. The determinants are

$$\begin{aligned} D = {} & \frac{\mathrm{i}}{x_\mathrm{c}} \left[-\frac{b_\mathrm{c}'}{b_\mathrm{t}} S_3 + \tilde{\eta}_0 x_\mathrm{s}'^2 S_2 \right] - \frac{1}{3} x_\mathrm{c}'^2 \left[-\frac{b_\mathrm{c}}{b_\mathrm{t}} \left(\frac{\mathrm{i}}{x_\mathrm{c}} - 1 \right) S_3 + \left(\left(x_\mathrm{s}^2 - 4 \right) \frac{\mathrm{i}}{x_\mathrm{c}} - x_\mathrm{s}^2 \right) S_2 \right] \\ & - S_1 \left[\frac{b_\mathrm{c}}{b_\mathrm{t}} \left(\frac{\mathrm{i}}{x_\mathrm{c}} - 1 \right) \tilde{\eta}_0 x_\mathrm{s}'^2 - \frac{b_\mathrm{c}'}{b_\mathrm{t}} \left(\left(x_\mathrm{s}^2 - 4 \right) \frac{\mathrm{i}}{x_\mathrm{c}} - x_\mathrm{s}^2 \right) \right], \end{aligned} \tag{C.24a}$$

$$\begin{aligned} D(A_0) = {} & \frac{1}{3} x_\mathrm{c}^2 \left[-\frac{b_\mathrm{c}'}{b_\mathrm{t}} S_3 + \tilde{\eta}_0 x_\mathrm{s}'^2 S_2 \right] - \frac{1}{3} x_\mathrm{c}'^2 \left[-\frac{b_\mathrm{c}}{b_\mathrm{t}} S_3 + x_\mathrm{s}^2 S_2 \right] \\ & - S_1 \left[\frac{b_\mathrm{c}}{b_\mathrm{t}} \tilde{\eta}_0 x_\mathrm{s}'^2 - \frac{b_\mathrm{c}'}{b_\mathrm{t}} x_\mathrm{s}^2 \right]. \end{aligned} \tag{C.24b}$$

The functions S_1, S_2, and S_3 are all the same order of magnitude. We may simplify the above expressions using that $b_\mathrm{c}/b_\mathrm{t} \sim b_\mathrm{c}'/b_\mathrm{t} \sim (k_0 \delta_\mathrm{t})^2 \ll 1$ as well as $x_\mathrm{c}^2 \sim x_\mathrm{c}'^2 \ll 1$ in

accordance with our general scheme of approximation. Then

$$D \simeq \frac{\mathrm{i}}{x_\mathrm{c}} \tilde{\rho}_0 x_\mathrm{s}^2 S_2, \tag{C.25a}$$

$$D(A_0) \simeq \frac{1}{3} \tilde{\rho}_0 x_\mathrm{s}^2 \left[x_\mathrm{c}^2 - \frac{x_\mathrm{c}'^2}{\tilde{\rho}_0} \right] S_2 - \tilde{\rho}_0 x_\mathrm{s}^2 \frac{b_\mathrm{c}}{b_\mathrm{t}} \left(1 - \frac{\tilde{\alpha}_p}{\tilde{\rho}_0 \tilde{C}_p} \right) S_1, \tag{C.25b}$$

where we have used that $\tilde{\eta}_0 x_\mathrm{s}'^2 = \tilde{\rho}_0 x_\mathrm{s}^2$ in the equation for D and that $b_\mathrm{c}'/b_\mathrm{c} = \tilde{\alpha}_p/\tilde{C}_p$ in the equation for $D(A_0)$. The last of these identities is obtained by combining Eq. (2.15b) with Eq. (2.41a).

The monopole scattering coefficient $A_0 = D(A_0)/D$ is evaluated from these expressions and the final result is most conveniently written on the form

$$A_0 = -\frac{\mathrm{i}}{3} x_\mathrm{c}^3 \left[1 - \tilde{\kappa}_s + 3(\gamma - 1) \left(1 - \frac{\tilde{\alpha}_p}{\tilde{\rho}_0 \tilde{C}_p} \right)^2 H(x_\mathrm{t}, x_\mathrm{t}', \tilde{k}_\mathrm{th}) \right], \tag{C.26a}$$

$$H(x_\mathrm{t}, x_\mathrm{t}', \tilde{k}_\mathrm{th}) = \frac{1}{x_\mathrm{t}^2} \left[\frac{1}{1 - \mathrm{i}x_\mathrm{t}} - \frac{1}{\tilde{k}_\mathrm{th}} \frac{\tan x_\mathrm{t}'}{\tan x_\mathrm{t}' - x_\mathrm{t}'} \right]^{-1}, \tag{C.26b}$$

where we have used that $(x_\mathrm{c}'/x_\mathrm{c})^2 = \tilde{\rho}_0 \tilde{\kappa}_s$ and that $b_\mathrm{c}/b_\mathrm{t} \simeq (\mathrm{i}/2)(\gamma - 1)(k_\mathrm{c}\delta_\mathrm{t})^2$, with the last identity correct within our approximation scheme where $\Gamma_\mathrm{s}, \Gamma_\mathrm{t} \ll 1$ are neglected relative to 1. The expression for the function H follows from evaluation of the functions S_1 and S_2 using the explicit expressions for the spherical Bessel and Hankel functions in Eq. (C.36) of Section C.6.

C.5 Dipole scattering coefficient: Calculations

The general system of equations for the expansion coefficients Eq. (5.9) for $n = 1$ are

$$\begin{aligned} & x_{\mathrm{c}} j_1'(x_{\mathrm{c}}) + A_1 x_{\mathrm{c}} h_1'(x_{\mathrm{c}}) + B_1 x_{\mathrm{t}} h_1'(x_{\mathrm{t}}) - 2C_1 h_1(x_{\mathrm{s}}) \\ & \quad = A_1' x_{\mathrm{c}}' j_1'(x_{\mathrm{c}}') + B_1' x_{\mathrm{t}}' j_1'(x_{\mathrm{t}}') - 2C_1' j_1(x_{\mathrm{s}}'), \end{aligned} \tag{C.27a}$$

$$\begin{aligned} & j_1(x_{\mathrm{c}}) + A_1 h_1(x_{\mathrm{c}}) + B_1 h_1(x_{\mathrm{t}}) - C_1 \left[x_{\mathrm{s}} h_1'(x_{\mathrm{s}}) + h_1(x_{\mathrm{s}}) \right] \\ & \quad = A_1' j_1(x_{\mathrm{c}}') + B_1' j_1(x_{\mathrm{t}}') - C_1' \left[x_{\mathrm{s}}' j_1'(x_{\mathrm{s}}') + j_1(x_{\mathrm{s}}') \right], \end{aligned} \tag{C.27b}$$

$$b_{\mathrm{c}} j_1(x_{\mathrm{c}}) + A_1 b_{\mathrm{c}} h_1(x_{\mathrm{c}}) + B_1 b_{\mathrm{t}} h_1(x_{\mathrm{t}}) = A_1' b_{\mathrm{c}}' j_1(x_{\mathrm{c}}') + B_1' b_{\mathrm{t}}' j_1(x_{\mathrm{t}}'), \tag{C.27c}$$

$$\begin{aligned} & k_{\mathrm{th}} b_{\mathrm{c}} x_{\mathrm{c}} j_1'(x_{\mathrm{c}}) + A_1 k_{\mathrm{th}} b_{\mathrm{c}} x_{\mathrm{c}} h_1'(x_{\mathrm{c}}) + B_1 k_{\mathrm{th}} b_{\mathrm{t}} x_{\mathrm{t}} h_1'(x_{\mathrm{t}}) \\ & \quad = A_1' k_{\mathrm{th}}' b_{\mathrm{c}}' x_{\mathrm{c}}' j_1'(x_{\mathrm{c}}') + B_1' k_{\mathrm{th}}' b_{\mathrm{t}}' x_{\mathrm{t}}' j_1'(x_{\mathrm{t}}'), \end{aligned} \tag{C.27d}$$

$$\begin{aligned} & \eta_0 \Big(\left[x_{\mathrm{c}} j_1'(x_{\mathrm{c}}) - j_1(x_{\mathrm{c}}) \right] + A_1 \left[x_{\mathrm{c}} h_1'(x_{\mathrm{c}}) - h_1(x_{\mathrm{c}}) \right] + B_1 \left[x_{\mathrm{t}} h_1'(x_{\mathrm{t}}) - h_1(x_{\mathrm{t}}) \right] \\ & \qquad -(C_1/2) x_{\mathrm{s}}^2 h_1''(x_{\mathrm{s}}) \Big) \\ & \quad = \eta_0' \Big(A_1' \left[x_{\mathrm{c}}' j_1'(x_{\mathrm{c}}') - j_1(x_{\mathrm{c}}') \right] + B_1' \left[x_{\mathrm{t}}' j_1'(x_{\mathrm{t}}') - j_1(x_{\mathrm{t}}') \right] \\ & \qquad -(C_1'/2) x_{\mathrm{s}}'^2 j_1''(x_{\mathrm{s}}') \Big), \end{aligned} \tag{C.27e}$$

$$\begin{aligned} & \eta_0 \left[x_{\mathrm{s}}^2 j_1(x_{\mathrm{c}}) - 2x_{\mathrm{c}}^2 j_1''(x_{\mathrm{c}}) \right] + A_1 \eta_0 \left[x_{\mathrm{s}}^2 h_1(x_{\mathrm{c}}) - 2x_{\mathrm{c}}^2 h_1''(x_{\mathrm{c}}) \right] \\ & \qquad + B_1 \eta_0 \left[x_{\mathrm{s}}^2 M h_1(x_{\mathrm{t}}) - 2x_{\mathrm{t}}^2 h_1''(x_{\mathrm{t}}) \right] + 4C_1 \eta_0 \left[x_{\mathrm{s}} h_1'(x_{\mathrm{s}}) - h_1(x_{\mathrm{s}}) \right] \\ & \quad = A_1' \eta_0' \left[x_{\mathrm{s}}'^2 j_1(x_{\mathrm{c}}') - 2x_{\mathrm{c}}'^2 j_1''(x_{\mathrm{c}}') \right] + B_1' \eta_0' \left[x_{\mathrm{s}}'^2 M' j_1(x_{\mathrm{t}}') - 2x_{\mathrm{t}}'^2 j_1''(x_{\mathrm{t}}') \right] \\ & \qquad + 4C_1' \eta_0' \left[x_{\mathrm{s}}' j_1'(x_{\mathrm{s}}') - j_1(x_{\mathrm{s}}') \right], \end{aligned} \tag{C.27f}$$

Taking Eq. (C.27d) and multiplying it by $1/k_{\mathrm{th}} b_{\mathrm{t}}$ we obtain

$$x_{\mathrm{c}} j_1'(x_{\mathrm{c}}) \frac{b_{\mathrm{c}}}{b_{\mathrm{t}}} + A_1 x_{\mathrm{c}} h_1'(x_{\mathrm{c}}) \frac{b_{\mathrm{c}}}{b_{\mathrm{t}}} + B_1 x_{\mathrm{t}} h_1'(x_{\mathrm{t}}) = A_1' x_{\mathrm{c}}' j_1'(x_{\mathrm{c}}') \tilde{k}_{\mathrm{th}} \frac{b_{\mathrm{c}}'}{b_{\mathrm{t}}} + B_1' x_{\mathrm{t}}' j_1'(x_{\mathrm{t}}') \tilde{k}_{\mathrm{th}} \frac{b_{\mathrm{t}}'}{b_{\mathrm{t}}}. \tag{C.28}$$

Comparing this equation to Eq. (C.27a) we see that the terms with A_1, A_1' and the inhomogeneous term are multiplied by the small factor $b_{\mathrm{c}}/b_{\mathrm{t}}$ or $b_{\mathrm{c}}/b_{\mathrm{t}}'$ of order $(k_{\mathrm{c}} \delta_{\mathrm{t}})^2$ as compared to Eq. (C.27a), which means that the terms with B_1, B_1' in Eq. (C.27a) are of negligible order. The same is true when comparing Eq. (C.27b) with Eq. (C.27c) multiplied by $1/b_{\mathrm{t}}$. Investigating the full system of equations the conclusion is that the terms with B_1, B_1' are of negligible order in all of the equations. Consequently terms with B_1, B_1' are omitted and the system of equations reduces to four equations with four unknowns, namely Eq. (C.27a), Eq. (C.27b), Eq. (C.27e), Eq. (C.27f) without the terms of B_1, B_1'.

Physically, this means that thermal effects are negligible in the dipole mode in the long wavelength limit. This is consistent with the dipole mode described as a back-and-forth motion of the undeformed particle relative to the fluid, for which we expect viscous effects to be dominant.

The simplified system of equations is

$$x_{\mathrm{c}} j_1'(x_{\mathrm{c}}) + A_1 x_{\mathrm{c}} h_1'(x_{\mathrm{c}}) - 2C_1 h_1(x_{\mathrm{s}}) = A_1' x_{\mathrm{c}}' j_1'(x_{\mathrm{c}}') - 2C_1' j_1(x_{\mathrm{s}}'), \tag{C.29a}$$

$$\begin{aligned} &j_1(x_{\mathrm{c}}) + A_1 h_1(x_{\mathrm{c}}) - C_1 \left[x_{\mathrm{s}} h_1'(x_{\mathrm{s}}) + h_1(x_{\mathrm{s}})\right] \\ &\quad = A_1' j_1(x_{\mathrm{c}}') - C_1' \left[x_{\mathrm{s}}' j_1'(x_{\mathrm{s}}') + j_1(x_{\mathrm{s}}')\right], \end{aligned} \tag{C.29b}$$

$$\begin{aligned} &\eta_0 \left[x_{\mathrm{c}} j_2(x_{\mathrm{c}}) + A_1 x_{\mathrm{c}} h_2(x_{\mathrm{c}}) + (C_1/2) x_{\mathrm{s}}^2 h_1''(x_{\mathrm{s}})\right] \\ &\quad = \eta_0' \left[A_1' x_{\mathrm{c}}' j_2(x_{\mathrm{c}}') + (C_1'/2) x_{\mathrm{s}}'^2 j_1''(x_{\mathrm{s}}')\right], \end{aligned} \tag{C.29c}$$

$$\begin{aligned} &\eta_0 \Big(\left[\left(x_{\mathrm{s}}^2 + 2x_{\mathrm{c}}^2\right) j_1(x_{\mathrm{c}}) - 4x_{\mathrm{c}} j_2(x_{\mathrm{c}})\right] + A_1 \left[\left(x_{\mathrm{s}}^2 + 2x_{\mathrm{c}}^2\right) h_1(x_{\mathrm{c}}) - 4x_{\mathrm{c}} h_2(x_{\mathrm{c}})\right] \\ &\qquad - 4C_1 x_{\mathrm{s}} h_2(x_{\mathrm{s}}) \Big) \\ &\quad = \eta_0' \left(A_1' \left[\left(x_{\mathrm{s}}'^2 + 2x_{\mathrm{c}}'^2\right) j_1(x_{\mathrm{c}}') - 4x_{\mathrm{c}}' j_2(x_{\mathrm{c}}')\right] - 4C_1' x_{\mathrm{s}}' j_2(x_{\mathrm{s}}')\right), \end{aligned} \tag{C.29d}$$

where we have used the following general relations in the last two equations,

$$x f_1'(x) - f_1(x) = -x f_2(x), \tag{C.30a}$$

$$f_1''(x) = -f_1(x) + (2/x) f_2(x), \tag{C.30b}$$

where f can be any spherical Bessel or Hankel function.

Next, we simplify the four equations of Eq. (C.29). For the first equation we multiply Eq. (C.29a) by (-1) and add it to Eq. (C.29b), then use the relation of Eq. (C.30a). For the second equation we multiply Eq. (C.29b) by 2 and add it to Eq. (C.29a) and use the relation $x f_1'(x) + 2 f_1(x) = x f_0(x)$ valid for any spherical Bessel or Hankel function f. The third equation is obtained by adding 4 times Eq. (C.29c) to Eq. (C.29d) while neglecting $x_{\mathrm{c}}^2, x_{\mathrm{c}}'^2$ relative to $x_{\mathrm{s}}^2, x_{\mathrm{s}}'^2$ consistent with our general scheme of approximation, and moreover making use of the relation in Eq. (C.30b). As the fourth equation we use Eq. (C.29c) without further manipulations. The new system of equations is

$$A_1 x_{\mathrm{c}} h_2(x_{\mathrm{c}}) + C_1 x_{\mathrm{s}} h_2(x_{\mathrm{s}}) - A_1' x_{\mathrm{c}}' j_2(x_{\mathrm{c}}') - C_1' x_{\mathrm{s}}' j_2(x_{\mathrm{s}}') = -x_{\mathrm{c}} j_2(x_{\mathrm{c}}), \tag{C.31a}$$

$$A_1 x_{\mathrm{c}} h_0(x_{\mathrm{c}}) - 2C_1 x_{\mathrm{s}} h_0(x_{\mathrm{s}}) - A_1' x_{\mathrm{c}}' j_0(x_{\mathrm{c}}') + 2C_1' x_{\mathrm{s}}' j_0(x_{\mathrm{s}}') = -x_{\mathrm{c}} j_0(x_{\mathrm{c}}), \tag{C.31b}$$

$$\eta_0 x_{\mathrm{s}}^2 \left[A_1 h_1(x_{\mathrm{c}}) - 2C_1 h_1(x_{\mathrm{s}})\right] - \eta_0' x_{\mathrm{s}}'^2 \left[A_1' j_1(x_{\mathrm{c}}') - 2C_1' j_1(x_{\mathrm{s}}')\right] = -\eta_0 x_{\mathrm{s}}^2 j_1(x_{\mathrm{c}}), \tag{C.31c}$$

$$\begin{aligned} &\eta_0 \left[A_1 x_{\mathrm{c}} h_2(x_{\mathrm{c}}) + (C_1/2) x_{\mathrm{s}}^2 h_1''(x_{\mathrm{s}})\right] - \eta_0' \left[A_1' x_{\mathrm{c}}' j_2(x_{\mathrm{c}}') + (C_1'/2) x_{\mathrm{s}}'^2 j_1''(x_{\mathrm{s}}')\right] \\ &\quad = -\eta_0 x_{\mathrm{c}} j_2(x_{\mathrm{c}}). \end{aligned} \tag{C.31d}$$

Next, we apply the Rayleigh limit of long wavelength in comparison to the particle size to neglect $x_{\mathrm{c}}^2, x_{\mathrm{c}}'^2$ relative to 1. Using the approximate expressions for the spherical Bessel

and Hankel functions given in Eq. (C.37) of section Section C.6, Eq. (C.31) simplifies to give

$$-\frac{3\mathrm{i}}{x_\mathrm{c}^2}A_1 + C_1 x_\mathrm{s} h_2(x_\mathrm{s}) - C_1' x_\mathrm{s}' j_2(x_\mathrm{s}') = 0, \tag{C.32a}$$

$$-2C_1 x_\mathrm{s} h_0(x_\mathrm{s}) - A_1' x_\mathrm{c}' + 2C_1' x_\mathrm{s}' j_0(x_\mathrm{s}') = -x_\mathrm{c}, \tag{C.32b}$$

$$\frac{1}{\tilde{\rho}_0}\left[\frac{3\mathrm{i}}{x_\mathrm{c}^2}A_1 + 6C_1 h_1(x_\mathrm{s})\right] + A_1' x_\mathrm{c}' - 6C_1' j_1(x_\mathrm{s}') = \frac{1}{\tilde{\rho}_0}x_\mathrm{c}, \tag{C.32c}$$

$$-\frac{3\mathrm{i}}{x_\mathrm{c}^2}A_1 + \frac{1}{2}C_1 x_\mathrm{s}^2 h_1''(x_\mathrm{s}) - \frac{1}{2}C_1'\tilde{\eta}_0 x_\mathrm{s}'^2 j_1''(x_\mathrm{s}') = 0, \tag{C.32d}$$

Subtracting Eq. (C.32a) from Eq. (C.32d) and using Eq. (C.30b) we obtain a relation that serves to eliminate C_1',

$$C_1' = \frac{x_\mathrm{s}^2 h_1(x_\mathrm{s})}{\tilde{\eta}_0 x_\mathrm{s}' Q(x_\mathrm{s}')}C_1, \tag{C.33a}$$

$$Q(x_\mathrm{s}') = x_\mathrm{s}' j_1(x_\mathrm{s}') - 2(1 - 1/\tilde{\eta}_0) j_2(x_\mathrm{s}'). \tag{C.33b}$$

Using this relation to eliminate C_1' in Eq. (C.32a) gives the first of the two equations in Eq. (C.34). The second equation is obtained by adding Eq. (C.32b) and Eq. (C.32c) in order to eliminate A_1', then making use of the general relation $3f_1(x) - xf_0(x) = xf_2(x)$ for any spherical Bessel or Hankel function f. This approach gives the following two equations with A_1 and C_1 unknowns

$$-\frac{3\mathrm{i}}{\tilde{\rho}_0 x_\mathrm{c}^2}A_1 + C_1\left[\frac{1}{\tilde{\rho}_0}x_\mathrm{s} h_2(x_\mathrm{s}) - \frac{x_\mathrm{s}^2 h_1(x_\mathrm{s}) j_2(x_\mathrm{s}')}{\tilde{\rho}_0\tilde{\eta}_0 Q(x_\mathrm{s}')}\right] = 0, \tag{C.34a}$$

$$\frac{3\mathrm{i}}{\tilde{\rho}_0 x_\mathrm{c}^2}A_1 + 2C_1\left[\frac{3}{\tilde{\rho}_0}h_1(x_\mathrm{s}) - x_\mathrm{s} h_0(x_\mathrm{s}) - \frac{x_\mathrm{s}^2 h_1(x_\mathrm{s}) j_2(x_\mathrm{s}')}{\tilde{\eta}_0 Q(x_\mathrm{s}')}\right] = (1/\tilde{\rho}_0 - 1)x_\mathrm{c}. \tag{C.34b}$$

These two equations are easily solved and we finally obtain the expression for the expansion coefficient A_1 of the scattered propagating wave

$$A_1 = \frac{-(\mathrm{i}/3)x_\mathrm{c}^3(1/\tilde{\rho}_0 - 1)\left[h_2(x_\mathrm{s})Q(x_\mathrm{s}') - (1/\tilde{\eta}_0)x_\mathrm{s} h_1(x_\mathrm{s}) j_2(x_\mathrm{s}')\right]}{\left[(3/\tilde{\rho}_0)h_2(x_\mathrm{s}) + 2(1/\tilde{\rho}_0 - 1)h_0(x_\mathrm{s})\right]Q(x_\mathrm{s}') - (1/\tilde{\eta}_0)(1/\tilde{\rho}_0 + 2)x_\mathrm{s} h_1(x_\mathrm{s}) j_2(x_\mathrm{s}')}. \tag{C.35}$$

This result, but with a small error in the numerator, was first obtained by Epstein and Carhart [8] using the same approach as that employed here. Unfortunately, their seminal paper is full of misprints and minor errors. In the calculation of A_1 as given in the appendix of their paper almost every equation is incorrect, and with the final result disagreeing with that of Allegra and Hawley, apparently unaware of it [9], we felt a need to go through the tedious calculations in this work. Allegra and Hawley derived the correct result by modifying the final result obtained using the stress tensor of an elastic solid particle into a result valid for a fluid droplet.

Using that $A_1 = (\mathrm{i}/6)x_\mathrm{c}^3 f_1$, dividing the numerator and denominator by $Q(x_\mathrm{s}')h_0(x_\mathrm{s})$, and making use of the explicit expressions for the Bessel and Hankel functions in Eq. (C.36) one obtains the expression for the dipole scattering coefficient f_1 given in Eq. (5.14).

C.6 Spherical Bessel and Hankel functions

Explicit expressions for the spherical Bessel functions j_n and Hankel functions $h_n = h_n^{(1)}$ needed to derive the monopole and dipole scattering coefficients are given in this section. The functions of low order are [51]

$$j_0(x) = \frac{\sin x}{x}, \qquad j_1(x) = \frac{1}{x}\left(\frac{\sin x}{x} - \cos x\right), \tag{C.36a}$$

$$j_2(x) = \frac{1}{x}\left[\left(\frac{3}{x^2} - 1\right)\sin x - \frac{3}{x}\cos x\right], \tag{C.36b}$$

$$h_0(x) = -\mathrm{i}\frac{\mathrm{e}^{\mathrm{i}x}}{x}, \qquad h_1(x) = -\frac{\mathrm{e}^{\mathrm{i}x}}{x}\left(1 + \frac{\mathrm{i}}{x}\right), \tag{C.36c}$$

$$h_2(x) = \mathrm{i}\frac{\mathrm{e}^{\mathrm{i}x}}{x}\left(1 + \frac{3\mathrm{i}}{x} - \frac{3}{x^2}\right). \tag{C.36d}$$

Expanding the spherical Bessel and Hankel functions and neglecting terms of order x^2 relative to 1, the Bessel and Hankel functions and their derivatives are approximated as

$$j_0(x) \simeq 1, \qquad j_0'(x) \simeq -\frac{x}{3}, \quad j_0''(x) \simeq -\frac{1}{3}, \tag{C.37a}$$

$$h_0(x) \simeq 1 - \frac{\mathrm{i}}{x}, \quad h_0'(x) \simeq \frac{\mathrm{i}}{x^2}, \quad h_0''(x) \simeq -\frac{2\mathrm{i}}{x^3}, \tag{C.37b}$$

$$j_1(x) \simeq \frac{x}{3}, \qquad j_2(x) \simeq \frac{x^2}{15}, \tag{C.37c}$$

$$h_1(x) \simeq -\frac{\mathrm{i}}{x^2}, \qquad h_2(x) \simeq -\frac{3\mathrm{i}}{x^3}. \tag{C.37d}$$

Bibliography

[1] H. Bruus, J. Dual, J. Hawkes, M. Hill, T. Laurell, J. Nilsson, S. Radel, S. Sadhal, and M. Wiklund, *Forthcoming Lab on a Chip tutorial series on acoustofluidics: Acoustofluidics-exploiting ultrasonic standing wave forces and acoustic streaming in microfluidic systems for cell and particle manipulation.* Lab Chip **11**(21), 3579–3580 (2011).

[2] A. Lenshof, C. Magnusson, and T. Laurell, *Acoustofluidics 8: Applications of acoustophoresis in continuous flow microsystems.* Lab Chip **12**, 1210–1223 (2012).

[3] M. Evander and J. Nilsson, *Acoustofluidics 20: applications in acoustic trapping.* Lab on a chip **12**(22), 4667–76 (2012).

[4] F. Petersson, A. Nilsson, C. Holm, H. Jönsson, and T. Laurell, *Separation of lipids from blood utilizing ultrasonic standing waves in microfluidic channels.* Analyst **129**(10), 938–943 (2004).

[5] C. Grenvall, P. Augustsson, J. R. Folkenberg, and T. Laurell, *Harmonic Microchip Acoustophoresis: A Route to Online Raw Milk Sample Precondition in Protein and Lipid Content Quality Control.* Anal Chem **81**(15), 6195–6200 (2009).

[6] P. Augustsson, C. Magnusson, M. Nordin, H. Lilja, and T. Laurell, *Microfluidic, Label-Free Enrichment of Prostate Cancer Cells in Blood Based on Acoustophoresis.* Analytical Chemistry **84**(18), 7954–7962 (2012).

[7] R. Barnkob, *Physics of microparticle acoustophoresis: Bridging theory and experiment.* Phd thesis, DTU, Department of Micro- and Nanotechnology, www.fysik.dtu.dk/microfluidics (2012).

[8] P. S. Epstein and R. R. Carhart, *The Absorption of Sound in Suspensions and Emulsions. I. Water Fog in Air.* The Journal of the Acoustical Society of America **25**(3) (1953).

[9] J. R. Allegra and S. A. Hawley, *Attenuation of Sound in Suspensions and Emulsions: Theory and Experiments.* The Journal of the Acoustical Society of America **51**(5B) (1972).

[10] N. Rott, *Damped and thermally driven acoustic oscillations in wide and narrow tubes.* Zeitschrift Fur Angewandte Mathematik Und Physik **20**(2), 230–243 (1969).

[11] G. W. Swift, *Thermoacoustic engines*. The Journal of the Acoustical Society of America **84**(4), 1145–1180 (1988).

[12] L. D. Landau and E. M. Lifshitz, *Fluid Mechanics, Course of Theoretical Physics, vol. 6* (Butterworth-Heinemann, Oxford), 2nd edn. (1987).

[13] H. Bruus, *Theoretical Microfluidics* (Oxford University Press, Oxford) (2008).

[14] H. Bruus, *Acoustofluidics 2: Perturbation theory and ultrasound resonance modes*. Lab Chip **12**, 20–28 (2012).

[15] M. Settnes and H. Bruus, *Forces acting on a small particle in an acoustical field in a viscous fluid*. Phys Rev E **85**(1), 16327 (2012).

[16] L. Prandtl, *Über Flüssigkeitsbewegung bei sehr kleiner Reibung*. Verhandl. III. Intern. Math. Kongr. Heidelberg 484 (1904).

[17] H. Schlichting, *Berechnung ebener periodischer Grenzeschichtströmungen*. Physik Z **33**, 327–335 (1932).

[18] L. Rayleigh, *On the Circulation of Air Observed in Kundt's Tubes, and on Some Allied Acoustical Problems*. Philosophical Transactions of the Royal Society of London **175**, 1–21 (1884).

[19] W. L. Nyborg, *Acoustic streaming near a boundary*. J Acoust Soc Am **30**(4), 329–339 (1958).

[20] M. F. Hamilton, Y. A. Ilinskii, and E. A. Zabolotskaya, *Acoustic streaming generated by standing waves in two-dimensional channels of arbitrary width*. The Journal of the Acoustical Society of America **113**(1), 153 (2003).

[21] M. F. Hamilton, Y. A. Ilinskii, and E. A. Zabolotskaya, *Thermal effects on acoustic streaming in standing waves*. J Acoust Soc Am **114**(6, Part 1), 3092–3101 (2003).

[22] A. Y. Rednikov and S. S. Sadhal, *Acoustic/steady streaming from a motionless boundary and related phenomena: generalized treatment of the inner streaming and examples*. J Fluid Mech **667**, 426–462 (2011).

[23] P. B. Muller, *Acoustofluidics in microsystems: investigation of acoustic streaming*. Msc thesis, DTU, Department of Micro- and Nanotechnology, www.fysik.dtu.dk/microfluidics.

[24] P. B. Muller, R. Barnkob, M. J. H. Jensen, and H. Bruus, *A numerical study of microparticle acoustophoresis driven by acoustic radiation forces and streaming-induced drag forces*. Lab Chip **12**, 4617–4627 (2012).

[25] P. B. Muller, M. Rossi, A. G. Marín, R. Barnkob, P. Augustsson, T. Laurell, C. J. Kähler, and H. Bruus, *Ultrasound-induced acoustophoretic motion of microparticles in three dimensions*. Phys. Rev. E **88**(2), 23006 (2013).

[26] L. D. Landau and E. M. Lifshitz, *Statistical Physics, Part 1, Course of Theoretical Physics, vol. 5* (Butterworth-Heinemann, Oxford), 3rd edn. (1980).

[27] P. Augustsson, R. Barnkob, S. T. Wereley, H. Bruus, and T. Laurell, *Automated and temperature-controlled micro-PIV measurements enabling long-term-stable microchannel acoustophoresis characterization*. Lab Chip **11**(24), 4152–4164 (2011).

[28] R. Barnkob, P. Augustsson, T. Laurell, and H. Bruus, *Acoustic radiation- and streaming-induced microparticle velocities determined by microparticle image velocimetry in an ultrasound symmetry plane*. Phys Rev E **86**(5), 56307 (2012).

[29] W. M. Haynes, *CRC Handbook of Chemistry and Physics* (CRC Press/Taylor and Francis, Boca Raton, FL), 94th edn.

[30] C. S. Miner and N. N. Dalton, *Glycerol. American Chemical Society Monograph Series*, vol. 117 (Reinhold Publishing Corp, New York) (1953).

[31] A. S. Dukhin and P. J. Goetz, *Bulk viscosity and compressibility measurement using acoustic spectroscopy*. J Chem Phys **130**(12) (2009).

[32] P. M. Morse and K. U. Ingard, *Theoretical Acoustics* (Princeton University Press, Princeton, New Jersey) (1986).

[33] R. Barnkob, P. Augustsson, T. Laurell, and H. Bruus, *Measuring the local pressure amplitude in microchannel acoustophoresis*. Lab Chip **10**(5), 563–570 (2010).

[34] O. Christensen, *Differentialligninger og uendelige rækker* (Danmarks Tekniske Universitet, Institut for matematik, Lyngby) (2009).

[35] A. Kundt and O. Lehmann, *Longitudinal vibrations and acoustic figures in cylindrical columns of liquids*. Ann. Phys. Chem. **153**, 1 (1874).

[36] W. Wagner and A. Pruss, *The IAPWS Formulation 1995 for the Thermodynamic Properties of Ordinary Water Substance for General and Scientific Use*. Journal of Physical and Chemical Reference Data **31**(2), 387–535 (2002).

[37] M. L. Huber, R. A. Perkins, A. Laesecke, D. G. Friend, J. V. Sengers, M. J. Assael, I. N. Metaxa, E. Vogel, R. Mareš, and K. Miyagawa, *New International Formulation for the Viscosity of H2O*. Journal of Physical and Chemical Reference Data **38**(2), 101–125 (2009).

[38] M. L. Huber, R. A. Perkins, D. G. Friend, J. V. Sengers, M. J. Assael, I. N. Metaxa, K. Miyagawa, R. Hellmann, and E. Vogel, *New International Formulation for the Thermal Conductivity of H2O*. Journal of Physical and Chemical Reference Data **41**(3), 033102 (2012).

[39] L. V. King, *On the Acoustic Radiation Pressure on Spheres*. P Roy Soc Lond A Mat **147**(861), 212–240 (1934).

[40] K. Yosioka and Y. Kawasima, *Acoustic radiation pressure on a compressible sphere.* Acustica **5**, 167–173 (1955).

[41] L. P. Gorkov, *On the Forces Acting on a Small Particle in an Acoustical Field in an Ideal Fluid.* Soviet Physics - Doklady **6**(9), 773–775 (1962).

[42] A. A. Doinikov, *Acoustic radiation force on a spherical particle in a viscous heat-conducting fluid. I. General formula.* The Journal of the Acoustical Society of America **101**(2), 713–721 (1997).

[43] A. A. Doinikov, *Acoustic radiation force on a spherical particle in a viscous heat-conducting fluid. II. Force on a rigid sphere.* The Journal of the Acoustical Society of America **101**(2), 722–730 (1997).

[44] A. A. Doinikov, *Acoustic radiation force on a spherical particle in a viscous heat-conducting fluid. III. Force on a liquid drop.* The Journal of the Acoustical Society of America **101**(2), 731–740 (1997).

[45] S. D. Danilov and M. A. Mironov, *Mean force on a small sphere in a sound field in a viscous fluid.* J Acoust Soc Am **107**(1), 143–153 (2000).

[46] L. L. Foldy, *The Multiple Scattering of Waves. I. General Theory of Isotropic Scattering by Randomly Distributed Scatterers.* Phys. Rev. **67**(3-4), 107–119 (1945).

[47] P. Lloyd and M. V. Berry, *Wave propagation through an assembly of spheres: IV. Relations between different multiple scattering theories.* Proceedings of the Physical Society **91**(3), 678 (1967).

[48] D. J. McClements and M. J. W. Povey, *Scattering of ultrasound by emulsions.* Journal of Physics D: Applied Physics **22**(1), 38 (1989).

[49] R. E. Challis, M. J. W. Povey, M. L. Mather, and A. K. Holmes, *Ultrasound techniques for characterizing colloidal dispersions.* Reports on Progress in Physics **68**(7), 1541–1637 (2005).

[50] C. A. Balanis, *Advanced Engineering Electromagnetics* (John Wiley & Sons, Inc., New Jersey), 2nd edn. (2012).

[51] G. B. Arfken and H. J. Weber, *Mathematical Methods for Physicists* (Elsevier Inc, Burlington), 6th edn. (2005).

[52] H. Bruus, *Acoustofluidics 7: The acoustic radiation force on small particles.* Lab Chip **12**, 1014–1021 (2012).

[53] J. N. Coupland and D. J. McClements, *Physical properties of liquid edible oils.* Journal of the American Oil Chemists' Society **74**(12), 1559–1564 (1997).

[54] B. Hammarstrom, T. Laurell, and J. Nilsson, *Seed particle-enabled acoustic trapping of bacteria and nanoparticles in continuous flow systems.* Lab Chip **12**(21), 4296–4304 (2012).